

# MELTING AND CRYSTALLIZATION STUDIES IN A PARTIALLY EXCLUDING COPOLYMER

by

**RAVI KANT VERMA**

DISSERTATION SUBMITTED TO THE FACULTY OF THE  
VIRGINIA POLYTECHNIC INSTITUTE & STATE UNIVERSITY  
IN PARTIAL FULFILLMENT OF THE REQUIREMENTS FOR THE DEGREE

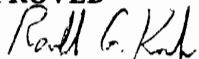
of

**Doctor of Philosophy**


in

**Materials Engineering Science**


**APPROVED**



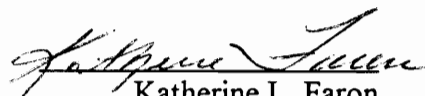
Ronald G. Kander  
Chairman, Advisory Board



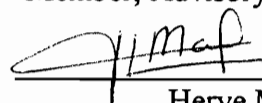
Benjamin S. Hsiao  
Member, Advisory Board



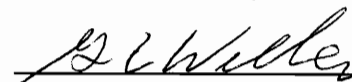
Thomas C. Ward  
Member, Advisory Board



Katherine L. Faron  
Member, Advisory Board



Herve Marand  
Member, Advisory Board



Garth L. Wilkes  
Chairman, MESC Program

Blacksburg, Virginia

OCTOBER, 1994

# MELTING AND CRYSTALLIZATION STUDIES IN A PARTIALLY EXCLUDING COPOLYMER

by

**Ravi Kant Verma**

Committee Chairman: Ronald G Kander  
Materials Engineering Science

## (ABSTRACT)

The crystallization and melting behavior of copolymers (specially of those which partially exclude the 2<sup>nd</sup> component) has not been well understood. Poly(ether ketone ketone) PEKK is such a partially excluding copolymer in which the crystalline phase tends to exclude one of two similar monads. Previous studies on PEKK have focused on effects of changing overall composition on the melting and crystallization behavior. These studies have demonstrated that PEKK tends to exclude one of two chemically similar monads from the crystalline phase, and the crystallization and melting behavior is affected as a result of this exclusion. However, the effect of changing linear chain architectures on the thermal behavior of such copolymers has not been investigated.

In this study, the effect of changing architectures of the linear chain (blockiness) on the crystallization and melting behavior has been studied. The overall composition of the copolymer is maintained at 50% 2<sup>nd</sup> comonomer, and a series of samples prepared with different block lengths and amounts of branching. The crystallization and melting behavior of these samples is then studied using hot stage optical microscopy, scattering (small and wide angle X-ray scattering) and thermal analysis techniques (differential scanning calorimetry).

It has been demonstrated that, upon changing from an alternating to a non-alternating structure, substantial amounts of 2<sup>nd</sup> component are excluded from the crystalline phase and the melting temperature is raised considerably. Further, because of

increased amounts of branching which accompanies the change in blockiness, the crystallization kinetics is slowed down. These results have been analyzed in terms of existing theories of copolymer crystallization, and some speculative arguments have been presented on the factors which affect the crystallization mechanism in such partially excluding copolymers. The validity of equilibrium thermodynamics based on the enthalpic approach has been analyzed.

# ACKNOWLEDGEMENTS

I sincerely believe that one's research (and everything else) is defined by one's personality. Well, my research (and everything else) has defects because I have defects. Life is a learning experience. I have learnt a little from the mistakes that I have made and, God willing, I will continue to learn some from the mistakes that I know I will make. My only prayer is that I don't repeat the mistakes that I have already made. However, I know that at the end of it all, I will still be ignorant of many things. Having said that, let me thank all those who have showered me with love for the qualities that I have. I thank them for glossing over my defects and highlighting my qualities. Let me also thank all those who have directed their anger at me for the qualities that I don't have. They are the ones who have highlighted my defects and overlooked my qualities (I will not name them, but if you are one, I say thank you!). I think I could not have improved without it all.

My parents, who taught me 'that if at first I don't succeed, then try-try again'. My Dad used to tease me that even little froggies could learn their lessons (implying that I could not!). I might never, but I will keep trying. My sister for showing me how to strive hard and how to keep one's faith, even in the most difficult of times. My two younger brothers who were always a pain in the rear end. Life would not be the same without them. Vivek, who was the first real friend I had. My friends in IIT who made life alternately miserable and ecstatic for me. Shouvik and Suman and Kaushik and Arpan and Subtrata and Shantanu (I shall, in the interest of decorum, refrain from calling them by their real names!). My friends in Blacksburg who put up with my judgemental attitude and my "final statements" for 3 long years. Srinivas (Watson) for putting up with my endless 'hand waving'/'definite proofs'. Joel for all those discussions on life and all it's miseries. Saikat (Ko) for all the advice he gave (and also for those he did not). Hemanshu (Paps) for always putting a new insight into things. Venky for being the target of my wrath the one time in the last 4 years when I lost my temper (and also for rechristening me with a name that I fear I will live with for a very long time). And 'Blacksburg's answer to

Motley Cruie': Diane and Shannon and Helene and Sue (somebody sure does have a preference for women!) and Rick and Mike.

I also thank several people for teaching me what I know about Science. I have been very fortunate to have been exposed to several mature thinkers during the course of my Graduate studies. I have tried to learn from all of them. From my advisor, Dr Kander, I learnt (very belatedly) that the best way to teach is to help people learn on their own. From Dr. Marand, I learnt that while a stitch in time can save nine, a stitch before time can save ninety nine. From Dr Hsiao (Ben), I learnt how to separate science from friendship. From Dr. Faron (Kate), I learnt that I am no chemist and never will be. Dr Ward tried to teach me thermodynamic (something that I am incapable of understanding). For me, he personifies respect. Dr Biswas (Amit), for showing me what a fool I was (I did not see something obvious to him). Dr Gardner (Kenn), for introducing me to the crazy world of inverse spacings and funny convolutions. Dr Sauer (Bryan) for making me understand that I could not force a marriage on 2 unwilling people.

*To all of them and countless others, I say 'Thank You, and I will always owe you!'*

This work is dedicated to:

*My Parents 'Veena and Krishna Verma'*

who seem more excited about it than I will ever be!

# TABLE OF CONTENTS

	Page
<b>INTRODUCTION</b> .....	<b>1</b>
<b>CHAPTER 2. LITERATURE REVIEW</b> .....	<b>5</b>
2.1 Poly(ether ketones) .....	5
2.2 Poly(ether ketone ketone).....	8
2.3 Synthesis of Poly(ether ketone ketone) .....	16
Historical Perspective: .....	16
Acid Promoted Electrophilic Reactions: .....	17
Nucleophilic Aromatic Substitution:.....	21
Poly(aryl ether ketone ketone): .....	24
2.4 Crystallization of Copolymers.....	28
2.5 SAXS data analysis: .....	31
2.6 Thermal Analysis.....	40
<b>CHAPTER 3. SYNTHESIS AND CHARACTERIZATION</b> .....	<b>45</b>
3.1 Synthesis .....	45
3.2 Characterization .....	49
3.3 Chain Defects .....	55
<b>CHAPTER 4. CRYSTALLIZATION AND MELTING STUDIES</b> .....	<b>61</b>
4.1 Experimental .....	61
4.2 Results .....	66
<b>CHAPTER 5. DISCUSSION</b> .....	<b>83</b>
5.1 Linear Chain Defects .....	85
5.2 Defect Exclusion .....	87
5.3 Elevation of $T_m^{Eq}$ .....	92
5.4 Crystallization kinetics.....	96
<b>CHAPTER 6. CONCLUSION</b> .....	<b>99</b>
<b>CHAPTER 7. FUTURE WORK</b> .....	<b>104</b>
<b>BIBLIOGRAPHY</b> .....	<b>109</b>
<b>VITA</b> .....	<b>113</b>

## List of Figures

- Figure 1.1: Simplified synthesis route for PEKK showing the -DT- and -DI- repeat units<sup>2</sup>.
- Figure 2.1: The chemical structure of different poly(aryl ether ketones).
- Figure 2.2: Orthorhombic unit cell parameters as a function of ketone content for different poly(aryl ether ketones)<sup>2</sup>.
- Figure 2.3: The glass transition ( $T_g$ ) and equilibrium melting ( $T_m^{eq}$ ) temperature as a function of ketone content for different poly(aryl ether ketones)<sup>2</sup>. The solid line at 400°C denotes the degradation temperature.
- Figure 2.4: The proposed Form 1 and Form 2 structures for PEKK<sup>2</sup>.
- Figure 2.5: Typical DSC traces for cold crystallized and melt crystallized PEKK 50/50 copolymer<sup>2</sup>.
- Figure 2.6: WAXD peak position vs the overall composition for poly(aryl ether ketone ketone) PEKK<sup>2</sup>.
- Figure 2.7: Unique arrangement of -DT- and -DI- monads within the lamellae that results in partial exclusion of one of the two monads.
- Figure 2.8: The equilibrium melting ( $T_m^0$ ) and the glass transition temperature ( $T_g$ ) vs the overall composition for poly(aryl ether ketone ketone) PEKK<sup>2</sup>.
- Figure 2.9: The crystallization kinetics as measured by DSC peak time for crystallization vs. the overall composition for poly(aryl ether ketone ketone) PEKK<sup>2</sup>.
- Figure 2.10: WAXD data analysis technique used by Gardner et al. for estimating the crystallinity and the composition of the crystalline phase. The dashed lines denote the amorphous halo. The solid lines denote the peaks corresponding to different crystallographic planes and the dark line denote the sum of all the fitted curves.
- Figure 2.11: The composition of the crystalline phase as estimated by Gardner et al. using the technique illustrated in Figure 2.10.
- Figure 2.12(a): 4-phenoxybenzoic acid.
- Figure 2.12(b): 4-(4' phenoxy phenoxy) benzoic acid.
- Figure 2.12(c): 4-(4' phenoxy phenyl) benzoic acid.
- Figure 2.13: Example Raw SAXS data. Sample: PEEK 450 G melted at 385°C for 4 minutes, followed by rapid quenching to 307°C. Data collected for 50 seconds after a hold of 600 seconds. Also shown in the plot is the Porod Law extrapolation for high angles.



- Figure 2.14: Lorentz corrected plot of the data depicted in Figure 2.13. Also shown in the plot is the Porod Law extrapolation for high angles. Extrapolation to low angles (in the region covered by the beam stop) was done with a straight line between the origin and the 1<sup>st</sup> useful data point in the plot.
- Figure 2.15: Porod Law plot of  $I \cdot q^4$  vs  $q^4$  to estimate  $I_b$ .
- Figure 2.16: Porod law plot of  $\text{Ln}[(I-I_b) \cdot q^4]$  vs  $q^2$  to estimate the factor  $\sigma$ .  $s$  is related to the thickness of the crystal-liquid transition zone  $E$  by the relation  $E = \sqrt{12} \cdot \sigma$
- Figure 2.17: Porod Law plot of  $[(I-I_b) \cdot q^4 \cdot \exp(\sigma^2 q^2)]$  vs  $q$ . This plot should resemble the one depicted in Figure 2.18. Also shown in the plot is the estimated Porod Law constant  $K$ . The constant  $K$  was estimated following the procedure of Biswas<sup>52</sup>.
- Figure 2.18: Porod Law plot of  $I \cdot q^4$  vs  $q$  for an ideal 2 phase lamellar system<sup>51</sup>. The plot resembles a decaying sine function, which has a value  $K$  at large values of  $q$ .
- Figure 2.19: One dimensional correlation function for the data depicted in Figure 2.13. Also marked in the plot are the 1st zero ( $B$ ), the 1st minima ( $L_c^m/2$ ) and the 1st maxima ( $L_c^M$ ). Note that the correlation function does not have any curvature at  $r=0$ . This results from the analysis procedure suggested by Biswas<sup>52</sup>.
- Figure 2.20: An example Hoffman-Weeks estimate for data obtained from the L-H theory.  $l_{\min}$ ,  $\delta l$  and  $l_{\text{act}}$  are estimated from the L-H<sup>61</sup> theory using  $T_m^0$ : 618 K;  $\sigma_e$ : 12 kcal\*nm/mole;  $\sigma$ : 1 kcal\*nm/mole;  $\Delta H$ : 15 kcal/mole  $\psi$ : 0.9 a: 0.49 nm; b: 0.5 nm. Melting temperatures (open circles) are estimated from  $l_{\text{act}}$  using Equation 2.7. Melting temperatures in an arbitrary 'observable range' are extrapolated to the  $T_m=T_c$  line for a  $T_m^{\text{HW}}$  estimate of 570 K.
- Figure 2.21: The Gibbs-Thomson-Tammann plot for the data depicted in Figure 2.20.
- Figure 3.1: The Friedel Crafts Acylation synthesis reaction for PEKK.
- Figure 3.2: Control of the Prepolymerization Step
- Figure 3.3: An <sup>1</sup>H NMR scan typical for PEKK 50/50.
- Figure 3.4: The different types of protons in the linear PEKK 50/50 chain.
- Figure 3.5: KBr pellet IR spectra for the Random PEKK 50/50 sample.
- Figure 3.6: A Gel Permeation Chromatography (GPC) trace for the sample labeled ABL 5 typical of all synthesized PEKK 50/50 samples.

- Figure 3.7: DSC traces of quenched PEKK 50/50 samples depicting the glass transition temperature at about 156 °C. All traces have been shifted vertically for visual clarity.
- Figure 3.8: Chart depicting the glass transition temperature from the DSC traces depicted in Figure 3.7.
- Figure 3.9: Formation of a xanthate type compound from a 1,2 substituted phenyl ring<sup>34</sup>.
- Figure 3.10: Formation of triphenyl hydroxyl group consistent with the <sup>1</sup>H NMR data.
- Figure 3.11: <sup>1</sup>H NMR scan of reaction bath after the prepolymerization step.
- Figure 3.12: Mass Spectroscopy analysis of reaction bath after the prepolymerization step.
- Figure 4.1(a): Tutorial example illustrating the peak time estimated as from the heat flow exotherm; and the half time estimated from the cumulative area plot.
- Figure 4.1(b): Tutorial example depicting the baseline used for estimating the heat of fusion of the two endotherms. Sample: PEKK 50/50 ABL 5; Crystallized at 225°C for 6 hrs.
- Figure 4.2: Crystallization kinetics as manifest in the DSC half time (ABL 1, ABL 3, ABL 5, and Random) and DSC peak time (perfectly alternating and ABL 2) vs crystallization temperature.
- Figure 4.3: Spherulitic growth rate vs crystallization temperature for the different synthesized PEKK 50/50 samples, and also a perfectly alternating sample.
- Figure 4.4: Example of raw SAXS data after parasitic correction (plot A) and after Lorentz correction (plot B). Sample: PEKK 50/50 ABL 2 crystallized at different temperatures (arrow indicates increasing crystallization temperature).
- Figure 4.5: Plots summarizing the lamellar variables (plot A) and the Gibbs-Thomson-Tammann plot (plot B) for PEKK 50/50 ABL 2.  $L_b$ ,  $l_1$  and  $l_2$  in plot A refer to the long spacing, lamellar thickness and amorphous layer thickness.  $L_b$  is determined from the maxima in the Lorentz corrected desmeared plot and  $l_1$  is assumed to be 35 Å.
- Figure 4.6: Plots summarizing the lamellar variables (plot A) and the Gibbs-Thomson-Tammann plot (plot B) for PEKK 50/50 ABL 2.  $L_c^M$ ,  $l_1$  and  $l_2$  in plot A refer to the long spacing, lamellar thickness and amorphous layer thickness determined from a correlation function analysis.
- Figure 4.7: Plots summarizing the lamellar variables (plot A) and the Gibbs-Thomson-Tammann plot (plot B) for PEKK 50/50 ABL 3.  $L_c^M$ ,  $l_1$  and

$l_2$  in plot A refer to the long spacing, lamellar thickness and amorphous layer thickness determined from a correlation function analysis.

Figure 4.8: Plots summarizing the lamellar variables (plot A) and the Gibbs-Thomson-Tammann plot (plot B) for PEKK 50/50 ABL 5.  $L_c^M$ ,  $l_1$  and  $l_2$  in plot A refer to the long spacing, lamellar thickness and amorphous layer thickness determined from a correlation function analysis.

Figure 4.9: Plots summarizing the lamellar variables (plot A) and the Gibbs-Thomson-Tammann plot (plot B) for PEKK 50/50 Random.  $L_c^M$ ,  $l_1$  and  $l_2$  in plot A refer to the long spacing, lamellar thickness and amorphous layer thickness determined from a correlation function analysis.

Figure 4.10: The ratio between the end surface free energy and the heat of fusion for the different PEKK 50/50 samples. For ABL 1, lamellar thickness is estimated as  $L_b-35$  A.

Figure 4.11: The Hoffman-Weeks type extrapolation for the 5 different synthesized PEKK 50/50 samples.

Figure 4.12: The equilibrium melting temperature estimated by the Hoffman-Weeks and the Gibbs-Thomson-Tammann analysis for the different PEKK 50/50 samples.

Figure 4.13: The estimated crystallinity index vs crystallization temperature for the different PEKK 50/50 samples.

Figure 4.14: The estimated crystalline phase composition vs crystallization temperature for the different PEKK 50/50 samples.

Figure 4.15: The heat of fusion vs crystallization temperature for the different PEKK 50/50 samples. The two traces for each sample are for the low and high endotherm.

Figure 5.1: Defect exclusion vs melting temperature calculated using the Helfand-Lauritzen equilibrium theory. The values used were (see Equation 2.1 and 2.2)  $\epsilon$  : 0.7 kcal/mole;  $\Delta H_f$  : 7.7 kCal/mole; and  $T_m^{eq}$  : 350 °C.

Figure 5.2: Summary of crystallization kinetics and time scale for molecular motion vs crystallization temperature. These factors affect the kinetics of defect exclusion as discussed in the text.

Figure 5.3: Summary of the end surface free energy as determined by the GTT analysis (Chart A); the crystallization kinetics as determined by DSC studies (Chart B) and the branching ratio estimated from  $^1\text{H}$  NMR (Chart C).

## INTRODUCTION

Poly(aryl ether ketone ketone) PEKK is a high temperature, high performance thermoplastic being developed at duPont<sup>1-2</sup>. PEKK belongs to the same family of poly(aryl ether ketones) as poly(aryl ether ether ketone) PEEK, and has similar crystallization and melting behavior<sup>1-10</sup>. PEKK can be synthesized by the Friedel-Crafts acylation reaction of diphenyl ether (DPE) with either terephthaloyl chloride (TCl) or isophthaloyl chloride (ICl)<sup>11</sup>. As depicted in Figure 1.1, the two reactions result in the formation of -DT- and -DI- type monads, which are identical except for the presence of a 1,3 (meta) linked phenyl ring in the case of the -DI- monad. Because of this unique synthesis route, PEKK can be thought of as a copolymer of the monads -DT- and -DI-<sup>2</sup>. However, PEKK is a copolymer which demonstrates some unusual traits. First, the crystal structure does not change as the 2<sup>nd</sup> comonomer (which can be considered as a defect) is incorporated in the crystalline phase<sup>2</sup>. PEKK crystallizes in an orthorhombic unit cell, and the unit cell dimensions are only marginally affected by the presence of -DI- monads in the crystalline phase<sup>2</sup>. Second, the defects tend to be partially excluded from the crystalline phase. There are several copolymer systems in which the 2<sup>nd</sup> monad is either completely included or completely excluded from the crystalline phase. PEKK is a

unique copolymer in which the two comonomers are chemically identical except for the presence of a meta-linked phenyl ring in the -DI- monad. As a result of this similarity, the 2<sup>nd</sup> comonomer is neither completely excluded from, nor completely included in the crystalline phase. These unique characteristics provide an opportunity to gain an insight into the crystallization behavior of copolymers.

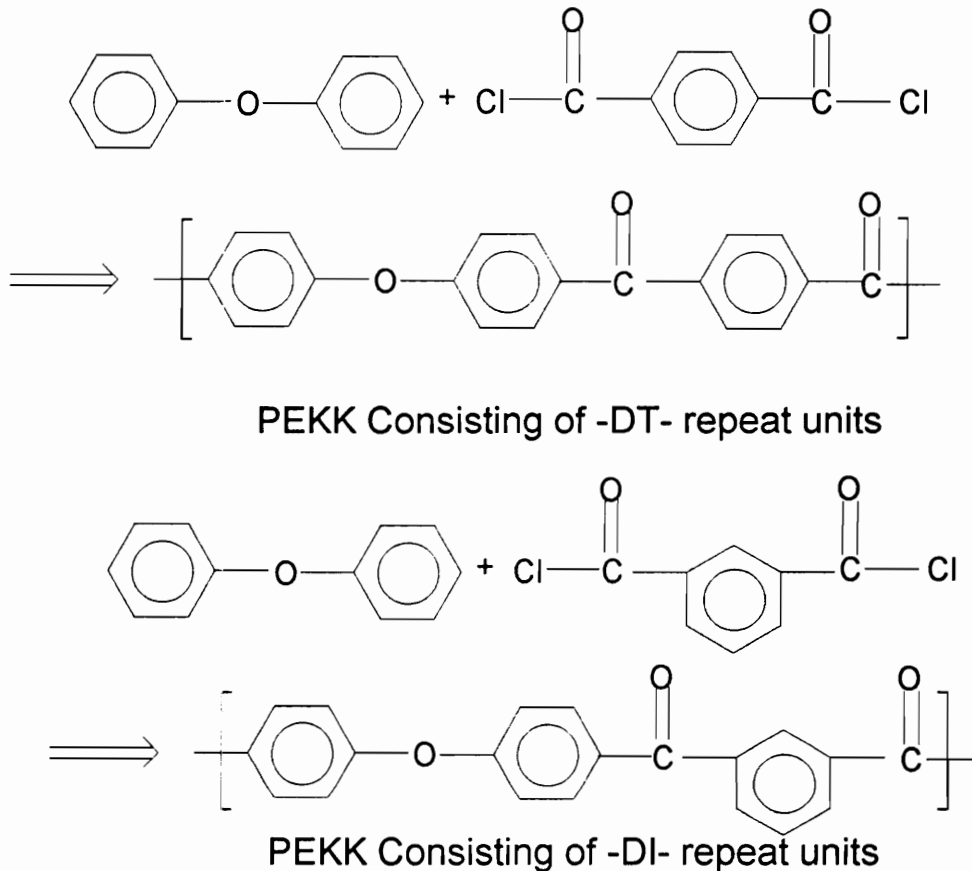


Figure 1.1: Simplified synthesis route for PEKK showing the -DT- and -DI- repeat units<sup>2</sup>.

From a practical viewpoint, PEKK is a high performance, high temperature semi-crystalline thermoplastic with numerous potential applications as a fiber and also as a matrix resin in composite parts<sup>1</sup>. The mechanical performance of such thermoplastics is largely governed by the amount and morphology of the crystalline phase. Therefore, it is

essential to have a complete understanding of the factors which affect the formation of the crystalline phase in such systems.

Gardner et al. have studied the crystallization behavior of PEKK as a function of the overall composition<sup>2</sup>. They have controlled the ratio of the -DT- and -DI- monads in the crystalline phase by controlling the ratio of terephthaloyl and isophthaloyl chloride (T/I Ratio) in the synthesis reaction. They have demonstrated that changing the overall T/I Ratio (PEKK T/I) substantially affects the thermal (crystallization, melting and glass transition) behavior of the copolymer. They have demonstrated that for T/I Ratios in the range of 65/35 (PEKK 65/35) to 80/20 (PEKK 80/20), substantial amounts of DI monads are excluded from the crystalline phase. Their synthesis route results in a perfectly alternating structure for the copolymer with the T/I Ratio of 50/50 (PEKK 50/50). Their use of a perfectly alternating PEKK 50/50 structures makes the exclusion of the DI monads from the crystalline phase impossible. Their work addresses the effect of changing overall composition on the crystallization process of the copolymer. However, the effect of changing chain architectures on the crystallization and melting behavior of the copolymer has not been addressed. This study therefore addresses the issue of changing chain architectures on the crystallization and melting process.

Towards this end, a series of non-alternating PEKK 50/50 samples has been synthesized. The blockiness of the final copolymer cannot be quantitatively characterized. However, the synthesis route was manipulated so as to result in copolymers with average expected block lengths (ABL) in the range of 1-5. Synthesis and characterization of these samples is described in Chapter 3. The crystallization and melting behavior of these samples have been studied. Results of these studies are described in Chapter 4. It has been demonstrated that upon changing the PEKK 50/50 structure from alternating to non-alternating,

1. The crystallization kinetics is substantially slowed while the melting temperature is raised substantially.
2. The T/I Ratio in the crystalline phase is found to be substantially higher than that of the overall melt.
3. The tendency for the exclusion of such DI units increases with increasing crystallization temperatures.

These results are analyzed in Chapter 5. Where possible, the results are explained in light of existing theories of copolymer crystallization, otherwise some speculative explanations for the observed behavior are provided. The entire work is summarized along with the conclusions in Chapter 6, and possible avenues for further research are summarized in Chapter 7.

## CHAPTER 2

### LITERATURE REVIEW

#### *2.1 Poly(ether ketones)*

Poly(ether ketones) are an important class of thermoplastic polymers with numerous industrial applications. This family of materials includes poly(aryl ether ether ketone) PEEK and poly(aryl ether ketone ketone) PEKK. Poly(aryl ether ketones)<sup>2-10</sup> demonstrate glass transition temperatures in the range of 110-170°C. They crystallize into a 2 chain orthorhombic unit cell and have equilibrium melting temperatures in the range of 290-400°C<sup>2-10</sup>. The structures of various poly(ether ketones) are given in Figure 2.1. The orthorhombic unit cell parameters as a function of ketone content for various poly(aryl ether ketones) has been summarized in Figure 2.2. The thermal (glass transition and equilibrium melting temperature) behavior of poly(aryl ether ketones) has been summarized in Figure 2.3. Among the family of poly(aryl ether ketones), poly(aryl ether ether ketone) PEEK is the most widely known. The thermal (glass transition, melting and crystallization) behavior of PEKK is similar to that of PEEK. However, there are important differences.



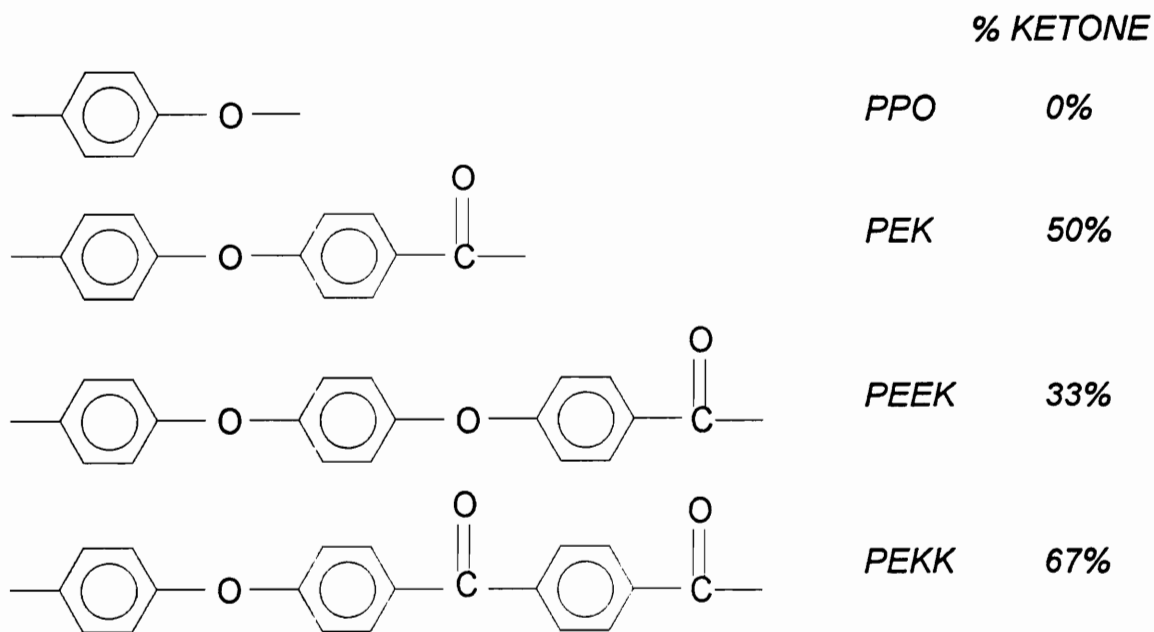


Figure 2.1: The chemical structure of different poly(aryl ether ketones).

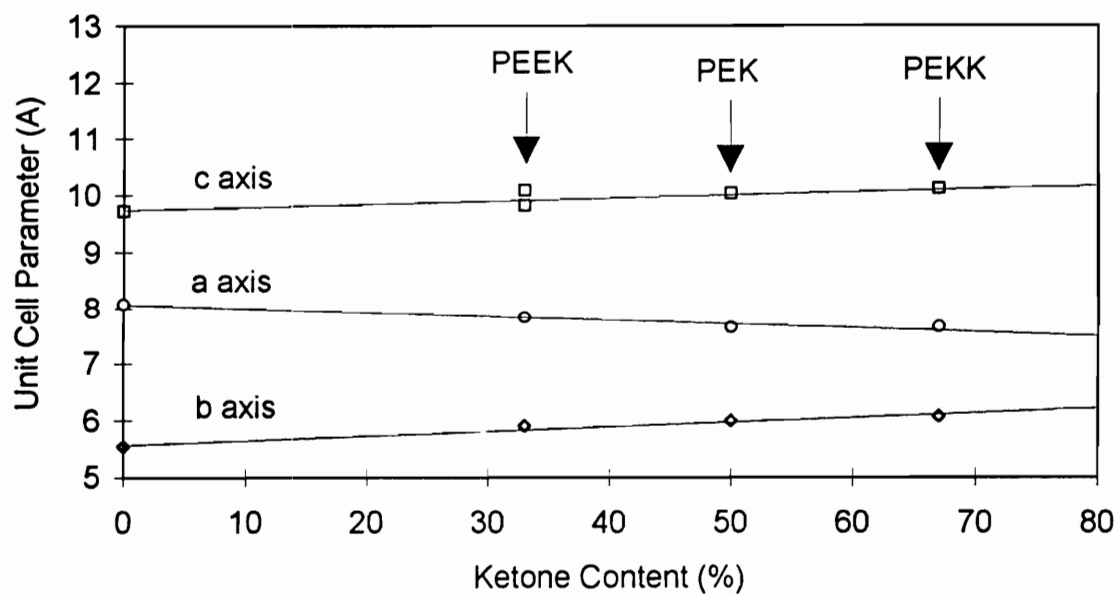


Figure 2.2: Orthorhombic unit cell parameters as a function of ketone content for different poly(aryl ether ketones)<sup>2</sup>.

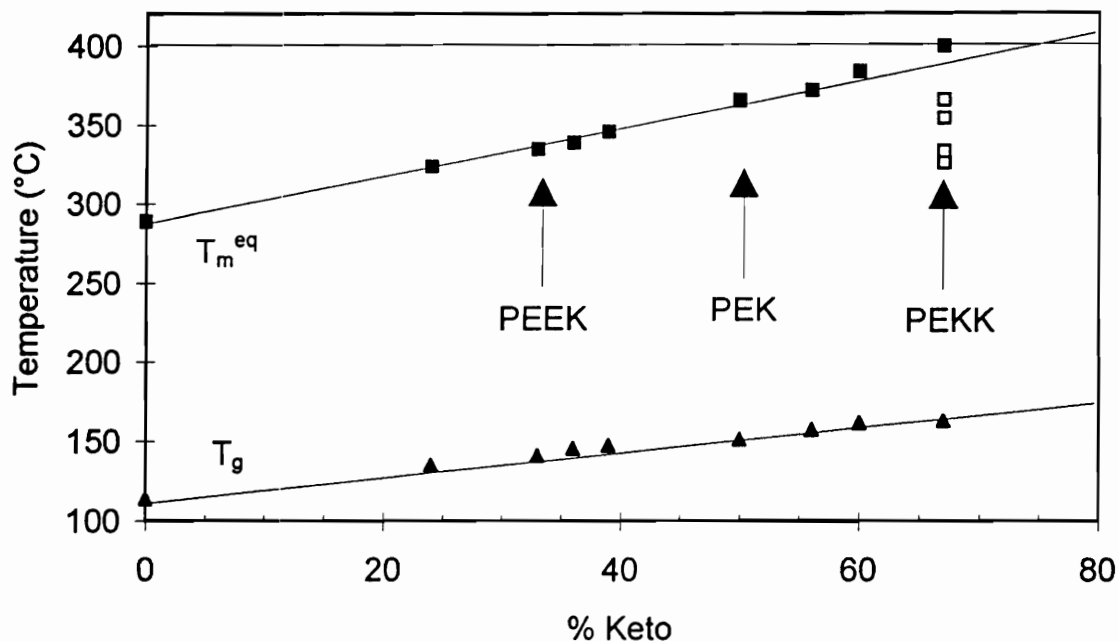


Figure 2.3: The glass transition ( $T_g$ ) and equilibrium melting ( $T_m^{eq}$ ) temperature as a function of ketone content for different poly(aryl ether ketones)<sup>2</sup>. The solid line at 400°C denotes the degradation temperature.

PEEK has two ether units for every keto unit. Unlike PEEK, PEKK has one ether bond for every two keto bonds. Since keto units have a relatively higher rotational conformation energy barrier, they are stiffer than ether units. As a result, PEKK, while very similar to PEEK, has a higher glass transition temperature ( $T_g$ ) and melting temperature ( $T_m$ ), and slower crystallization rates.

## 2.2 Poly(ether ketone ketone)

PEKK is typically prepared by a Friedel Crafts condensation reaction (discussed in more detail in Section 2.3) of diphenyl ether (DPE), terephthaloyl chloride (T) and isophthaloyl chloride (I) (see Figure 1.1)<sup>11</sup>. Because of this unique synthetic route, PEKK can be thought of as a copolymer of the 'monads' DPE-T (DT) and DPE-I (DI)<sup>2</sup>. The DI monad has a meta (1,3) linked phenyl ring, whereas the DT monad is all para (1,4) linked. The amount of such meta linkages can be controlled by changing the ratio of terephthaloyl chloride to isophthaloyl chloride (T/I ratio) used in the synthesis.

Gardner et al. have studied the effect of changing T/I Ratios on the crystallization and melting behavior of PEKK<sup>2</sup>. They have varied the T/I Ratio from 50/50 (PEKK 50/50) to 100/0 (PEKK 100/0). The PEKK samples used by Gardner et al. were synthesized using a special two-step process (discussed in Section 2.3). This reaction scheme results in the formation of a perfectly alternating PEKK 50/50 structure. They have studied the crystallization and melting behavior of these samples as a function of overall T/I Ratio. Their results are summarized below.

Melt crystallized PEKK gives a Wide Angle X-ray Diffraction (WAXD) pattern which can be indexed by a two chain orthorhombic unit cell ( $a = 0.769$  nm,  $b = 0.606$  nm and  $c = 1.016$  nm)<sup>2</sup>. PEKK can be crystallized from the melt, from solution and from the glassy state. Upon crystallization from solution (e.g. methylene chloride) and from the glassy state, PEKK exhibits a WAXD peak at ca.  $2\theta = 15.6^\circ$  in addition to those observed in melt crystallized samples. Gardner et al.<sup>2</sup> have ascribed this additional peak to the formation of a one-chain orthorhombic unit cell (which they have labeled Form 2 as opposed to Form 1 formed by melt crystallization) with  $a = 0.393$  nm,  $b = 0.575$  nm and  $c = 1.016$  nm. The proposed Form 1 & Form 2 structures are similar as depicted in Figure 2.4. Form 2 has an edge to face phenyl packing as opposed to the face to face phenyl packing in Form 1.

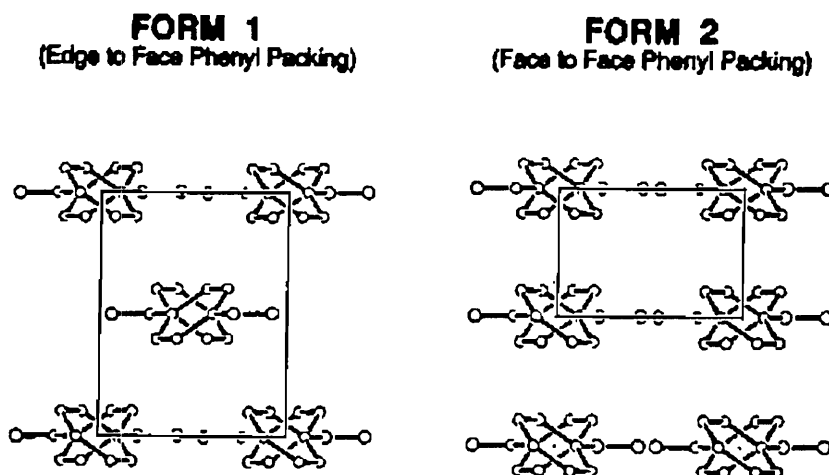


Figure 2.4: The proposed Form 1 and Form 2 structures for PEKK<sup>2</sup>.

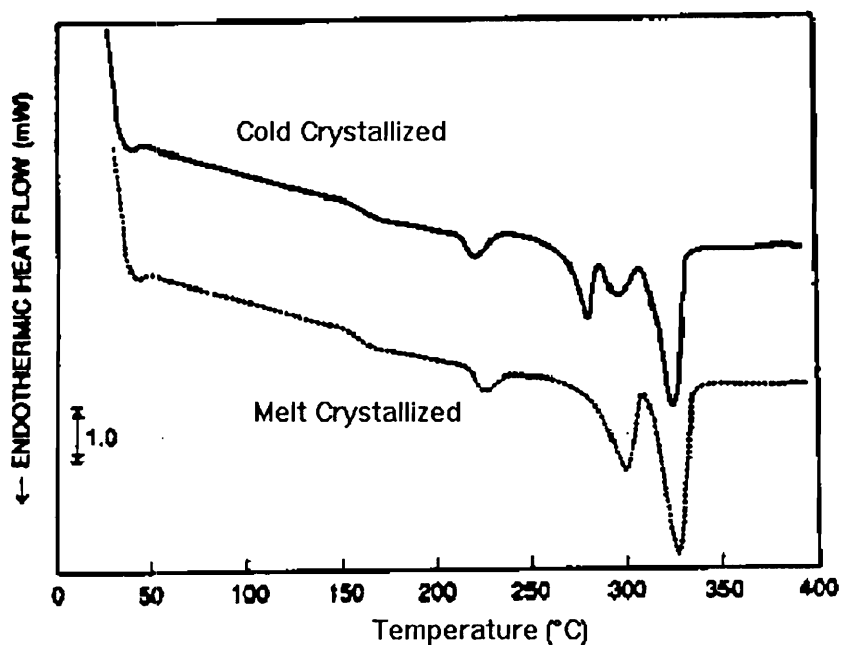


Figure 2.5: Typical DSC heating traces for cold crystallized and melt crystallized PEKK 50/50 copolymer<sup>2</sup>.

Figure 2.5 depicts typical DSC traces of cold crystallized and melt crystallized PEKK 50/50 samples<sup>2</sup>. Melt crystallized PEKK 50/50 samples demonstrate a triple endotherm melting behavior. The three endotherms have been explained by Gardner et al.

as follows. The low temperature endotherm at about  $T_c+10^\circ\text{C}$  (where  $T_c$  is the crystallization temperature) is similar in nature to the low endotherm observed in PEEK and other semi-crystalline polymers<sup>12</sup>. The origin of this low temperature endotherm in PEEK is the subject of immense recent controversy. Most authors ascribe the dual endotherm melting behavior in PEEK and other polymers either to a melting-recrystallization phenomena<sup>13,14</sup> or to the melting of a dual population of lamellar thickness<sup>12,15,16</sup>. However, recent work suggests that the origin of the low endotherm might lie in the enthalpic recovery of a rigid amorphous fraction<sup>17-18</sup>. The high temperature endotherm corresponds to melting of the crystalline lamellae. Gardner et al.<sup>2</sup> have used this endotherm to construct a Hoffman-Weeks  $T_m$ - $T_c$  plot and determined the equilibrium melting temperature ( $T_m^{\text{HW}}$ ). The third endotherm lies at temperatures higher than the second endotherm, and is heating rate dependent. Gardner et al.<sup>2</sup> have suggested that the origin of this endotherm might lie in a melting-recrystallization phenomena. Cold crystallized PEKK samples demonstrate 4 endotherms during a melting scan. The additional endotherm typically occurs at temperatures intermediate to the 1<sup>st</sup> and the 2<sup>nd</sup> endotherms in melt crystallized PEKK. Gardner et al.<sup>2</sup> have ascribed this additional endotherm to the melting of the Form 2 structure which forms upon cold crystallization.

Increasing the overall T/I Ratio does not change the unit cell parameters. This is manifest in constant peak positions in the WAXD patterns as depicted in Figure 2.6<sup>2</sup>. This unique feature is made possible by the unique arrangements of the DI and DT monads along the PEKK chain as depicted in Figure 2.7. However, the thermal behavior (crystallization, melting and glass transition) of the copolymer is dramatically altered by changes in the overall composition. The changes in the thermal behavior are summarized in Figures 2.8 & 2.9<sup>2</sup>. Figure 2.8 summarizes the glass transition and equilibrium melting ( $T_g$  and  $T_m^{\text{eq}}$ ) temperatures for the different PEKK samples with varying overall compositions. Figure 2.9 summarizes the crystallization kinetics of the different PEKK 50/50 samples.

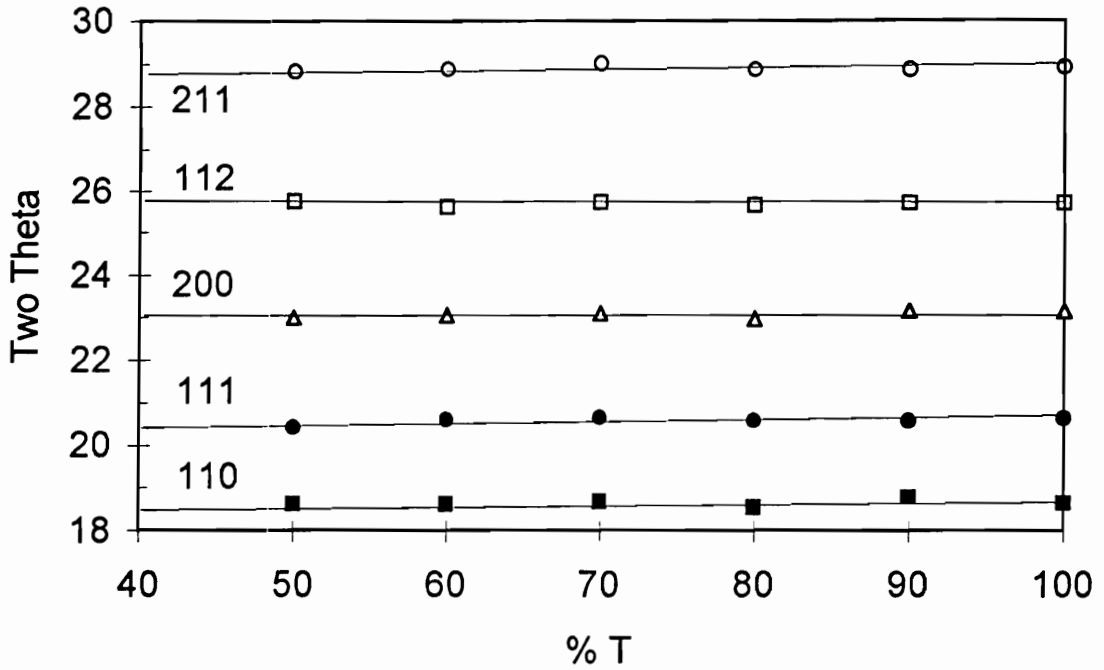


Figure 2.6: WAXD peak position vs the overall composition for poly(aryl ether ketone ketone) PEKK<sup>2</sup>.

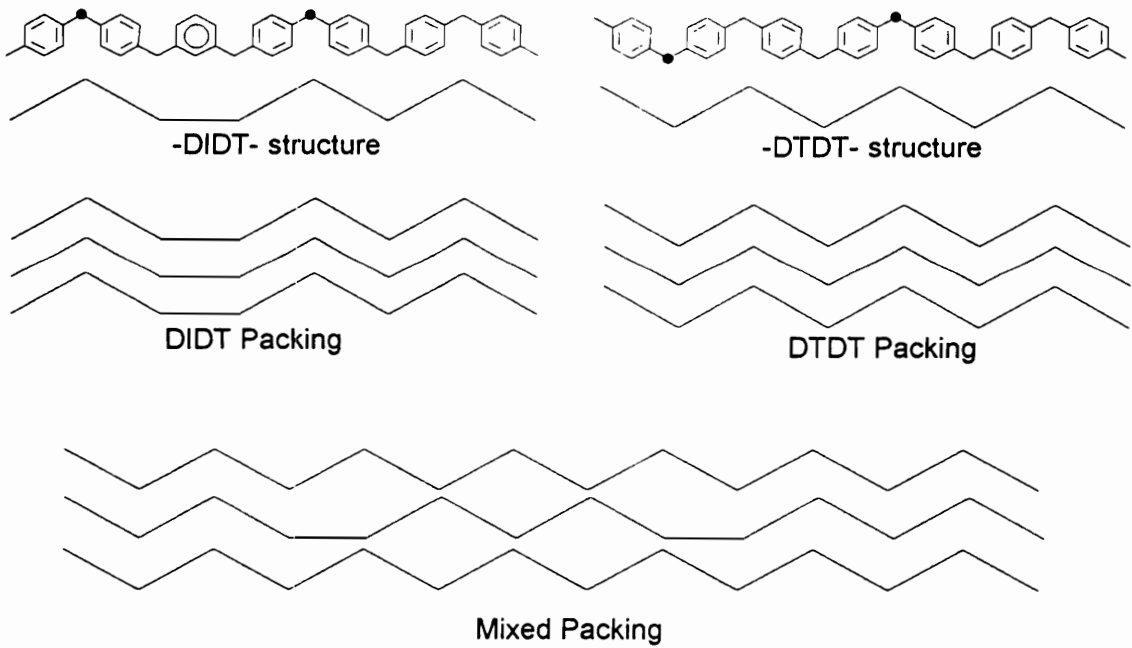


Figure 2.7: Unique arrangement of -DT- and -DI- monads within the lamellae that results in partial exclusion of one of the two monads.

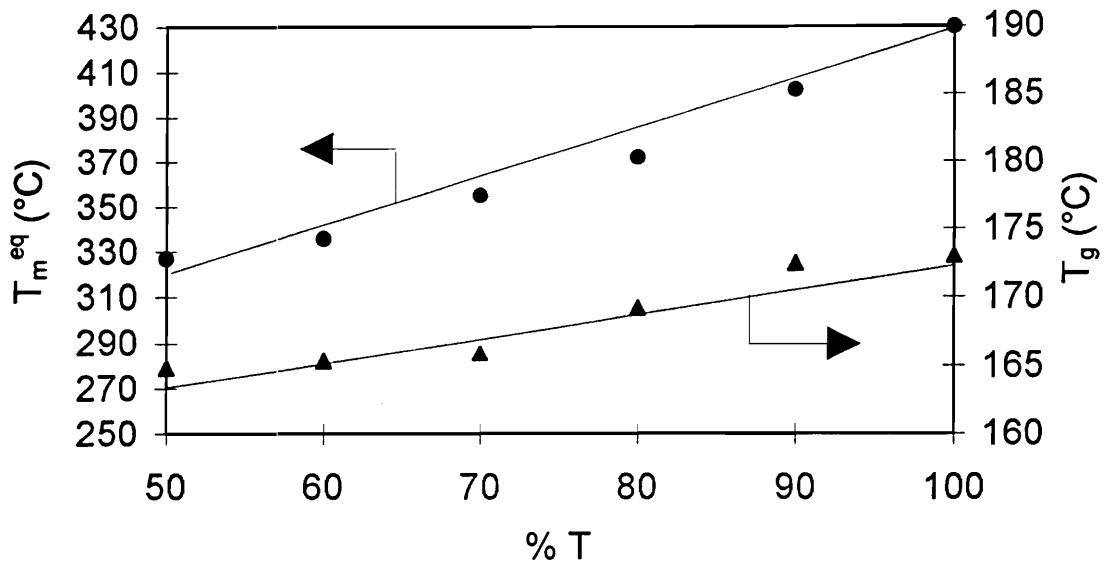


Figure 2.8: The equilibrium melting ( $T_m^0$ ) and the glass transition temperature ( $T_g$ ) vs the overall composition for poly(aryl ether ketone ketone) PEKK<sup>2</sup>.

Increasing the T/I Ratio increases both  $T_m^{eq}$  and  $T_g$ . Also, since  $T_m^{eq}$  rises faster than  $T_g$ , the crystallization process is generally speeded up. The only exception to this general rule is PEKK 50/50 which crystallizes faster than PEKK 60/40. This anomaly has been ascribed by Gardner et al. to the fact that their PEKK 50/50 sample is a perfectly alternating copolymer, which therefore crystallizes faster than PEKK 60/40, which is a 'random' copolymer.

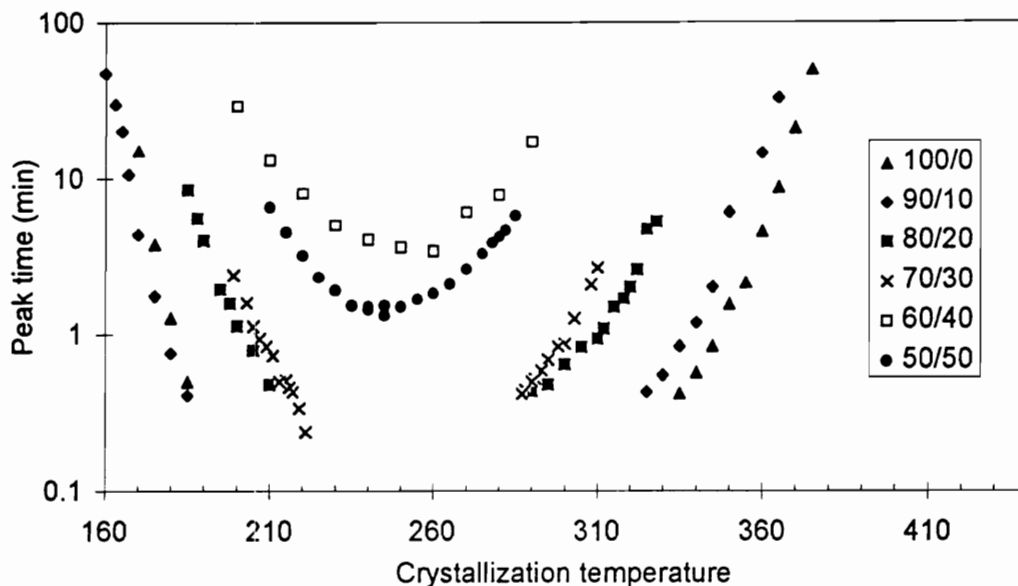


Figure 2.9: The crystallization kinetics as measured by DSC peak time for crystallization vs. the overall composition for poly(aryl ether ketone) PEKK<sup>2</sup>.

As already mentioned, the isophthalic monads (DI) tend to get excluded from the crystalline phase. This has been determined by Gardner et al. using WAXD. A typical WAXD pattern of a melt crystallized PEKK sample is depicted in Figure 2.10. The WAXD patterns can be fitted with Gaussian shaped peaks, which are also depicted in Figure 2.10. As in other polymers, this peakfitting technique can be used to index the crystallinity ( $X_C$ ), but for PEKK, it can also be used to estimate the composition of the crystalline phase. This technique has been illustrated by Gardner et al.<sup>2</sup> They have plotted the ratio of the areas of the peaks corresponding to the 111 and the 110 crystallographic planes (111/110 Intensity Ratio) against the overall T/I Ratio. Such a plot is depicted in Figure 2.11<sup>2</sup> Gardner et al. propose that this ratio is reflective of the T/I Ratio in the crystalline phase. Following their arguments, the solid line depicted in Figure 2.11 reflects the theoretical ratio if the crystalline phase were to have the same T/I Ratio as the overall melt. They base their conclusion on the following facts. First, for PEKK 100/0, the crystalline phase is 100 % T. Second, for PEKK 0/100, the crystalline phase is 100 % I.



Finally, for perfectly alternating PEKK 50/50 sample, the crystalline phase is 50% T. Figure 2.11 suggests that in the overall composition range of PEKK 0/100 to PEKK 35/65, the crystalline phase consists of the diads II; in the composition range PEKK 35/65 to PEKK 65/35, the crystalline phase consists largely of diads of the type TI and finally in the overall composition range of PEKK 65/35 to PEKK 100/0, the crystalline phase consists largely of the diads TT.

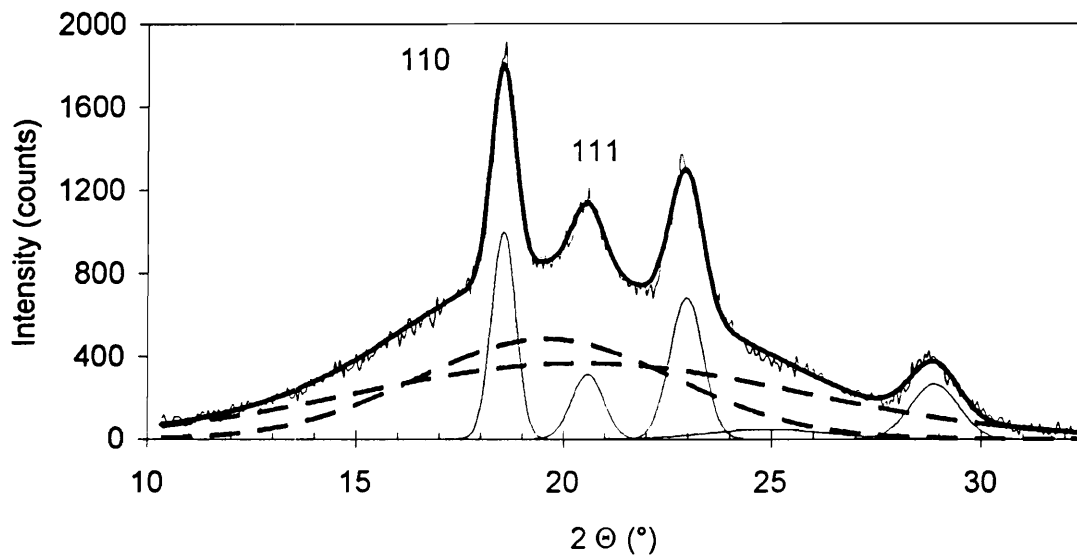


Figure 2.10: WAXD data analysis technique used by Gardner et al.<sup>2</sup> for estimating the crystallinity and the composition of the crystalline phase. The dashed lines denote the amorphous halo. The solid lines denote the peaks corresponding to different crystallographic planes and the dark line denote the sum of all the fitted curves.

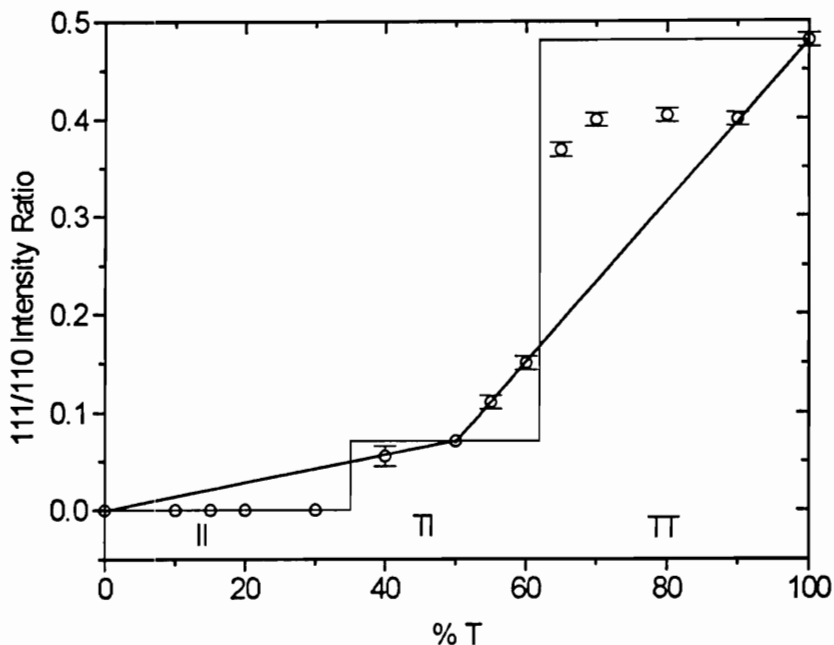


Figure 2.11: The composition of the crystalline phase as estimated by Gardner et al. using the technique illustrated in Figure 2.10.

Their work suggests that the crystallizing copolymer tends to exclude the 2<sup>nd</sup> monad (e.g. -DI- in the composition range of PEKK 65/35 to PEKK 100/0). However, their unique synthesis route results in the formation of perfectly alternating PEKK 50/50. They have not investigated PEKK 50/50 samples with non alternating structures. However, their work does suggest that the architecture of the crystallizing chain affects the crystallization kinetics (for example, perfectly alternating PEKK 50/50 crystallizes faster than “random” PEKK 60/40 in spite of a lower equilibrium melting temperature). Therefore in this study, several PEKK 50/50 samples with non alternating structures have been synthesized. The crystallization and melting behavior of these samples has been characterized and is compared to the reported crystallization and melting behavior of perfectly alternating PEKK 50/50 samples.

## 2.3 Synthesis of Poly(ether ketone ketone)

In this section, the several reactions used to produce different poly(aryl ether ketones) are discussed from an historical perspective. Next, the nucleophilic and the electrophilic routes for the synthesis of most poly(ether ketones) is discussed. Finally, the Friedel Crafts Acylation Synthesis reaction for PEKK is described.

### Historical Perspective:

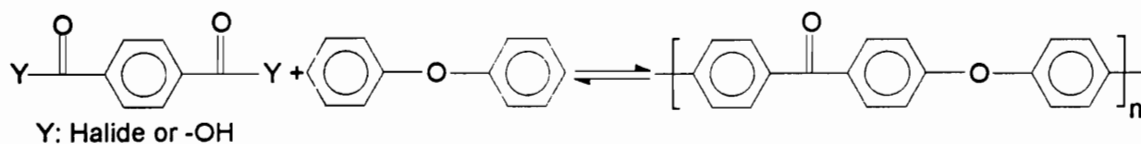
Poly(aryl ether ketones) were first prepared by Bonner in 1962.<sup>19</sup> He synthesized a low molecular weight (MW) PEKK by the Friedel Crafts polycondensation of diphenyl ether (DPE) and isophthaloyl chloride, using nitrobenzene as a solvent and aluminum chloride as a catalysts. In 1964, Goodman et al.<sup>20</sup> prepared a series of poly(aryl ether ketones) using similar reactions on analogous reactants. They were also the first to prepare a poly(aryl ether ketone) without any meta linkages. Iwakura et al.<sup>21</sup> prepared polymers with the same structure in 1968. They noted that the polymer was insoluble in all common inorganic solvents. This becomes a problem when the growing polymer chain drops out of solution before high MW can be achieved. Iwakura had used poly(phosphoric acid) as the solvent. Marks<sup>22</sup> devised a better solvent for these reactions in 1969. He used liquid hydrogen fluoride as the solvent and he found that the  $\text{BF}_3\text{HF}$  complex was an excellent catalyst for the polycondensation reaction. Marks obtained poly(aryl ether ketones) with reasonably high molecular weights using his catalyst. He proposed that the  $\text{BF}_3\text{HF}$  complex was a good solvent because of the protonation of the carbonyl group. In 1976, Dahl et al.<sup>23</sup> improved this solvent system. In 1977, Niume et al.<sup>24</sup> prepared poly(ether ketones) by the acid promoted electrophilic reaction of diphenyl ether and isophthaloyl chloride. They used polyphenyl alcohol as the solvent along with  $\text{AlCl}_3$  catalyst. However, the polymer obtained did not have very high molecular weights because of premature precipitation. In 1988, Colquhoun et al.<sup>25</sup> prepared poly(ether ketones) using a similar method. However, they used trifluoromethane sulphonic acid as the solvent. This solvent is relatively involatile (b.p.  $162^\circ\text{C}$ ) and thus can be used without

worrying about solvent degradation etc. Ueda et al.<sup>26</sup> used phosphorus pentoxide/methane sulphonic acid (PPMA) as their solvent in 1989. This solvent also gave relatively high molecular weights.

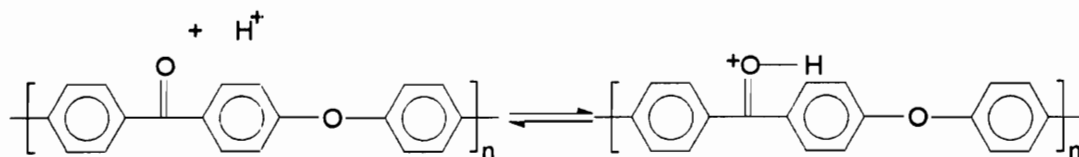
An alternative route to the synthesis of poly(aryl ether ketones) was suggested by Clendinning et al. in 1967.<sup>27</sup> They suggested a synthesis route using nucleophilic aromatic substitution. The solvent problem in such reactions was found to be more acute because protic solvents cannot be used. Hence the solvent is maintained at higher temperatures in order to prevent premature crystallization. Clendinning et al. used sulpholane or dimethyl sulphoxide as their solvents and they recognized the fact that they could not obtain high molecular weights because of premature crystallization of the polymer. Use of higher temperatures leads to undesirable reactions like solvent degradation etc. In 1980, Attwood et al.<sup>28</sup> used certain diaryl sulphones as their solvents at temperatures close to the polymer melting temperature and they obtained copolymers of poly(aryl ether ketones) and poly(aryl ether sulphones) of high molecular weights. The copolymer has a higher solubility and does not precipitate out prematurely. However, they could not obtain high molecular weights for copolymers containing less than 20% by weight poly(aryl ether sulphones). Mohanty et al.<sup>29</sup> approached the problem of premature crystallization by incorporating bulky alkyl substituents (e.g. t-butyl) on the phenyl rings and cleaving them with strong acids after polymerization. Lyon et al.<sup>30</sup> used a similar technique but they made ketimine derivatives of the poly(ether ketones) instead of incorporating substituents on the alkyl rings.

### **Acid Promoted Electrophilic Reactions:**

All the early synthesis of poly(aryl ether ketones) involved the use of acid promoted electrophilic reactions<sup>19-26</sup>. A typical acid promoted electrophilic reaction is given in Scheme 2.1a. The polymer solution is stable even at low temperatures due to the protonation of the carbonyl group shown in Scheme 2.1b.



Scheme 2.1a: Acid Promoted Electrophilic Reaction



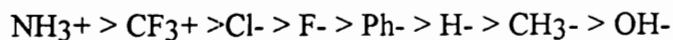
Scheme 2.1b: Protonation of the Carbonyl Group

One of the earliest solvents used was dichloromethane. As a result of premature crystallization, very low molecular weight polymers were obtained. To this date, premature crystallization of the polymer from the solvent is a problem (for both electrophilic and nucleophilic routes). The first solvent to give reasonably high molecular weights was anhydrous hydrogen fluoride. This solvent prevents premature crystallization by protonation of the carbonyl group. However, anhydrous hydrogen fluoride is very corrosive, volatile and toxic. Hence, aluminum chloride in polyphosphoric acid was tried as a solvent. This solvent gave polymers of moderate molecular weights. Phosphorous pentoxide in methane sulphonic acid was also tried as a solvent and this also gave polymers of moderate molecular weights.

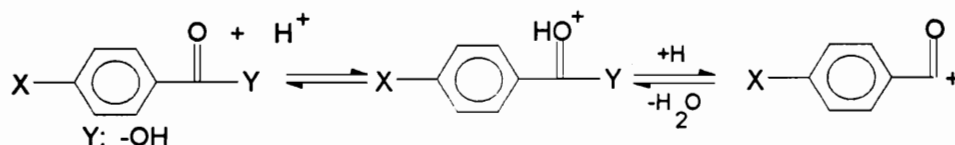
One of the best solvents available to date is trifluoromethane sulphonic acid  $\text{CF}_3\text{SO}_3\text{H}$ .  $\text{CF}_3\text{SO}_3\text{H}$  promotes the condensation reaction of carboxylic acids with activated aromatics to give para substituted ketones. Hence this solvent leads to high molecular weights even at room temperatures.  $\text{CF}_3\text{SO}_3\text{H}$  is also relatively involatile (b.p.  $162^\circ\text{C}$ ) hence solvent degradation is not a problem.

It has been experimentally determined that when electron withdrawing ring substituents ( $-\text{NO}_2$ ,  $-\text{NH}_3^+$  etc) are introduced into a carboxylic acid then the reactivity

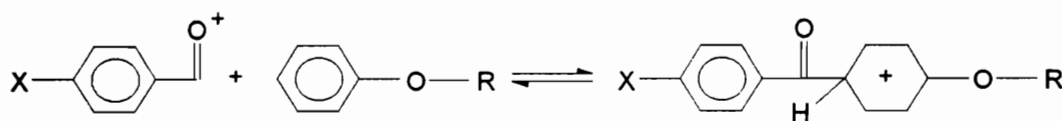
of the carboxylic acid decreases substantially. The half life increases in the order given below:



Therefore terephthalic acid should have a slow rate when reacted under these conditions. This apparent anomaly can be explained by the formation of a positively charged reaction intermediate (e.g.  $[\text{ArCO}]^+$  or  $[\text{ArCO}(\text{H})\text{OSO}_2\text{CF}_3]^+$ ). This step is hindered by the addition of electron withdrawing groups. Scheme 2.2a denotes the rate controlling step in the presence of electron withdrawing groups, while Scheme 2.2b denotes the rate controlling steps in the presence of electron donating groups.

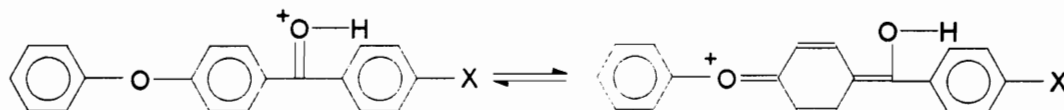


**Scheme 2.2a: Rate Controlling Step in the Presence of Electron Withdrawing Groups**



**Scheme 2.2b: Rate Controlling Step in the Presence of Electron Donating Groups**

A major stumbling block in the synthesis of poly(aryl ether ketones) is the so called "through bridge" effect<sup>25</sup>. Scheme 2.3 outlines this effect. Acylation of one ring of diphenyl ether deactivates the other ring by a factor of >500. This is because the mesomeric electron withdrawing power of a protonated para carbonyl group is transmitted to the bridging ether oxygen atom.



**Scheme 2.3: The Through bridge effect in Diphenyl Ether**

The through bridge effect is a problem only when using ethers like diphenyl ether. Ethers like 4,4'-diphenoxybenzophenone and 4,4' diphenoxy diphenyl sulphone are expected to behave similarly whereas, the through bridge effect is not a problem in ethers like 1,4 diphenoxybenzene and 4,4' diphenoxy diphenyl benzene because the phenoxy link is not susceptible to the through bridge effect and moreover, the ends are far apart.

There are a number of single monomer (A-B type) systems which can be polymerized to give a poly(ether ketone). These monomers are given below in Figures 2.2a through 2.2c.

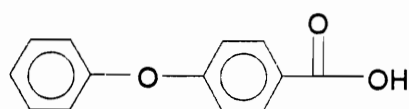


Figure 2.12a: 4-phenoxybenzoic acid

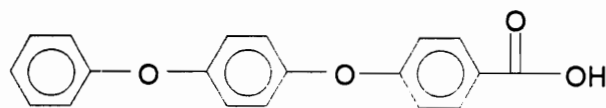


Figure 2.12b: 4-(4'-phenoxy phenoxy) benzoic acid

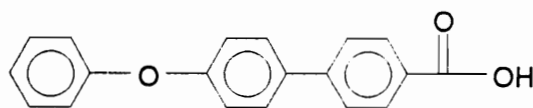
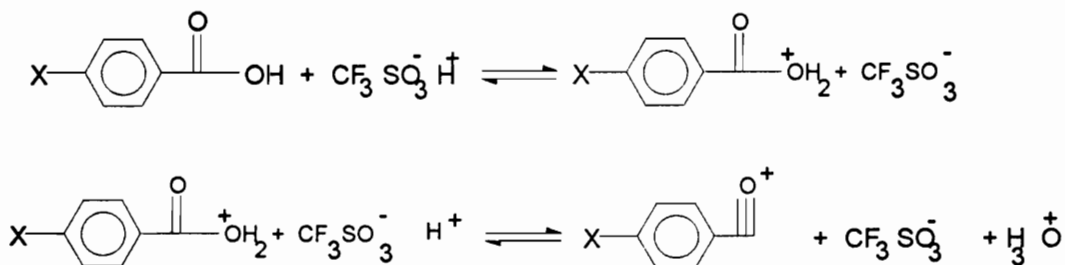


Figure 2.12b: 4-(4'-phenoxy phenyl) benzoic acid

These monomers self condense to give poly(ether ketones). However, the through bridge effect is a problem in the case of the 4-phenoxybenzoic acid monomer and it does not give high molecular weights.

The trifluoromethane sulphonic acid<sup>25</sup> (CF<sub>3</sub>SO<sub>3</sub>H) solvent takes part in the reaction according to the outline given in Scheme 2.4.



Scheme 2.4: Solvent Reaction in poly(aryl ether ketone) synthesis

From the solvent reaction given in Scheme 2.4, it can be seen that two moles of solvent are required for every mole of poly(ether ketone) synthesized. In actual practice, the solvent volume fraction is kept at around 10 times that of the monomer volume fraction. The half time of the reaction increases exponentially as the solvent to monomer ratio is decreases below 10.

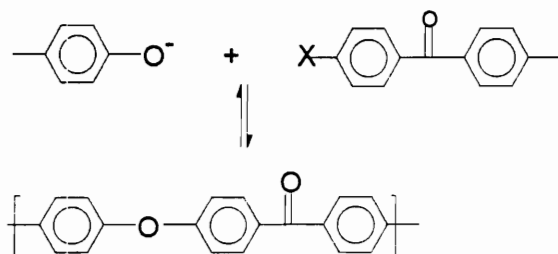
Another solvent recently reported in the literature is phosphorous pentoxide/methane sulphonic acid (PPMA). The PP:MA ratio is maintained at 1:10. The monomers which have been polymerized in this type of solvent include 4-(4'-phenoxy phenoxy)benzoic acid and 3-(4'-phenoxy phenoxy)benzoic acid.

Note that the through bridge effect cannot take place in the 3-(4'-phenoxy) benzoic acid. This polymer also has a higher solubility. Hence the molecular weights obtained with this compound are higher than for the 4-(4'-phenoxy phenoxy)benzoic acid. Also, when the electron donating groups are on the ortho or the para positions, the decarboxylation takes place more easily when compared to decarboxylation where electron donating groups are on the meta positions. Hence not only does the all para linked poly(ether ketone) have lower molecular weights, it also has slower rates of reaction.

### **Nucleophilic Aromatic Substitution:**

A typical nucleophilic substitution reaction<sup>27-30</sup> is given in Scheme 2.5.

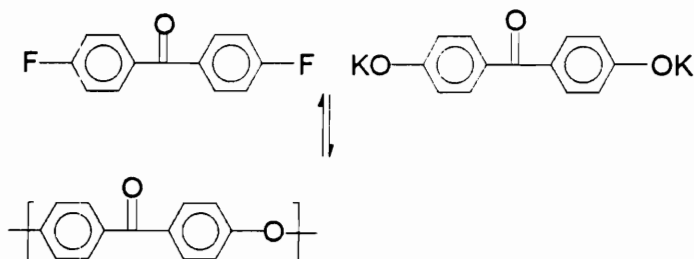




Scheme 2.5: Base Promoted Nucleophilic Reaction

Protic solvents cannot be used in this route. Hence higher temperatures are required in order to prevent premature crystallization. This results in undesirable side reactions like solvent degradation etc. Most solvents are unstable at high temperatures and the polymer crystallizes out prematurely at lower temperatures.

Clendinning et al.<sup>27</sup> used sulfolanes or diphenyl sulphoxide as their solvent. They did not obtain high molecular weight polymers. Their reaction is outlined in Scheme 2.6.



Scheme 2.6: Clendinning's Reaction

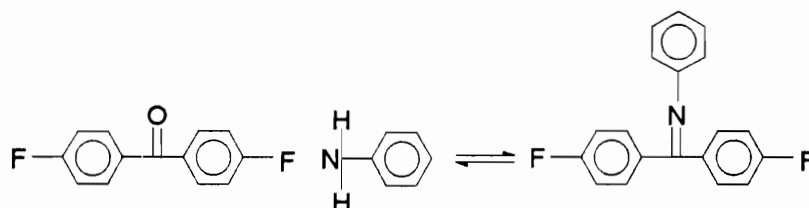
Clendinning synthesized the polymer from a fluorophenoxide as well as from the difluoride and bisphenoxide shown above. He found that there are considerable side reaction taking place in the fluorophenoxide system.

An improved solvent was suggested by Attwood et al.<sup>28</sup> in 1980. They used diaryl sulphones as their solvents at temperatures close to the melting point of the polymer. Diaryl sulphones are good solvents at high temperatures (close to the melting point of the

polymer). They have high thermal stability and do not react with the polycondensation reactants at to any significant degrees even at high temperatures.

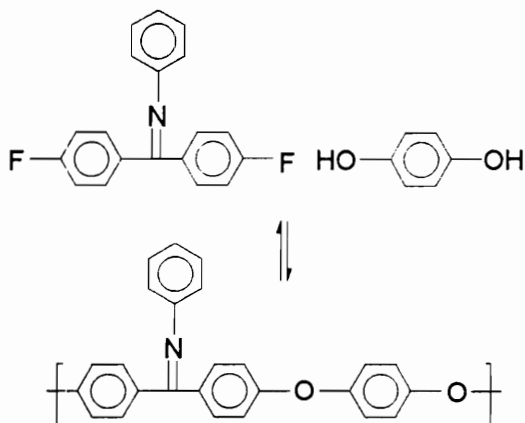
It is obvious that the product of Attwood's polycondensation is a copolymer. Characterization techniques reveal that it is a statistical or random copolymer. The copolymer has a lower melting point and crystallizes less readily. The only problem with this method is that it results in copolymers only. The molecular weights decreases significantly as the poly(ether sulphone) content is decreased below 20%.

Another approach to solve the problem of premature crystallization was suggested by Mohanty et al.<sup>29</sup> and later by Lyon et al.<sup>30</sup> Mohanty et al. incorporated bulky alkyl substituents (e.g. t-butyl) and cleaved it after polymerization using strong acids. Lyon et al. prepared ketimine derivatives of the activated halide as an intermediate. The ketimine was then polymerized. The poly ketimine has a higher solubility thus the reaction can be carried out at relatively moderate conditions (e.g. 150°C). The preparation of a ketimine derivative is outlined in Scheme 2.7.



Scheme 2.7: Synthesis of bis(4-fluorophenyl) ketimine

The nucleophilic aromatic substitution step polymerization reaction is given in Scheme 2.8.



Scheme 2.8: Polymerization of the ketimine derivative

The only disadvantage of this route is that it requires that two ether groups be next to each other. This means that poly(ether ketones) which have only one ether link separated by two ketone links cannot be prepared by this reaction.

### Synthesis of PEKK:

High molecular weight PEKK cannot be synthesized by any of the standard methods reported above. Most attempts to synthesize high molecular weight PEKK have met with little or no success. However, PEKK can be prepared by a Friedel Crafts Acylation reaction of diphenyl ether with terephthaloyl chloride or isophthaloyl chloride. Gay and Brunette<sup>11</sup> have reported the synthesis of a series of high molecular weight PEKK copolymers from the Friedel Crafts Acylation reaction of diphenyl ether (DPE) with terephthaloyl chloride (TCl) and isophthaloyl chloride (ICl). They have used ortho-dichlorobenzene as the solvent and large excesses of  $\text{AlCl}_3$  as the catalyst (>3 part catalyst for every repeat unit in the molecule).

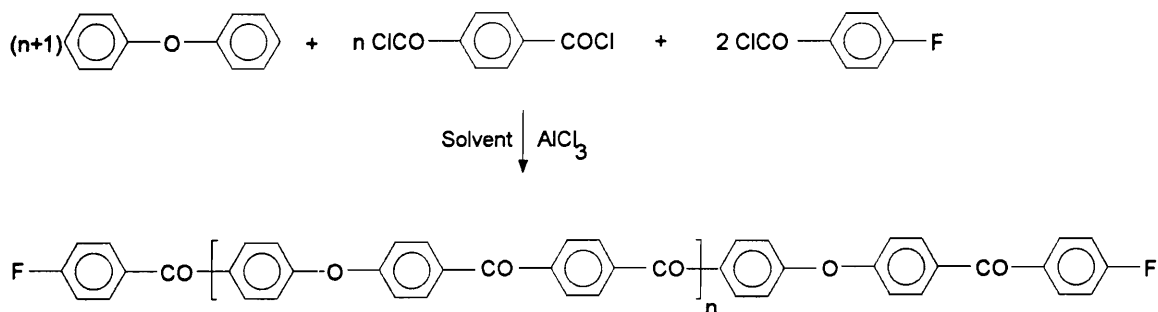
Their method is cumbersome, demanding and cannot be easily manipulated. However, they have success in synthesizing PEKK of high molecular weights. Since this

study uses their procedures (or slight modifications of it) to synthesize novel PEKK 50/50 copolymers, one of their procedures (Example 1 in Reference # 11) is reproduced below:

*A two liter resin kettle with a shell for heating and cooling was equipped with a high speed Teflon ® fluorocarbon resin clad tantalum stirrer, a dry nitrogen inlet, a gas outlet to a scrubber and a port for introducing reagents. 0.075 mole (15.23 g) distilled terephthaloyl chloride and 0.15 mole (25.53 g) diphenyl ether was dissolved in 150 g o-dichlorobenzene and added to the reactor. The solution was cooled to -10° to -15°C with solid carbon dioxide/methanol. 0.30 mole (40.00 g) anhydrous aluminum chloride was added portion wise over 30 minutes with temperature maintained at -10°C. The reaction was warmed to +10°C for 10 min and then cooled to -10°C. Then 0.075 mole (15.23 g) distilled isophthaloyl chloride was added followed by 0.15 mole (20.00 g) anhydrous aluminum chloride with reaction temperature maintained at -10°C. When addition was complete, coolant was drained from the shell, and the stirrer was turned to high speed. 500 g o-dichlorobenzene preheated to 160°C was added and steam was introduced into the shell. Particle formation was observed in the dark red-brown system in about a minute. The system was held at 100°C for 30 minutes and then allowed to cool to 30°C over a period of 60 minutes. The reaction was then quenched by adding 1 liter of methanol chilled to -40°C. Stirring was continued until all color was gone, about an hour. The polymer was filtered and rewashed with twice with one liter of methanol. The polymer was transferred to a beaker and boiled in one liter of water until the liquid temperature was 98°C. After filtration, the polymer was soaked in 500 g glacial formic acid for 30 minutes, filtered and dried overnight in a vacuum oven at 170°C with a light nitrogen purge.*

Sakaguchi et al.<sup>31</sup> have synthesized PEKK 0/100 using DPE and ICl along with AlCl<sub>3</sub> catalyst. While they have used a similar Friedel Crafts Acylation reaction, their solvent (1,2 dichloroethane) differs from that of Gay and Brunette (o-dichlorobenzene). They have also studied the effects of various reaction conditions (amount of catalyst etc.)

on the synthesis reaction. Clendinning et al.<sup>32,33</sup> have synthesized a series of PEKK oligomers of controlled molecular weights using the reactions schemes given below.



Scheme 2.9: Poly(ether ketone ketone) synthesis by Clendinning et al.<sup>32,33</sup>

They use aliphatic chlorinated solvents (methylene chloride and 1,2-dichloroethane) which led to partially alkylated products. They have also investigated a number of other solvent including carbon disulphide (which gave heterogeneous reaction mixtures). 1,2-dichlorobenzene (the solvent used in this study) and trichlorobenzene resulted in very complex reaction mixtures in which the reaction flask, and the stirrer were coated with polymer and the remaining bath formed lumps of polymer. Use of nitrobenzene as a solvent resulted in very slow reaction rates. 'Undesirable byproducts' formed with 1,1,2-trichloroethane and trichloroethylene. Sulfolane led to incomplete reactions. Freon (with nitrobenzene or diethyl ether as cosolvents) led to heterogeneous reaction mixtures and little conversion. They therefore concluded that dichloroethane was the most attractive solvent and devoted considerable efforts towards reducing the formation of alkylated byproducts. They have also used these oligomers to synthesize a series of novel PEKK polymers and also blends of PEEK and PEKK.

## 2.4 Crystallization of Copolymers

The crystallization theory of copolymers is not well developed. However, a number of authors<sup>35-48</sup> have tried to formulate theories to describe the crystallization behavior of copolymers. For example, Flory<sup>35</sup> modeled the crystallization behavior of copolymers consisting of crystallizable and non-crystallization comonomers. He derived '*necessary and sufficient*' conditions for the crystallization of such copolymers. He then used these conditions to predict that the degree of crystallinity would be a function of crystallization temperature. Following his arguments, at temperatures slightly below the equilibrium melting temperature, the requirement of large lamellae for crystallization and the ensuing requirement of very long blocks free of non-crystallizing monads would drastically reduce the degree of crystallinity. As the crystallization temperature is reduced, this requirement of large lamellae, and the ensuing requirement of long blocks free of non-crystallizable monad is relaxed. Therefore, the degree of crystallinity rises as the crystallization temperature is decreased.

The composition and morphology of the crystalline phase will depend on the factors which affect the crystallization kinetics of different crystallizable entities. Helfand and Lauritzen<sup>38</sup> developed an equilibrium theory for copolymer crystallization. They contend that if crystal growth is slow enough, equilibrium concentrations of copolymer units will be achieved. While equilibrium conditions are never achieved, it is always helpful to start with equilibrium thermodynamics. For a crystallizing copolymer of comonomers A and B, they setup the problem with two free energy terms  $-\Delta F_0$  and  $\epsilon$ .  $-\Delta F_0$  is the free energy change upon incorporating a comonomer A into the crystalline phase and  $-\Delta F_0 + \epsilon$  is the free energy change upon incorporating a comonomer B in the crystalline phase. Using simple statistical mechanics arguments, they arrive at an expression relating the composition of the crystalline phase with the crystallization temperature. This relation is summarized below in Equation 2.1

$$c^{eq} = \frac{x \cdot e^{-\beta\epsilon}}{(1-x) + x \cdot e^{-\beta\epsilon}} \quad \text{Equation 2.1}$$

where  $c^{eq}$  is the composition (%B units) of the crystalline phase;  $\beta$  is  $1/kT$ ; and  $x$  is the overall composition of the copolymer.

The above expression predicts the composition of the crystalline phase when crystallized at different temperatures. They then continue the statistical mechanics arguments and arrive at melting temperatures for the different copolymers. This relation for the melting point depression is summarized below in Equation 2.2.

$$\Delta H_f \left( \frac{1}{T_m} - \frac{1}{T_m^0} \right) = -k \ln \left[ 1 - x + x \cdot \exp \left( -\frac{\epsilon}{kT_m} \right) \right] \quad \text{Equation 2.2}$$

Sanchez and Eby<sup>39,40</sup> further developed the equilibrium thermodynamics arguments of Helfand and Lauritzen<sup>38</sup>. They developed equations relating the equilibrium melting temperature of a copolymer of a given composition with the defect exclusion energy etc. Their equations are similar to Equation 2.2 and is depicted in Equation 2.3.

$$\frac{1}{T_m} = \frac{\frac{1}{T_m^0} + \frac{R}{\Delta H^0} \left\{ (1 - c^{eq}) \cdot \ln \left( \frac{1 - c^{eq}}{1 - x} \right) + c^{eq} \cdot \ln \left( \frac{c^{eq}}{x} \right) \right\}}{1 - \frac{\epsilon X_c}{\Delta H}} \quad \text{Equation 2.3}$$

In the above equations, superscript 0 refers to the homopolymer. Note that Equation 2.3 predicts that the equilibrium melting temperature of a partially excluding copolymer will always be lower than that of the corresponding homopolymer.

Sanchez and Eby<sup>39</sup> have also shown that in the limiting case, the equilibrium theory of Helfand and Lauritzen<sup>38</sup> can be reduced to the uniform inclusion and the uniform exclusion models<sup>36</sup>. They demonstrate<sup>39</sup> that melting temperature data alone cannot distinguish between the two models (both the inclusion and the exclusion models result in similar equations). However, the observed heat of fusion, in conjunction with an absolute estimate for crystallinity can be used to determine which model is more accurate.

Lauritzen, DiMarzio and Passaglia<sup>41</sup> (LDP) developed a general theory which deals with growth of a sequence composed of different elements. Their general theory was adapted for copolymer crystallization and a series of expressions were developed which

relate the crystal growth rate and the mean lamellar thickness to the crystallization temperature. While the final expressions are too cumbersome to be of practical use, it is instructive to analyze their approach. They start with the assumption that the crystallizing copolymer will initiate crystallization in various forms (lamellar thickness and composition) and that each of these forms will have different growth rates. The mean lamellar thickness and growth rate is then the overall effect of these individual growth rates and lamellar thickness.

A number of other attempts<sup>42-48</sup> have been made to model the crystallization behavior of copolymers. However, such attempts have had limited success so far largely because of two reasons. First, there is still some debate on the crystallization mechanism in homopolymers. Even for relatively simple homopolymers like polyethylene, there is some controversy on the chain reentry mechanism, the regime kinetics etc. For more complex homopolymers like PEEK, crystallization process is less clear. Given this relative lack of understanding on the crystallization process in homopolymers, it is not surprising that the crystallization process in copolymers is not understood. Secondly, it is difficult to synthesize good model systems to test any copolymer crystallization theory. Given this relative paucity of available data, it becomes even more difficult to formulate theories to model the crystallization process.

In this dissertation, a novel model copolymer system (PEKK 50/50) has been synthesized and characterized. The crystallization and melting behavior of this model copolymer system has been investigated and tested against the different copolymer crystallization theories. It will be shown, for example, that the degree of crystallinity does decrease as the crystallization temperature is increased. Further, it will be shown that the equilibrium thermodynamic arguments of Helfand and Lauritzen has limited success in modeling the crystallization process. However, it will also be shown that kinetic factors play a very important role in determining the morphology and composition of the crystalline phase.



## 2.5 SAXS data analysis:

Small Angle X-Ray Scattering (SAXS) techniques have been used to calculate the lamellar thickness of the crystallized copolymer. These values for lamellar thickness have then been used to estimate the equilibrium melting temperature using the Gibbs-Thomson-Tammann analysis described in Section 2.5. In this section, the SAXS data analysis to obtain the lamellar thickness has been outlined.

Raw SAXS data is first corrected for parasitic scattering. Corrected SAXS data (see example in Figure 2.13) can then be analyzed using the one dimension correlation function approach as outlined by Strobl and Schneider<sup>49</sup>. The correlation function is the inverse cosine Fourier transform of the corrected data as summarized in Equation 2.4.

$$\gamma_1(r) = \int_0^{\infty} (I - I_b) \cdot q^2 \cdot \exp(\sigma^2 \cdot q^2) \cdot \text{Cos}(qr) \cdot dq \quad \text{Equation 2.4}$$

In the above equation,  $\gamma_1(r)$  is the one dimension correlation function,  $I$  is the intensity at scattering vector  $q$ ; where  $q$  is  $(4\pi/\lambda) \cdot \sin(\Theta)$  (where  $2\Theta$  is the scattering angle). Before the inverse Fourier transform, the corrected SAXS data needs to be extrapolated to low and high angles and the component of scattering due to homogenous density fluctuations (liquid scattering profile  $I_b$ ) subtracted. Extrapolation to low angles (in the angular region covered by the beam stop) is relatively straightforward and involves a straight-line extrapolation from the origin to the first useful data point in the Lorentz-corrected  $((I - I_b) \cdot q^2$  vs  $q$ ) plot. An example of this extrapolation on the Lorentz corrected plot (sample: PEEK crystallized at 307°C for 10 minutes) is depicted in Figure 2.14. In the example, data was collected in the range  $q = 0.06$  to  $0.19 \text{ \AA}^{-1}$ . In the angular range  $q = 0$  to  $0.06 \text{ \AA}^{-1}$ , SAXS data was extrapolated using the straight line between the origin and the first useful data point (also depicted in the Figure). Figure 2.13 and 14 also depict the modified Porod Law fit to the experimental data. This Porod Law fit is then used to extrapolate the data to high angles. The modified Porod Law is summarized in Equation 2.5 below<sup>50</sup>.

$$I = I_b + \frac{K}{q^4} \cdot \exp(-\sigma^2 \cdot q^2)$$

Equation 2.5

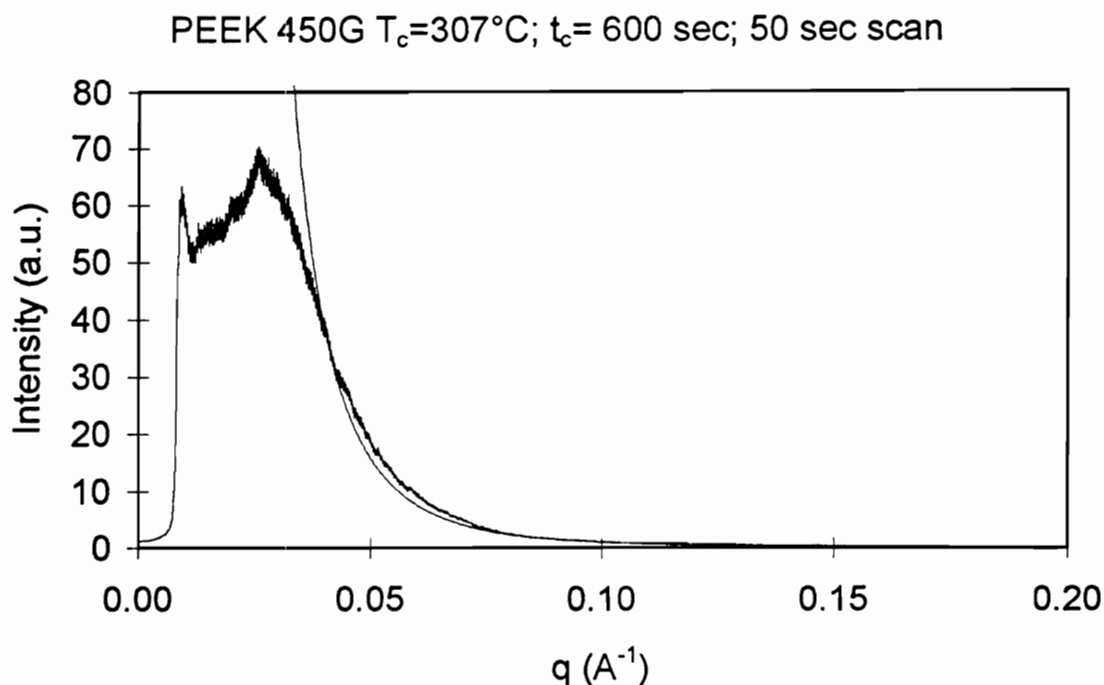


Figure 2.13: Example Raw SAXS data. Sample: PEEK 450 G melted at  $385^\circ\text{C}$  for 4 minutes, followed by rapid quenching to  $307^\circ\text{C}$ . Data collected for 50 seconds after a hold of 600 seconds. Also shown in the plot is the Porod Law extrapolation for high angles.

In the above equation,  $K$  is the Porod Law constant, and  $\sigma$  is related to the width of the crystal liquid transition zone (interphase)  $E$  by the relation

$$E = \sqrt{12} \cdot \sigma$$

In order to estimate a value for liquid scattering ( $I_b$ ), the term arising due to the presence of a finite interphase can be ignored. Under this assumption, a plot of  $Iq^4$  vs  $q^4$  (an example of which is depicted in Figure 2.15) will have a slope equal to  $I_b$ . This value for  $I_b$  can be used to construct a plot of  $\ln[(I-I_b) \cdot q^4]$  vs  $q^2$  depicted in Figure 2.16. From the negative slope of this plot, a value for  $\sigma$  can be estimated. This value of  $\sigma$  can be used

to construct another plot of  $(I-I_b) \cdot q^4 \cdot \exp(\sigma^2 \cdot q^2)$  vs  $q$  as depicted in Figure 2.17. For ideal lamellar two phase systems, this plot should resemble the plot depicted in Figure 2.18<sup>51</sup>. The differences between the two plots are obvious and will be discussed in more detail in a subsequent part of this section. The last step in the Porod Law fitting is the estimation of a value for  $K$ . This can be done by calculating the area under the plot depicted in Figure 2.17 in the available angular range ( $q = 0$  to  $0.2 \text{ \AA}^{-1}$ ) and dividing that by the angular range used ( $0.2 \text{ \AA}^{-1}$ ). It has been demonstrated by Biswas<sup>52</sup> that this procedure results in a correlation function without any curvature near the origin and thereby facilitates the Strobl and Schneider analysis for lamellar thickness estimation.

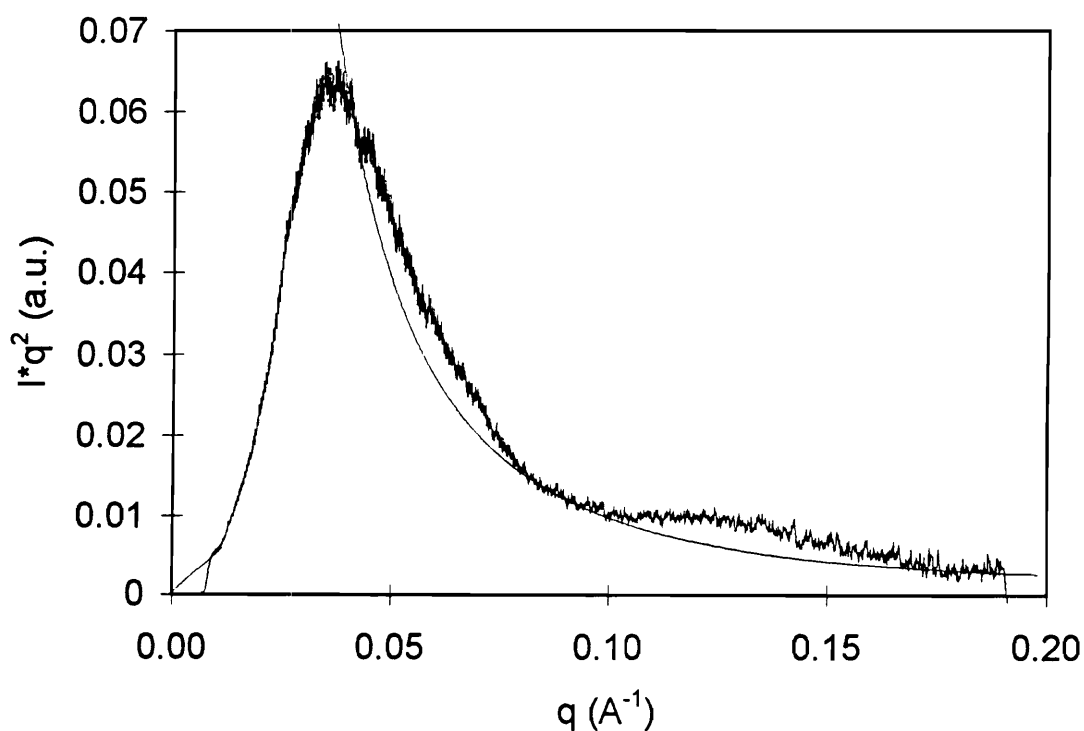


Figure 2.14: Lorentz corrected plot of the data depicted in Figure 2.13. Also shown in the plot is the Porod Law extrapolation for high angles. Extrapolation to low angles (in the region covered by the beam stop) was done with a straight line between the origin and the 1<sup>st</sup> useful data point in the plot.

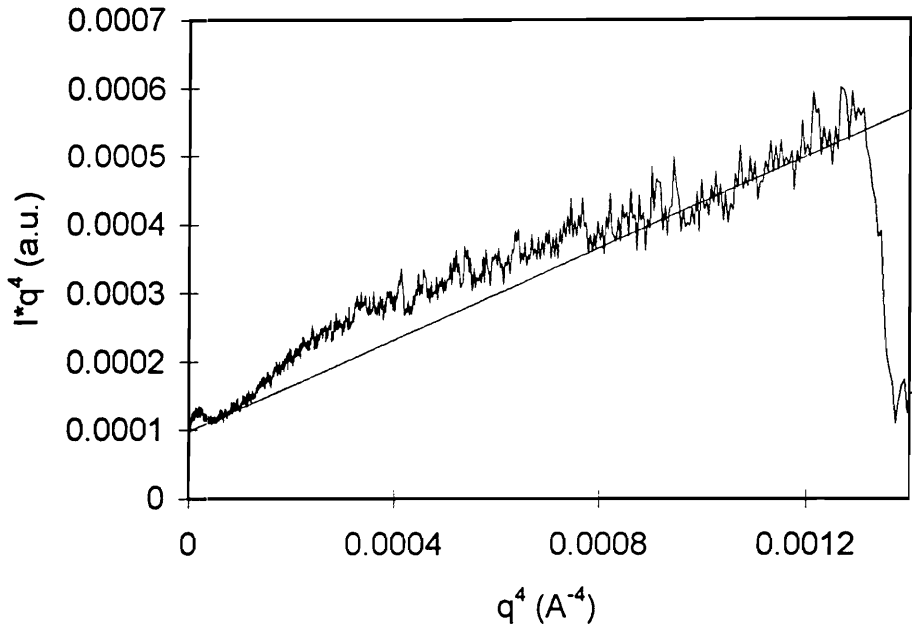


Figure 2.15: Porod Law plot of  $I \cdot q^4$  vs  $q^4$  to estimate  $I_b$ .

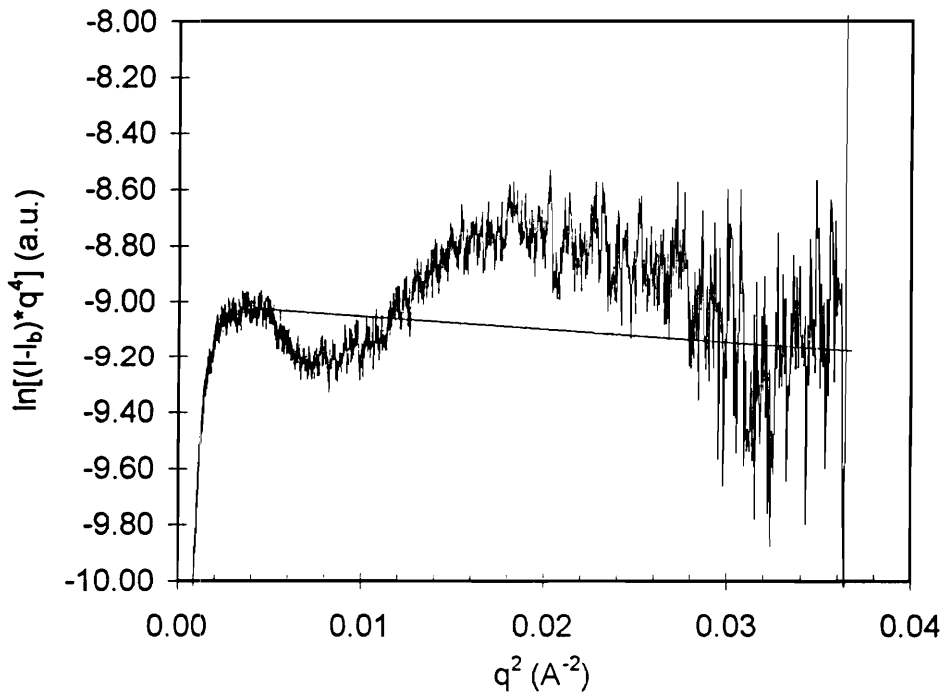


Figure 2.16: Porod law plot of  $\ln[(I - I_b) \cdot q^4]$  vs  $q^2$  to estimate the factor  $\sigma$ .  $s$  is related to the thickness of the crystal-liquid transition zone  $E$  by the relation  $E = \sqrt{12} \cdot \sigma$

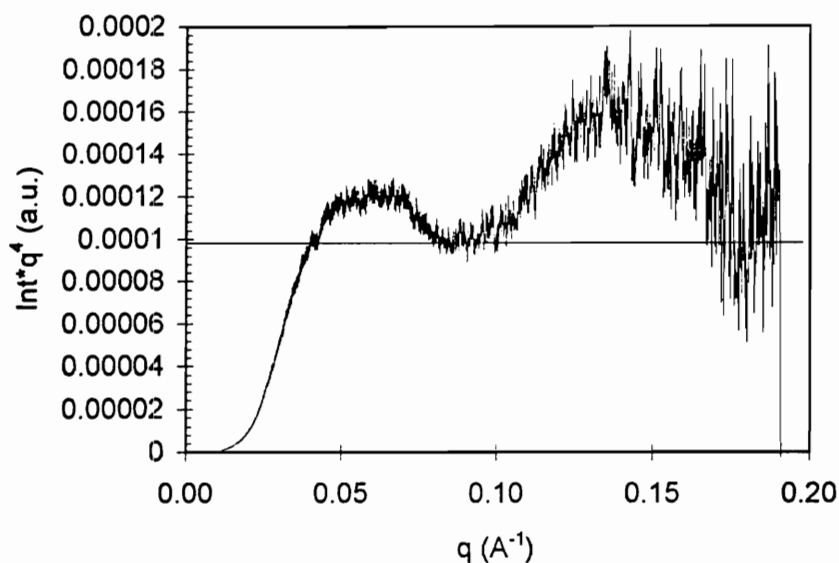


Figure 2.17: Porod Law plot of  $[(I-I_b)*q^4*\exp(\sigma^2q^2)]$  vs  $q$ . This plot should resemble the one depicted in Figure 2.18. Also shown in the plot is the estimated Porod Law constant  $K$ . The constant  $K$  was estimated following the procedure of Biswas<sup>52</sup>.

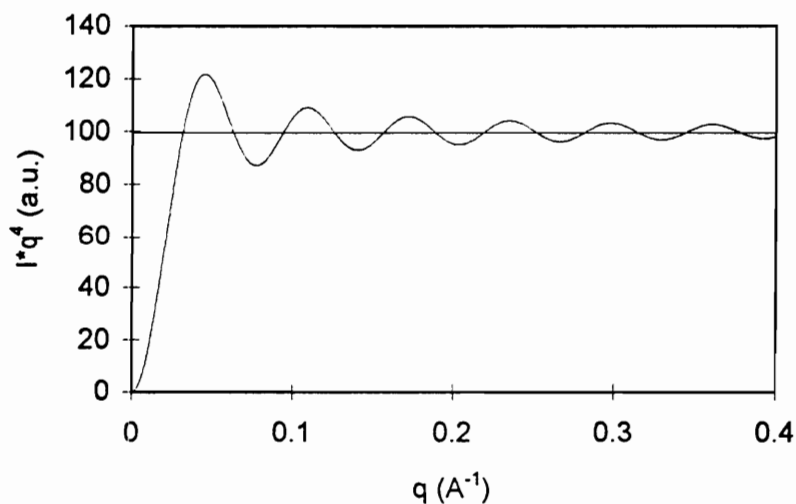


Figure 2.18: Porod Law plot of  $I^*q^4$  vs  $q$  for an ideal 2 phase lamellar system<sup>51</sup>. The plot resembles a decaying sine function, which has a value  $K$  at large values of  $q$ .

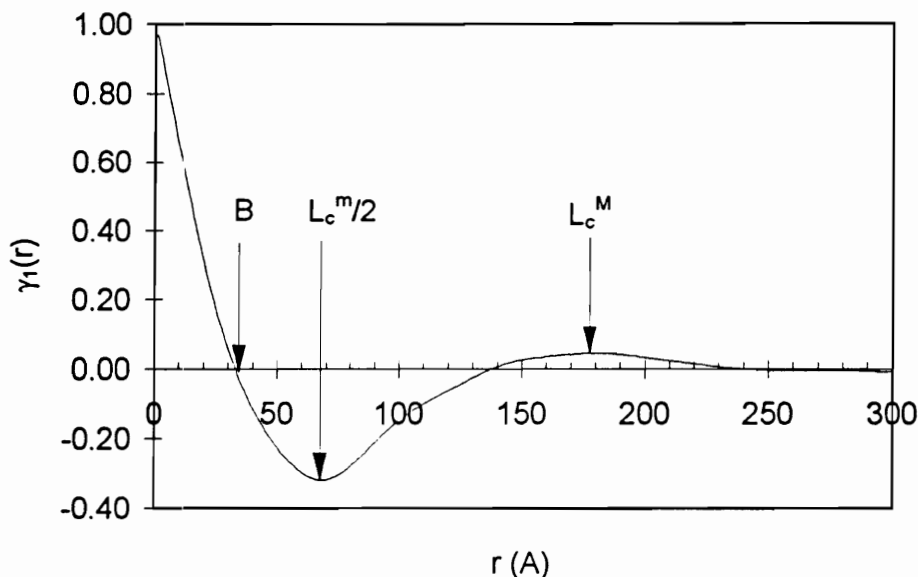


Figure 2.19: One dimensional correlation function for the data depicted in Figure 2.13. Also marked in the plot are the 1<sup>st</sup> zero (B), the 1<sup>st</sup> minima ( $L_c^m/2$ ) and the 1<sup>st</sup> maxima ( $L_c^M$ ). Note that the correlation function does not have any curvature at  $r=0$ . This results from the analysis procedure suggested by Biswas<sup>52</sup>.

The typical correlation function is depicted in Figure 2.19. Also depicted in the Figure are the 1<sup>st</sup> zero, the 1<sup>st</sup> minima and the 1<sup>st</sup> maxima. From the shape of the correlation function, the lamellar thickness, amorphous layer thickness and the long spacing (the sum of the two) can be extracted using the relation suggested by Strobl and Schneider<sup>49</sup>.

$$x_1 \cdot x_2 = \frac{B}{L_c^M}$$

In the above equation,  $x_1 + x_2 = 1$  and  $x_1 = x_{cl} = l_1/L_c^M$ ,  $l_1$  is the lamellar thickness, B is the position of the first zero in the correlation function and  $L_c^M$  is the long spacing as estimated by the first maxima in the correlation function.

As described, analysis of SAXS data is relatively complicated. There are a number of factors which can potentially affect the final calculated values of lamellar thickness.

Since one of the conclusions made in this dissertation relies on the accuracy of the Gibbs-Thomson-Tammann estimate for the lamellar thickness, the various problems associated with SAXS data analysis are described below.

First, it is not mathematically possible to distinguish between the high and low values of  $x_1$  for  $x_{cl}$ . For reasons listed later, the high value of  $x_1$  was used as the correct estimate for  $x_{cl}$ . For lamellar space filling semi-crystalline systems, the lamellar thickness should equal the long spacing multiplied by the overall degree of crystallinity. Such an approach results in substantially lower values for lamellar thickness when compared to those used in this dissertation. However, work by other authors suggests that PEEK (which is very similar to PEKK 50/50) does not have a lamellar space filling morphology. For example, electron microscopy results obtained by Lovinger et al.<sup>53</sup> suggests that PEEK crystallizes in the form of stacks of lamellae which are separated from each other by amorphous rich regions. Sauer and Hsiao<sup>54</sup> have used simple geometrical arguments on SAXS, WAXS and DSC data to suggest that for PEEK crystallized at 300°C, these lamellar stacks consist of about 5-6 lamellae which are separated from each other by thin amorphous regions. The work of Lovinger et al.<sup>53</sup> and the work of Sauer and Hsiao<sup>54</sup> clearly suggests that the choice of the low value of  $x_1$  for  $x_{cl}$  would be incorrect. Evidence to support the choice of the high value of  $x_1$  for  $x_{cl}$  is obtained by comparing SAXS results with calculations made on WAXD data. The degree of crystallinity within a lamellar stack (if it exists) has to be higher than the overall degree of crystallinity. Therefore, the estimated linear (or stack) degree of crystallinity  $x_{cl}$  should be higher than the overall degree of crystallinity estimated by WAXD. If the morphology is lamellar space filling, then the two should be equal. The linear degree of crystallinity can never be less than the overall degree of crystallinity. Calculations made on actual scattering data from PEKK 50/50 and also on PEEK<sup>18</sup> suggests that only the high value of  $x_1$  is consistent with this requirement. Further, a line broadening analysis<sup>55</sup> on the WAXD peaks can be used to estimate a lower limit for the lamellar thickness. This lower limit for lamellar thickness is consistent only with the choice of the high value of  $x_1$  for  $x_{cl}$ .

In a broader context, there is no unique solution for the correlation function. There are several possible electron density distributions which will give rise to the same correlation function. Therefore the correlation function by itself cannot be analyzed to obtain any information on the semi-crystalline morphology. However, in conjunction with some information on the morphology from other techniques, it is possible to analyze the correlation function. For example, the TEM work of Lovinger et al.<sup>53</sup> suggests that the morphology consists of lamellar stacks. With this information, the correlation function can be analyzed to obtain the average lamellar thickness within the lamellar stack. However, caution should be applied when using the results of such analysis.

The other problem relates to the extrapolation of the corrected SAXS data to high angles. This extrapolation is affected by the quality of the Porod law fit in the available angular range and will in turn affect the shape of the correlation function. Therefore the quality of the Porod Law fit will affect the final calculations. Sample calculations suggests that within “reasonable” upper and lower limits of the Porod Law constant, the final calculations for lamellar thickness do not differ by more than 5 %. However, extrapolation of scattering data in a limited angular range to high angles should be treated with some caution. The problem is illustrated in Figure 2.17 and 18. Figure 2.17 is a plot of  $[(I-I_b) \cdot q^4 \cdot \exp(\sigma^2 q^2)]$  vs  $q$ . As already mentioned, this plot should resemble a similar plot for the ideal two phase lamellar system depicted in Figure 2.18<sup>51</sup>. The differences between the two plots are obvious. For the real system depicted in Figure 2.17, the 1<sup>st</sup> maxima is lower than the 2<sup>nd</sup> maxima and the 1<sup>st</sup> minima is lower than the 2<sup>nd</sup> minima. For the ideal lamellar system, the 2<sup>nd</sup> and subsequent maximas are lower than the 1<sup>st</sup> maxima and the 2<sup>nd</sup> and subsequent minimas are higher than the 1<sup>st</sup> minima. The plot for the ideal lamellar system resembles an oscillation which decays to a constant of value  $K$ . For the real system, the plot resembles a similar decaying oscillation, but the oscillations appear to decay around a straight line of positive slope. This positive deviation from the ideal two phase system is probably caused by incorrect subtraction of the parasitic background and/or an incorrect subtraction of the liquid scattering profile  $I_b$ .



Moreover, work done by other researchers has demonstrated that the liquid scattering profile is not a constant as assumed in this work. For example, Vonk<sup>56</sup> has used a polynomial type fit and Ruland<sup>51</sup> has used an exponential type fit for the liquid scattering profile. These authors have collected scattering data in a large angular range (up to about  $5^\circ 2\Theta$ ). At large scattering angles, the liquid scattering becomes predominant over the lamellar scattering. These authors have used the scattering data at large angles ( $3\text{-}5^\circ 2\Theta$ ) to fit the liquid scattering profile, and then extrapolated the fit to lower angles. In this work, scattering data was collected in a small angular range only. Therefore no attempt was made to fit the liquid scattering profile to a non-constant background. Since the liquid scattering profile was approximated to a constant value, it is possible that the positive deviation depicted in Figure 2.17 is caused by this approximation. Hence results obtained from the Fourier analysis of such extrapolated data should be treated with some caution.

Note that there are several variations to the scheme described below. These variations relate to extrapolation of data to high and low angles and in the estimation of the lamellar thickness from the correlation function. These variations have been summarized in the literature<sup>49,50</sup>.

## 2.6 Thermal Analysis

The thermal analysis technique used in this study is differential scanning calorimetry (DSC). DSC techniques can be used to obtain the glass transition temperature, the melting temperature, and to study the crystallization kinetics<sup>56</sup>. The melting temperature can be obtained either by a Hoffman Weeks<sup>57</sup> (HW) type analysis or by a Gibbs Thomson Tamman<sup>58</sup> (GTT) type analysis. Excellent descriptions of the thermal analysis techniques and the measured material properties have been provided by Wunderlich<sup>58</sup> and Hoffman<sup>59</sup> respectively. Both the HW and the GTT techniques have been used in this study and are therefore described in this section. Some of the conclusions made in this thesis rely on melting temperature estimates from these two techniques. Therefore these techniques have been examined from a critical viewpoint also.

The Hoffman Weeks type analysis extrapolates the melting temperatures ( $T_m$ ) when plotted against the crystallization temperatures ( $T_c$ ) to the  $T_m=T_c$  line (see Figure 2.20). The melting and crystallization temperatures are related to the actual and minimum lamellar thickness ( $l_{act}$  and  $l_{min}$ ) as summarized in Equations 2.6 and 2.7

$$T_c = T_m^{eq} \left( 1 - \frac{2\sigma_e}{\Delta H_f^o \cdot l_{min}} \right) \quad \text{Equation 2.6}$$

$$T_m = T_m^{eq} \left( 1 - \frac{2\sigma_e}{\Delta H_f^o \cdot l_{act}} \right) \quad \text{[Gibbs Thomson Tamman Relation] Equation 2.7}$$

The minimum lamellar thickness is a thermodynamic manifestation of the crystallization temperature. The term  $l_{act}$  is a function of the kinetic processes that affect the lamellar flux distribution, and can be estimated for flexible macromolecules by the Lauritzen-Hoffman<sup>61</sup> kinetic theory (L-H theory). It is usually slightly greater than  $l_{min}$ , with the difference between them ( $\delta l = l_{act} - l_{min}$ ) decreasing with increasing  $T_c$ . Finally, the melting temperature is a thermodynamic manifestation of the actual lamellar thickness.

Taking the ratio of  $\Delta T_c$  ( $T_m^{eq}-T_c$ ) and  $\Delta T_m$  ( $T_m^{eq}-T_m$ ) and a few simple algebraic manipulations leads to the relation between  $\Delta T_c$  and  $\Delta T_m$  summarized in Equation 2.8

$$\Delta T_m = \Delta T_c \frac{2 \cdot \sigma_e}{\Delta H_f} \left( \frac{1}{l_{min}} - \frac{1}{l_{act}} \right) \quad \text{Equation 2.8}$$

The 1<sup>st</sup> derivative of the above relation results in Equation 2.9.

$$\frac{d\Delta T_m}{d\Delta T_c} = \frac{2\sigma_e}{\Delta H_f} \cdot \frac{d}{d\Delta T_c} \left( \frac{1}{l_{min}} - \frac{1}{l_{act}} \right) \quad \text{Equation 2.9}$$

The Hoffman-Weeks analysis is based on a straight line extrapolation of the  $T_m$  vs  $T_c$  plot to the  $T_m=T_c$  line. For  $T_c = T_m^{eq}$ ,  $l_{min}=l_{act}$ , therefore  $T_m=T_c=T_m^{eq}$ . Therefore an extrapolation of the  $T_m$  vs  $T_c$  data to the  $T_m=T_c$  line would give an estimate for the equilibrium melting temperature ( $T_m^{HW}$ ). For the straight line extrapolation to be valid, the  $d\Delta T_m/d\Delta T_c$  term should be a constant. Therefore, the 2<sup>nd</sup> derivative of the  $\Delta T_m$  vs  $\Delta T_c$  plot should be zero.

$$\frac{d^2\Delta T_m}{d\Delta T_c^2} = \frac{2\sigma_e}{\Delta H_f} \cdot \frac{d^2}{dT_m^2} \cdot \left( \frac{1}{l_{min}} - \frac{1}{l_{act}} \right) = 0$$

It is not obvious from the above relation that the 2<sup>nd</sup> derivative of the  $T_m$  vs  $T_c$  plot should be zero. In fact, calculations made using the L-H theory demonstrate that the slope is indeed a function of  $T_c$ . As  $T_c$  increases, both  $l_{min}$  and  $l_{act}$  increase while the difference between them continually decreases to 0 as  $T_c$  approaches  $T_m^{eq}$ . A hypothetical case depicting the trends in  $l_{min}$ ,  $l_{act}$  and  $\delta l$  (the difference between them) as a function of crystallization temperature is depicted in Figure 2.20. Based on these L-H estimates for  $l_{act}$ , the  $T_m$  for a given  $T_c$  can be estimated using Equation 2.7. These estimates for  $T_m$  are also plotted in Figure 2.20. For any real polymer system, melting temperature data will be available in a finite crystallization temperature range only. A hypothetical (but reasonable) finite crystallization temperature range is also depicted in Figure 2.20. Extrapolation of the melting temperature data in this temperature range to the  $T_m=T_c$  line will result in the hypothetical Hoffman-Weeks melting temperature. As the extrapolation indicates, the

estimated Hoffman-Weeks melting temperature is 570 K, whereas the actual equilibrium melting temperature is about 618 K.

As already mentioned, the equilibrium melting temperature can also be estimated if the lamellar thickness values are available for the different crystallization temperatures. This is done with the aid of the Gibbs-Thomson-Tamman relation given in Equation 2.7. As suggested by Equation 2.7, a plot of  $T_m$  vs  $1/l_{act}$  should result in a straight line with slope  $2\sigma_e/\Delta H_f^\circ$  and an intercept equal to the equilibrium melting temperature ( $T_m^{GTT}$ ). Such a plot for the data depicted in Figure 2.20 is illustrated in Figure 2.21. As can be seen from Figure 2.21 the estimated Gibbs-Thomson-Tammann melting temperature is 618 K, which compares favorably with the Hoffman Weeks estimate of 570 K and the actual equilibrium melting temperature of 618 K.

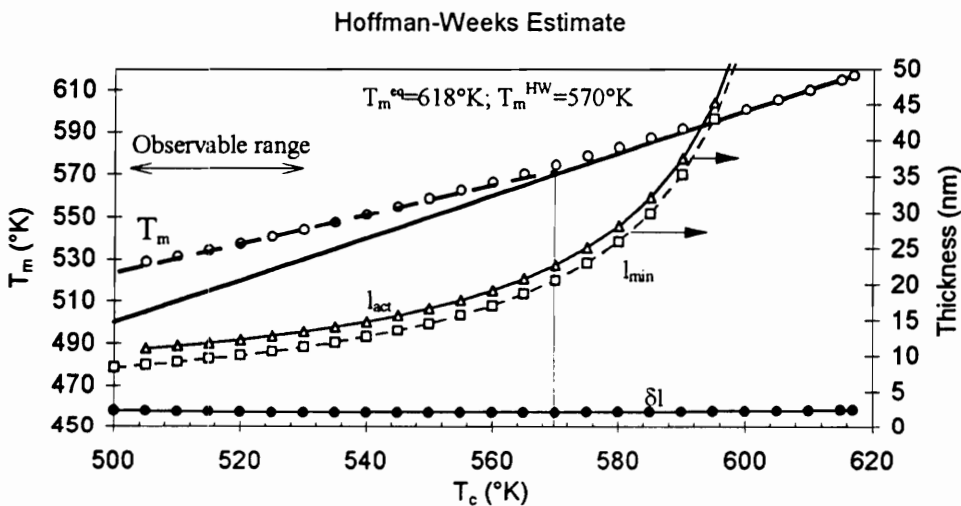


Figure 2.20: An example Hoffman-Weeks estimate for data obtained from the L-H theory.  $l_{min}$ ;  $\delta l$  and  $l_{act}$  are estimated from the L-H<sup>61</sup> theory using  $T_m^{eq}$ : 618 K;  $\sigma_e$ : 12 kcal/mole;  $\sigma$ : 1;  $\Delta H$ : 15 kcal/mole  $\psi$ : 0.9 a: 0.49; b: 0.5. Melting temperatures (open circles) are estimated from  $l_{act}$  using Equation 2.7. Melting temperatures in an arbitrary 'observable range' are extrapolated to the  $T_m=T_c$  line for a  $T_m^{HW}$  estimate of 570 K.

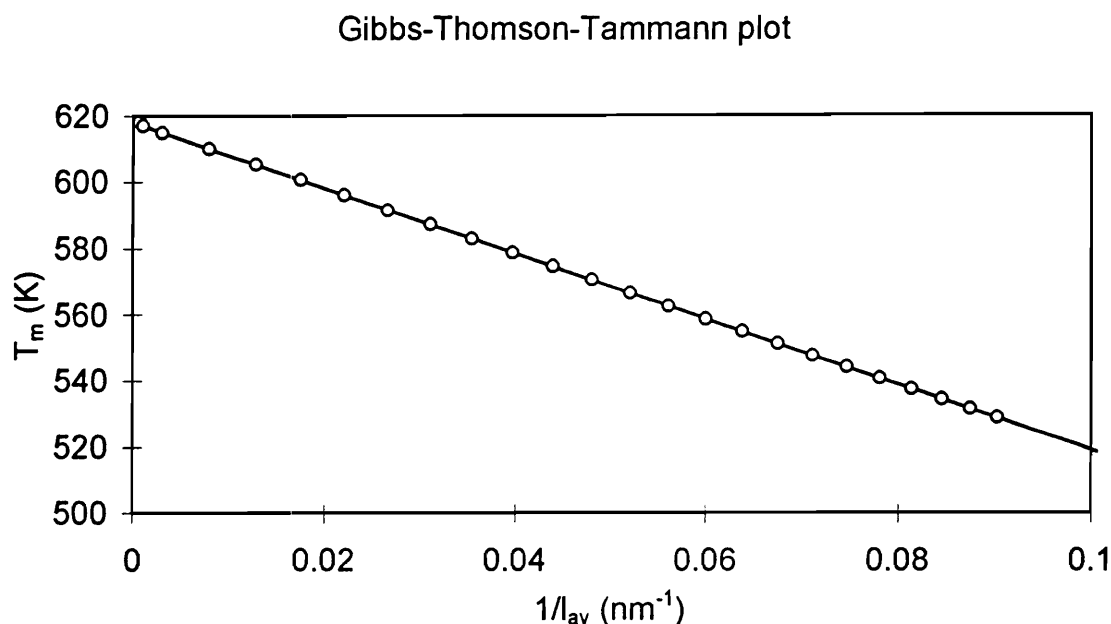


Figure 2.21: The Gibbs-Thomson-Tammann plot for the data depicted in Figure 2.20.

It should be noted that calculations for  $l_{act}$  have been made using the Lauritzen-Hoffman theory and values for the required thermodynamic variables which were reasonable for PEEK. Care should be taken in using the results of such calculations on relatively rigid macromolecules like PEEK because the L-H theory was developed for flexible macromolecules with chain folded lamellae. However, the conclusion being made from Figure 2.20 (that the Hoffman Weeks analysis results in an underestimate) is independent of the polymer system being used. It should also be noted that while theoretical calculations suggest that the Gibbs-Thomson-Tammann approach is better than the Hoffman-Weeks approach, for real polymer systems, that might not be the case. For real polymer systems, estimation of lamellar thickness is not always straightforward. As already discussed in the previous section, the usual method of estimating the SAXS long spacing and multiplying that by the overall degree of crystallinity does not hold for polymers which demonstrate a lamellar stacking morphology. Therefore other approaches

(such as the correlation function approach) have to be adopted. These approaches are relatively complicated, difficult to implement and prone to operator error. To summarize, while the Hoffman-Weeks approach is experimentally easy to implement, it underestimates the equilibrium melting temperature considerably. In comparison, the Gibbs-Thomson-Tammann approach is theoretically sound, but experimentally difficult to implement.

## CHAPTER 3: SYNTHESIS AND CHARACTERIZATION

### *3.1 Synthesis*

A series of non-alternating PEKK 50/50 samples were synthesized using the Friedel Crafts Acylation synthesis reaction (see Figure 3.1). Details of the synthesis reaction have been provided by Gay & Brunette and is also described in Section 2.3. Briefly, the reaction consists of a prepolymerization step at about 25°C, and a high temperature polymerization step at about 100°C. Oligomers (e.g. of the type D-I-D-I-D etc.) were synthesized during the prepolymerization step from diphenyl ether (DPE) and either terephthaloyl chloride (TCl) or isophthaloyl chloride (ICl). These oligomers were subsequently chain extended during the high temperature polymerization step.

The prepolymerization step was manipulated in order to synthesize a series of non-alternating PEKK 50/50 samples. This prepolymerization step control has been depicted in Figure 3.2. For example, a DPE:ICl ratio of 6:5 during the prepolymerization step resulted in an oligomer of the type labeled I5. This oligomer was then chain extended with 5 parts of TCl and 4 parts of DPE, which resulted in a PEKK 50/50 structure with an

Average Block Length (ABL) of 5. Using this and similar prepolymerization steps, the ABL was manipulated and a series of PEKK 50/50 samples with ABL of 1, 3 & 5 were prepared. Another sample was prepared using a DPE:TCl ratio of 3:2 in the prepolymerization step (ABL 2). In addition, a PEKK 50/50 structure labeled Random was also prepared by adding all the reactants during the prepolymerization step.

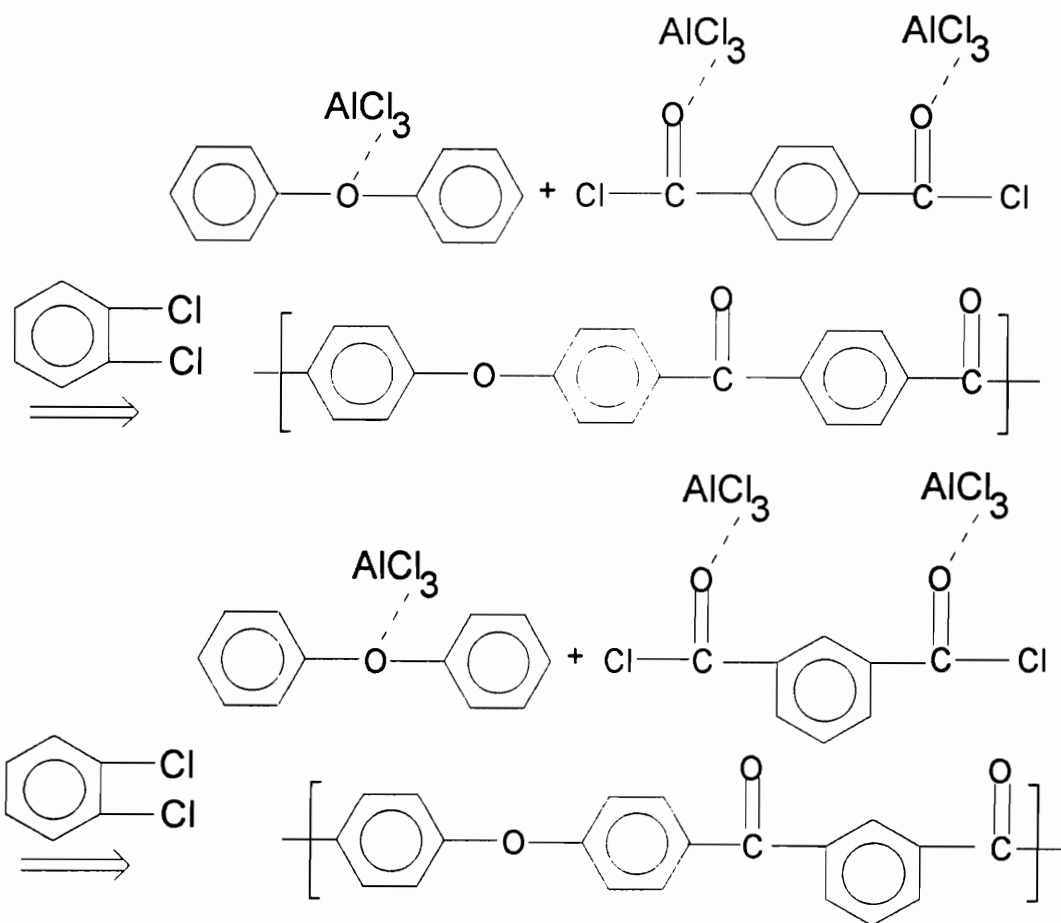


Figure 3.1: The Friedel Crafts Acylation synthesis reaction for PEKK.



6•DPE + 5•ICl I5 + 5•TCI + 4•DPE	-I-D- I -D-I-D-I-D-I-D (IIII or I5) -TDTDTDTDTD-IDIDIDIDID- (T5I5)
	Average Block Length: 5
4•DPE + 3•ICl I3 + 3•TCI + 2•DPE	D-I-D-I-D-I-D (III or I3) -TDTDTD-IDIDID- (T3I3)
	Average Block Length: 3
2•DPE + ICl I1 + TCI	D-I-D (I or I1) -TD-ID- (T1I1)
	Average Block Length: 1
3•DPE + 2•TCI T2 + 2•ICl + DPE	D-T-D-T-D (TT or T2) -TDTD-IDID- (T2I2)
	Average Block Length: 2
2•DPE + TCI + ICl	-DIDTDIDIDTDIDTDT-

#### Random Structure

Figure 3.2: Control of the Prepolymerization Step

Note that the prepolymerization step is not expected to result in the formation of one stoichiometric type of oligomer. Rather, it is expected that a series of oligomers will be formed, and that the average molecular weight of those oligomers would be close to that predicted by stoichiometric considerations alone. Indeed, a Mass Spectroscopy analysis of the reaction bath frozen after the prepolymerization step suggested the presence of compounds which are compatible with the above expectation.

Also note that the PEKK 50/50 polymer labeled ABL 1 is not expected to have a perfectly alternating structure. This follows from observations made by earlier researchers that use of a DPE:ICl ratio of less than 4:1 leads to the formation of oligomers other than the D-I-D oligomer during the prepolymerization step. A DPE:ICl ratio of 2:1 should

result in the formation of compounds of the type D-ICI, D-I-D-ICI etc, while leaving some unreacted ICI in the reaction mixture. Therefore, the final copolymer is expected to have an average block length greater than 1, and the label ABL 1 is misleading. Only a perfectly alternating structure can have an ABL of 1. While the synthesized samples have been labeled as ABL 1, 3 & 5 and so on, it should be noted that there is no known technique that can be used to determine either the block length average or its distribution. Therefore the ABL labels should be loosely interpreted as Average Expected Block Lengths.

To summarize, several PEKK 50/50 copolymers were synthesized by manipulating the prepolymerization step. A series of copolymers were prepared with DPE and ICI in the prepolymerization step (ABL 1, 3 and 5). Another copolymer (ABL 2) was prepared with DPE and TCI in the prepolymerization step, while a Random copolymer was prepared with all the reactants in the prepolymerization step.

### 3.2 Characterization

The synthesized polymers were dried in vacuum at 150°C for 24 hrs and a series of characterization tests performed. These include (1) proton nuclear magnetic resonance ( $^1\text{H}$  NMR) to verify that the overall composition is PEKK 50/50 and also to analyze the defects in the linear chain structure; (2) Infra Red (IR) spectroscopy to determine the purity of the samples; (3) Gel Permeation Chromatography (GPC) to determine the molecular weight distribution; (4) Elemental Analysis to ensure that the  $\text{AlCl}_3$  catalyst has been washed away; (5) Thermo-Gravimetric Analysis (TGA) to characterize melt degradation; and (6) Differential Scanning Calorimetry (DSC) to determine glass transition temperature. Results of these characterization tests have been summarized in the following sections.

Solution  $^1\text{H}$  NMR was performed using a 0.1 % weight solution in tri-chloro acetic acid at 60°C. A DMSO coaxial lock and a dimethyl silane reference was used for calibration. A  $^1\text{H}$  NMR scan typical for PEKK 50/50 is depicted in Figure 3.3. Figure 3.4 depicts the different types of  $^1\text{H}$  in the linear PEKK 50/50 molecule. Table 3.1 summarizes the assignment of peaks in the  $^1\text{H}$  NMR spectra to these  $^1\text{H}$ , the area under the assigned peaks, along with the expected ratio for a PEKK 50/50 sample. Since the number of  $^1\text{H}$  in an average PEKK 50/50 repeat unit is 12, the areas under the assigned peaks have been accordingly normalized. The assignment of the individual peaks on the  $^1\text{H}$  NMR scan to protons in the linear chain structure were made on the basis of the expected splitting of the peaks (e.g. singlet vs doublet). As can be seen from Table 3.1, the final copolymer has a composition that is (within experimental errors) 50% T.

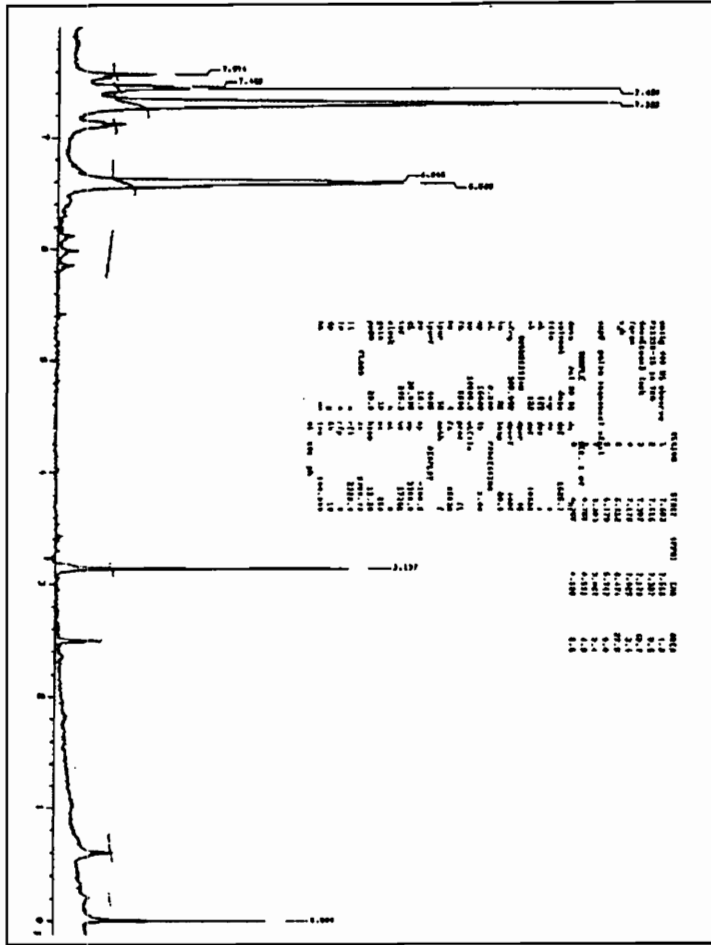


Figure 3.3: An <sup>1</sup>H NMR scan typical for PEKK 50/50.

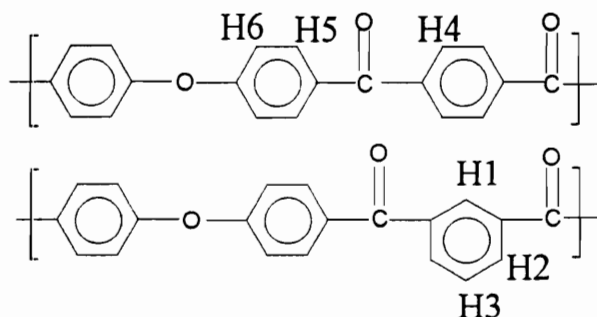


Figure 3.4: The different types of protons in the linear PEKK 50/50 chain.

Table 3.1: Analysis of proton NMR data to verify that the composition is PEKK 50/50. The 1<sup>st</sup> column refers to the types of expected <sup>1</sup>H in the PEKK 50/50 repeat unit (see Figure 3.4). The 2<sup>nd</sup> column refers to the number of such <sup>1</sup>H in an average PEKK 50/50 repeat unit, and the type of <sup>1</sup>H NMR peak expected. The 3<sup>rd</sup> column refers to the shifts of the assigned <sup>1</sup>H NMR peak and the last 5 columns refer to the normalized areas of the actual peaks.

type	#, fine structure	Shift (ppm)	ABL 1	ABL 2	ABL 3	ABL 5	Random
H1	0.5; singlet	7.60	0.585	0.647	0.5581	0.5059	0.589
H2	1; doublet	7.45	1.058	1.29	1.131	1.0119	1.15
H3	0.5; triplet	7.15	0.599	0.458	0.6046	0.5059	0.586
H4	2; singlet	7.35	5.809	5.892	5.736	6.07	5.82
H5	4; doublet						
H6	4; doublet	6.6	3.942	3.707	3.968	3.903	3.842
6 types	12		12	12	12	12	12

IR spectra were collected for all the samples using KBr pellets. An IR pattern typical of all the synthesized PEKK 50/50 sample is depicted in Figure 3.5. Gel Permeation Chromatography (GPC) was performed in penta-fluoro phenol at 120°C using a polystyrene standard. A GPC trace of one of the PEKK 50/50 samples is depicted in Figure 3.6. All the GPC traces had similar features. Note that since an absolute calibration scale was not used the results should be treated with caution. Table 3.2 summarizes the results of the GPC measurements on the different PEKK 50/50 samples.

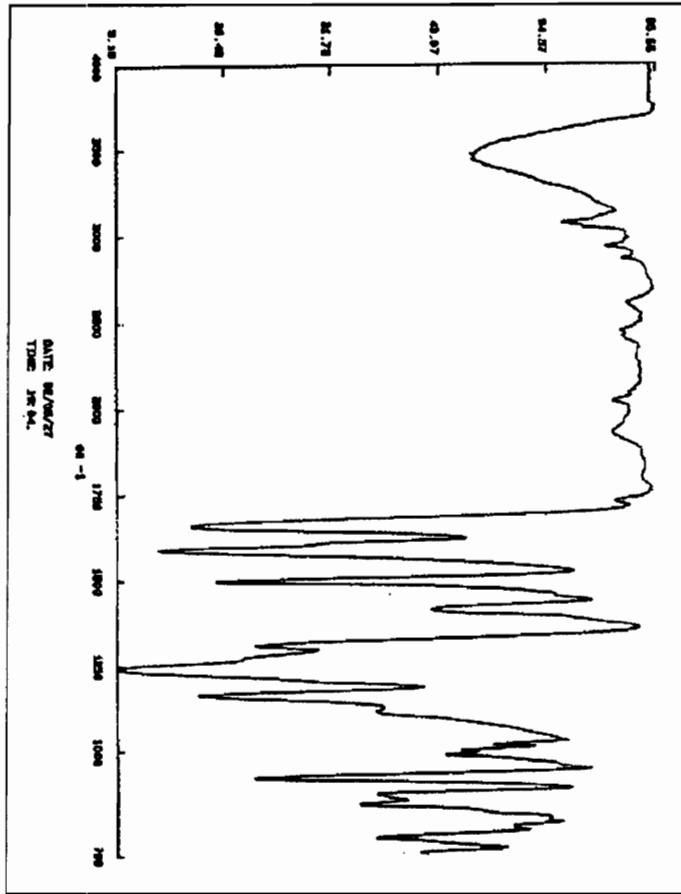


Figure 3.5: KBr pellet IR spectra for the Random PEKK 50/50 sample.

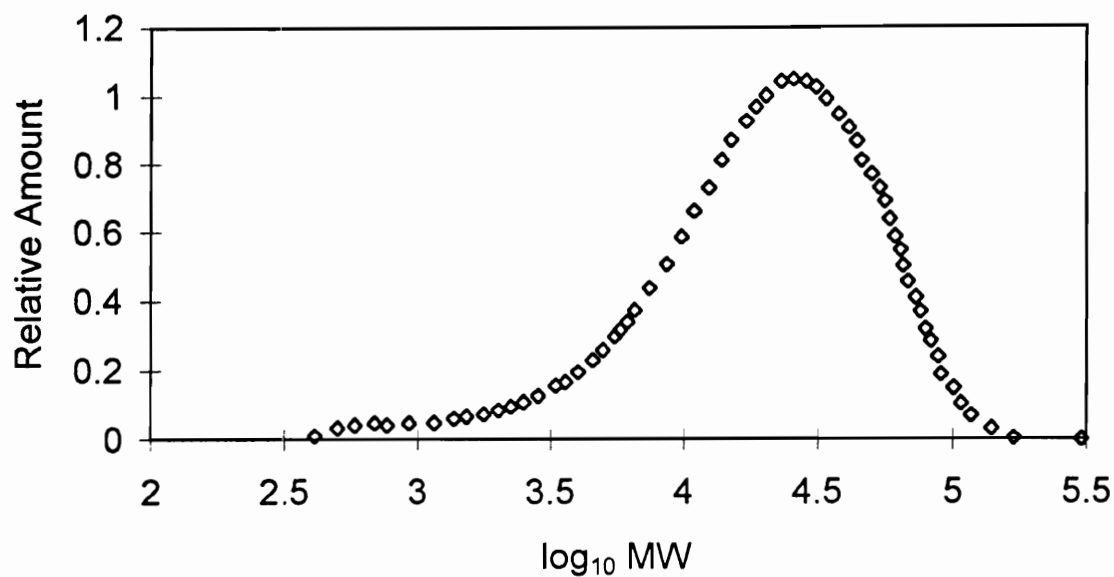


Figure 3.6: A Gel Permeation Chromatography (GPC) trace for the sample labeled ABL 5 typical of all synthesized PEKK 50/50 samples.

Table 3.2: Summary of GPC Data.

	ABL 1	ABL 2	ABL 3	ABL 5	Random
$\langle M_n \rangle$	8400	8800	8100	9150	7420
$\langle M_w \rangle$	25500	25900	24600	26300	26600
$\langle M_v \rangle$	23500	24100	23800	23500	23500
$\langle M_w \rangle / \langle M_n \rangle$	3.03	2.94	3.03	2.88	3.58
Int Viscosity	0.644	0.645	0.644	0.645	0.644

TGA scans were collected for the different PEKK samples, and it was determined that the 5% loss (under  $N_2$ ) temperature was higher than  $400^\circ\text{C}$  for all PEKK 50/50 samples. DSC tests were performed to determine the glass transition  $T_g$  temperature. The as polymerized samples were melted at  $370^\circ\text{C}$  for 2 min, then quenched to room temperature at  $200^\circ\text{C}/\text{min}$ , and then heated at  $10^\circ\text{C}$  to  $200^\circ\text{C}$  in order to determine the  $T_g$ . Figure 3.7 depicts the relevant DSC scans. Figure 3.8 summarizes the  $T_g$ 's of the different PEKK 50/50 samples as determined by DSC. All the different PEKK 50/50 samples appear to have about the same glass transition temperature. The presence of any trends within the 5 samples can be further investigated using other techniques such as dynamic mechanical analysis (DMA). For the scope of the present work, it suffices to state that all the glass transition temperatures are about the same and will therefore not affect the crystallization behavior.

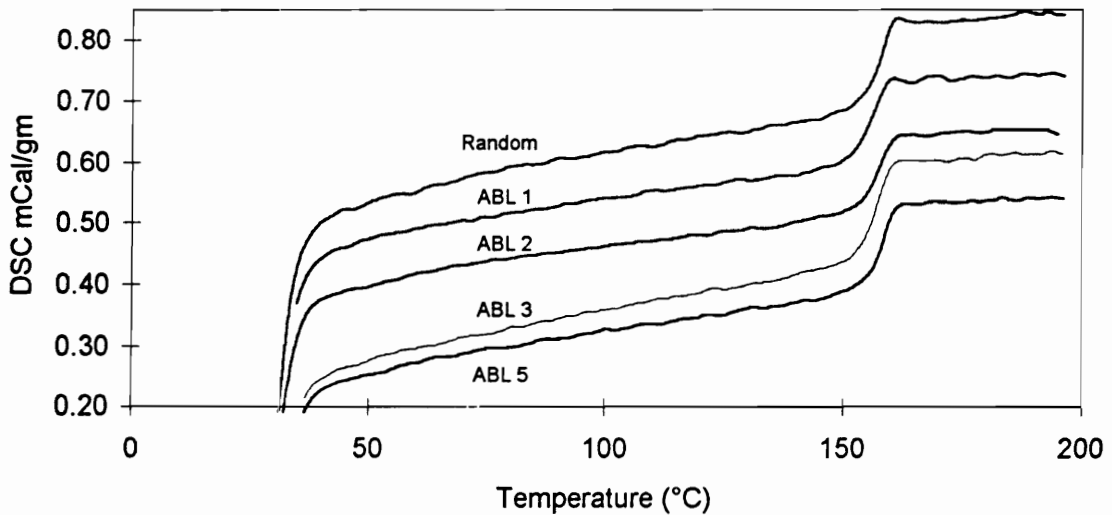


Figure 3.7: DSC traces of quenched PEKK 50/50 samples depicting the glass transition temperature at about  $156^\circ\text{C}$ . All traces have been shifted vertically for visual clarity.



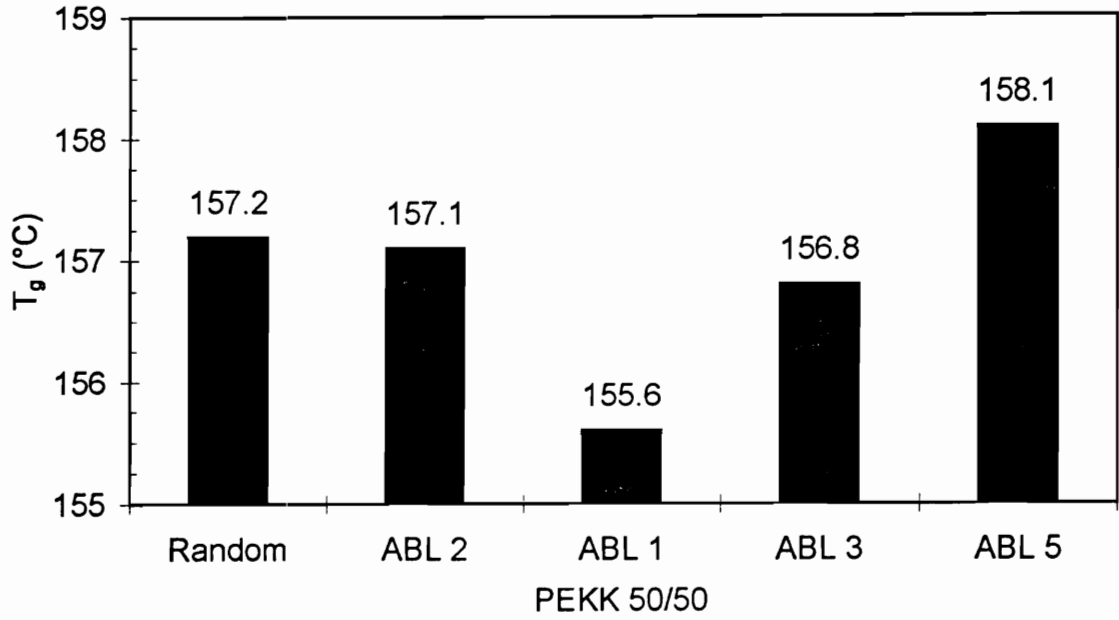


Figure 3.8: Chart depicting the glass transition temperature from the DSC traces depicted in Figure 3.7.

### 3.3 Chain Defects

Several side reactions are possible during the synthesis reaction of PEKK. One of these side reactions results in the formation of xanthate type groups and is depicted in Figure 3.9<sup>34</sup>. These compounds form from 1,2 substituted phenyl rings and are unstable at high temperatures. In the <sup>1</sup>H NMR scan depicted in Figure 3.3, there are some unassigned peaks at 5.7, 6.0 and 6.2 ppm. These peaks can be explained by the formation of triphenyl hydroxyl linkages present in the xanthate group and also of the type depicted in Figure 3.10. In order to support this hypothesis, PEKK oligomers were prepared and analyzed using solution NMR and Mass Spectroscopy (Mass Spec) techniques. PEKK oligomers were prepared using the synthesis route described in the experimental section, but the reaction bath was frozen after the prepolymerization step. The synthesized "oligomers" were then analyzed using solution NMR and Mass Spec. Results of the solution NMR and Mass Spec analysis are given in Figures 3.11 and 3.12 respectively. The NMR peaks are too numerous to be analyzed but the Mass Spec results have been analyzed and the results are also listed in Table 3.3. Figure 3.12 lists some potential monomeric groups which are consistent with the observed Mass Spec peaks. Note that the Mass Spec results are consistent with the NMR conclusions regarding the formation of triphenyl hydroxyl groups.

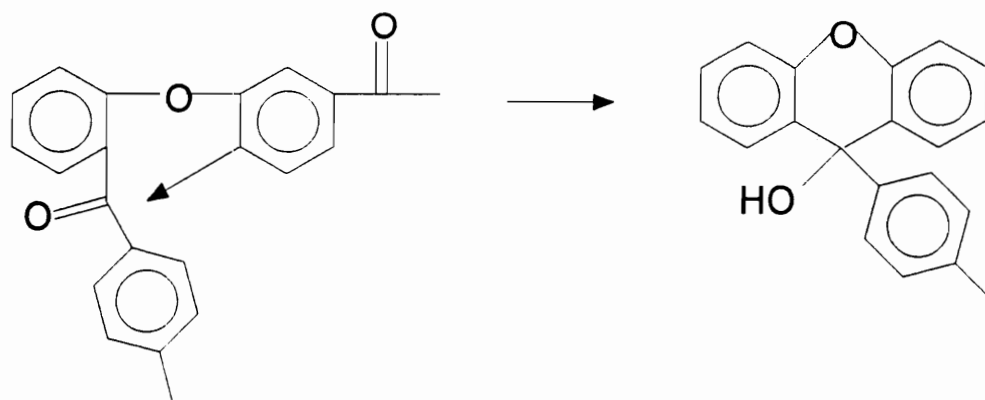


Figure 3.9: Formation of a xanthate type compound from a 1,2 substituted phenyl ring<sup>34</sup>.

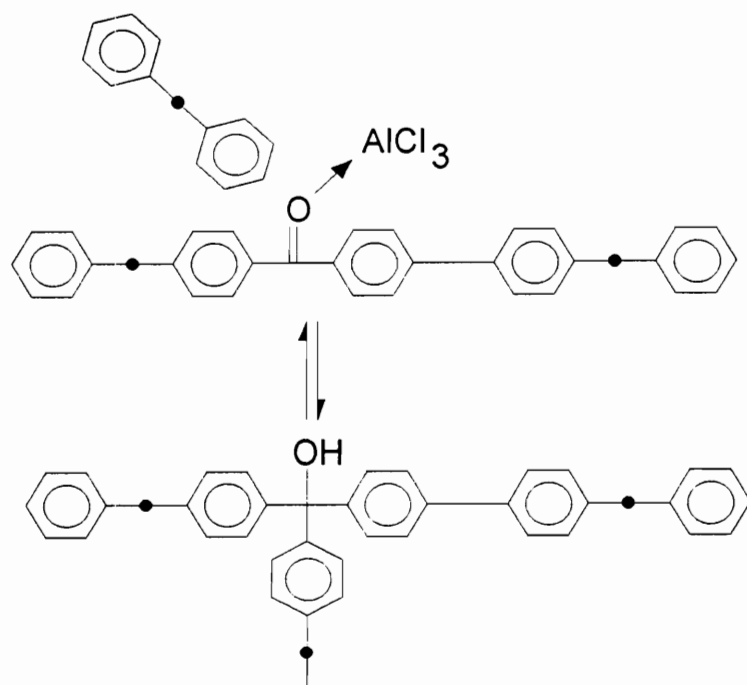


Figure 3.10: Formation of triphenyl hydroxyl group consistent with the  $^1\text{H}$  NMR data.

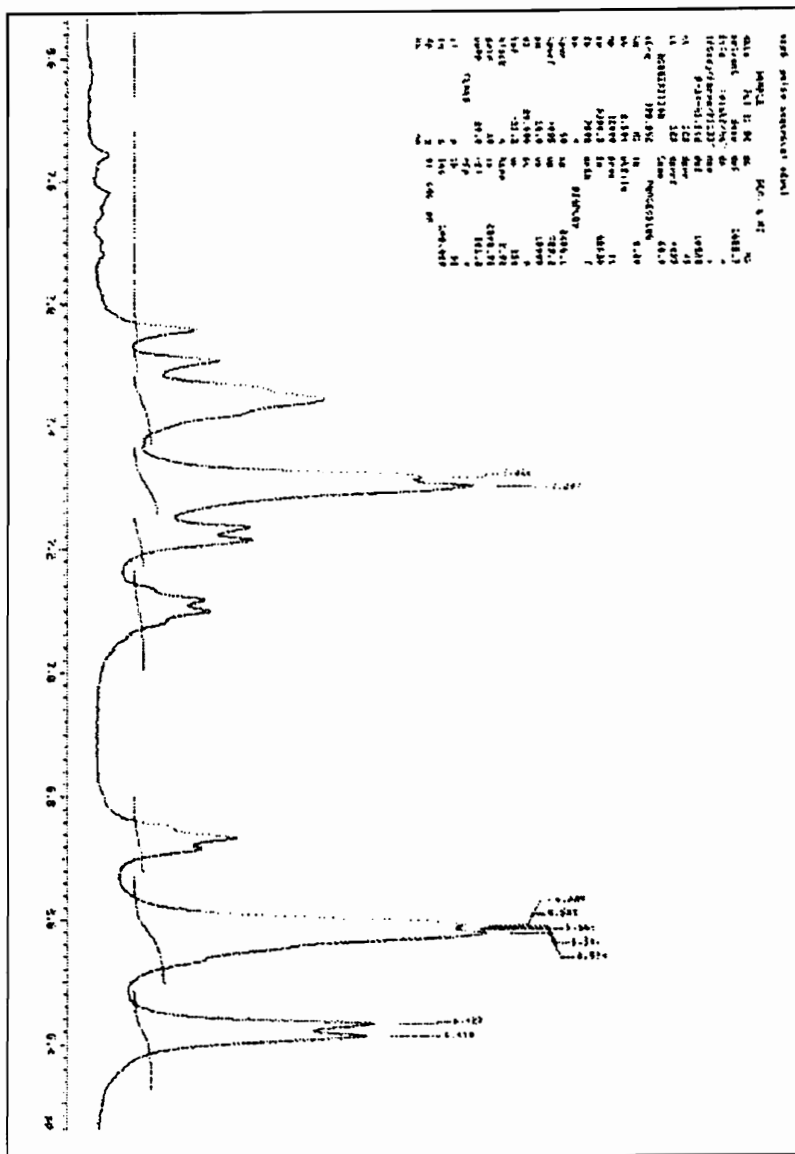


Figure 3.11:  $^1\text{H}$  NMR scan of reaction bath after the prepolymerization step.

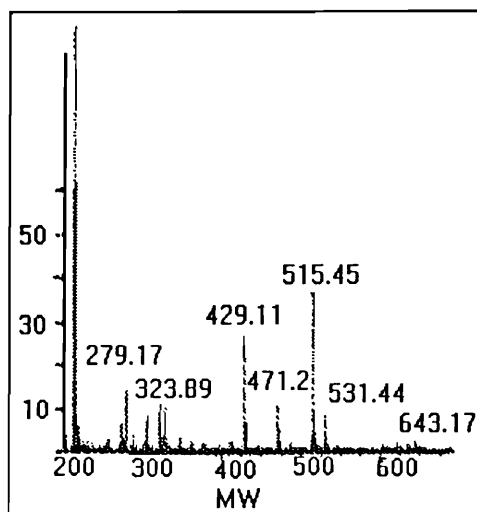


Figure 3.12: Mass Spectroscopy analysis of reaction bath after the prepolymerization step.

Table 3.3: Summary and analysis of Mass Spec signals suggesting the formation of triphenyl hydroxyl groups of the type depicted in Figure 3.10. The triphenyl hydroxyl compound should have an MW of 643 and is detected by the instrument.

SIGNAL MW	SIGNAL STRENGTH	COMPATIBLE COMPOUND & MW
279	moderate	
300	weak	D-T: 301
323	moderate	
429	strong	D-T-AlCl <sub>3</sub> : 430
471	moderate	DTD: 470
515	very strong	
531	weak	
643	faint	D(TD)D: 643

Table 3.4 lists the areas under the three <sup>1</sup>H NMR peaks assigned to the triphenyl hydroxyl type groups for the different PEKK samples. In order to compare them they have been normalized with the area under the doublet at 6.6 ppm. It can be seen that for the samples crystallized with DPE and ICl in the prepolymerization step, the calculated ratio follows the trend ABL 3 > ABL 1 > ABL 5. Therefore it can be deduced that the amount of branching in the linear chain structure in these 3 samples follows the trend ABL 3 > ABL 1 > ABL 5. ABL 5 and ABL 2 demonstrate no detectable traces of branching,

whereas the Random sample demonstrates intermediate amounts of branching. There does not seem to be any apparent correlation between the amount of branching and the blockiness of the samples. These trends, and the reasons affecting them are discussed in more detail in Section 5.1

Table 3.4: Analysis of proton NMR data to estimate the amount of branching type defects in the linear chain structure.

SAMPLE IDENTIFICATION	Ratio of NMR peaks between 5.7 & 6.2 ppm and 6.6 ppm
ABL 1	1.44
ABL 3	1.84
ABL 5	No detectable traces
ABL 2	No detectable trace
Random	0.224

To summarize, a series of PEKK 50/50 samples have been prepared by controlling the prepolymerization step. The composition of the samples (T/I ratio) has been verified using solution proton NMR. The molecular weights, purity etc. have also been characterized using different techniques. Defects in the linear chain system have been quantified using the peaks between 5.7 and 6.2 ppm in the proton NMR scans. It has been demonstrated that among the 3 samples synthesized with DPE and ICl in the prepolymerization step, the amount of branching follows the trend ABL 3 > ABL 1 > ABL 5. ABL 5 and ABL 2 do not demonstrate any detectable traces of branching, whereas the Random sample demonstrates intermediate amounts of branching.

The crystallization and melting behavior of these samples has been characterized and is reported in Chapter 4. These results are discussed in terms of the chain architecture and the synthesis route in Chapter 5.

## CHAPTER 4

# CRYSTALLIZATION AND MELTING STUDIES

### *4.1 Experimental*

The techniques used for studying crystallization and melting include differential scanning calorimetry (DSC), spherulitic growth rate measurements using hot stage optical microscopy, wide-angle X-ray diffraction (WAXD), and small angle X-ray scattering (SAXS). First, the crystallization and melting behavior of the synthesized copolymers was characterized using DSC and optical microscopy. Next, a series of melt crystallized samples were prepared in a hot press. These samples were crystallized at different temperatures. The lamellar morphology, crystallinity, crystalline phase composition, and melting behavior of these samples was characterized using SAXS, WAXD, and DSC techniques.

All spherulitic growth rate measurements were carried out in an Olympus microscope using a Linkam hot stage. Thin films of the copolymer were prepared by melt pressing between a glass slide and a cover slip. The films were equilibrated at 380°C under a light nitrogen purge for about 30 seconds and then quenched at 90°C/min to the

crystallization temperature. Images of the growing spherulites was captured using a Video Monitor and a VCR, and subsequently analyzed to obtain the spherulitic radii vs time. Growth rates were estimated in the linear region well before spherulitic impingement.

All DSC measurements were carried out either in a Polymer Laboratories DSC capable of cooling at 50°C/min or a Perkin Elmer DSC System 7 capable of cooling at 320°C/min. The weight of all samples was maintained between 9 and 11 mg. As polymerized samples were equilibrated at 375°C for 4 minutes and then quenched at fast rates to the crystallization temperature. The sample labeled ABL 2 demonstrates 'rapid' crystallization and was cooled at 320°C/min from the melt in a Perkin Elmer DSC. All other samples demonstrate 'slow' crystallization and were cooled at 50°C/min from the melt in a Polymer Laboratories DSC. After a suitable isothermal hold at the crystallization temperature, the sample was heated at 5°C/min to 385°C. The observed exotherm during crystallization was analyzed to extract the half time for crystallization. For the sample labeled ABL 2, the half time for crystallization could not be estimated because of the absence of any induction time. Therefore, for this sample, the peak time of the crystallization exotherm was used to characterize the crystallization kinetics. The melting scan was analyzed to extract the position and area of the two melting endotherm as depicted in Figure 4.1 a. The area under the low melting peak was estimated by drawing a straight line as shown in Figure 4.1 b.

Additional isothermally crystallized samples were prepared for further DSC and X-ray studies (both SAXS and WAXD). These samples had a nominal dimension of 0.1 mm X 5 mm X 40 mm and were prepared using a combination of two hot presses. As polymerized PEKK 50/50 powder was melted in a suitable mold without any platen pressure at 380°C for 5 minutes and then manually transferred to another hot press maintained at the crystallization temperature. Pressure was gradually increased as the mold cooled to the crystallization temperature. After a long enough hold (at least several



times the half time for crystallization), the mold was quenched to room temperature by transferring to the first hot press (now maintained at room temperature under a water quench). The samples were visually inspected for macroscopic voids. Only samples without any macroscopic voids were used in the SAXS studies.

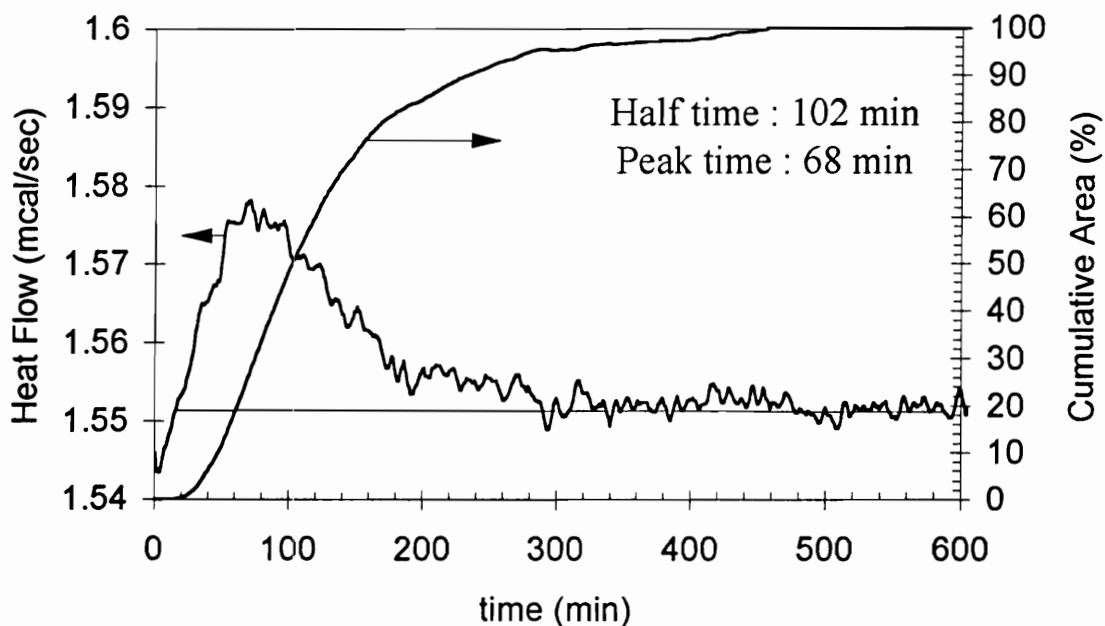


Figure 4.1(a): Tutorial example illustrating the peak time estimated as from the heat flow exotherm; and the half time estimated from the cumulative area plot.

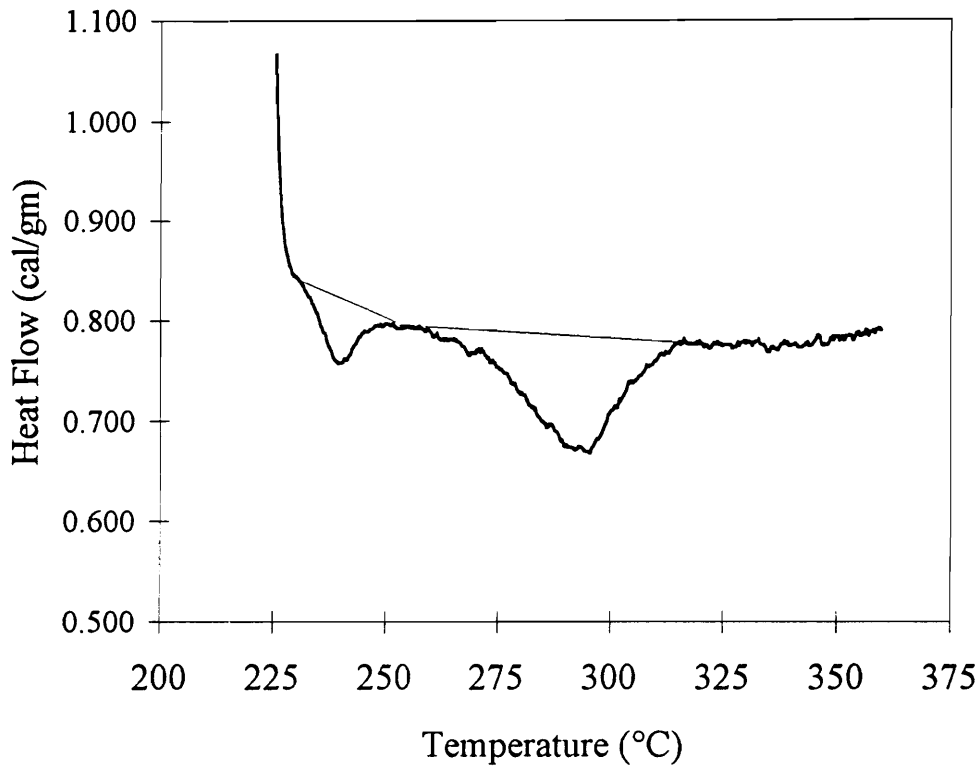


Figure 4.1(b): Tutorial example depicting the baseline used for estimating the heat of fusion of the two endotherms. Sample: PEKK 50/50 ABL 5; Crystallized at 225°C for 6 hrs.

WAXD measurements were carried out either in a Philips or a Nicolet Diffractometer. X-Ray data was collected in the  $5\text{-}37^\circ$  range at intervals of  $0.05^\circ$ . WAXD data was analyzed for the degree of crystallinity and the composition of the crystalline phase following the procedure of Gardner et al. This procedure has already been described in a preceding section (see Figure 2.10 and 2.11 in Chapter 2). Note that the method used for crystallinity estimation is an approximation of the method outlined by Ruland<sup>63</sup>. It does not take into account the loss of intensity of the crystalline peaks due to thermal vibration and other first order crystalline defect. Therefore, the estimated 'crystallinities' are used as an 'index of crystallinity' rather than as an absolute 'degree of crystallinity', with an understanding that the actual crystallinity is higher than the estimate.

SAXS measurements were carried out at the SUNY X3A2 beamline at the National Synchrotron Light Source using modified Kratky optics. Details of the experimental setup of the SUNY beamline have been provided by previous authors<sup>15,16</sup> and will not be discussed here. Briefly, data was collected in the angular range of 0-1.5° using a linear position sensitive detector using a sample to detector distance of 500 mm. Previous authors have demonstrated that the modified Kratky optics can be approximated as a pinhole. SAXS data was analyzed using the correlation function approach outlined by Strobl and Schneider<sup>49</sup>. Details of the data analysis has been described in Section 2.5 and will not be discussed here. Briefly, raw SAXS data was corrected for parasitic scattering. Corrected SAXS data was extrapolated to high angles using a modified Porod law<sup>50</sup> and to low angles using a straight line between the origin and the first useful data point in the Lorentz corrected plot. The extrapolated data was Fourier inversed to obtain the correlation function. From the shape of the correlation function, details of the lamellar level morphology was extracted using the method of Strobl and Schneider<sup>49</sup>.

For the sample labeled ABL 1, SAXS data was collected in a table top Kratky camera using slit collimation. Attempts to analyze the slit collimated data using the Fourier-Bessel transformation approach<sup>51</sup> were unsuccessful. Therefore, the slit collimated data was analyzed as follows: Raw SAXS data was corrected for parasitic scattering and desmeared using the iterative procedure of Glatter<sup>62</sup>. The desmeared data was Lorentz-corrected to obtain intensity vs solid angle. The long spacing ( $L_b$ ) was obtained by applying Bragg's law ( $n\lambda=2L_b\sin\theta$ ) on the maxima in the Lorentz corrected plot. Lamellar thickness was estimated from  $L_b$  by assuming that the interlamellar amorphous layer thickness is 35 Å. This arbitrary number was chosen after the more rigorous correlation function analysis of SAXS data from other samples suggests that the amorphous layer thickness is about 35 Å.

## 4.2 Results

Figure 4.2 depicts the crystallization half times as a function of crystallization temperature for the various PEKK 50/50 samples (Random, ABL 1, 3, & 5). It also depicts the peak times for the sample labeled ABL 2 and the perfectly alternating PEKK 50/50 sample studied by Gardner et al. (The last two samples crystallize too fast for accurate estimations of half times. Therefore peak times are used!). Note that the non-alternating samples crystallize at slower rates than the perfectly alternating sample. Further, for the 3 samples synthesized using the DPE + ICl route in the prepolymerization step, the crystallization kinetics follows the trend (ABL 5 > ABL 3 > ABL 1). Beyond that, there is no apparent correlation between blockiness and crystallization kinetics. For example, the sample labeled ABL 2 crystallizes relatively rapidly whereas ABL 1 and ABL 3 crystallize relatively slowly. Clearly then, there must be additional factors that affect the crystallization kinetics. These factors are discussed in more detail in Section 5.4. Figure 4.3 depicts the growth rates (as determined from hot stage optical microscopy) as a function of crystallization temperature for the different PEKK 50/50 samples. It depicts a similar trend when compared to Figure 4.2. However, there are differences between trends in the growth rate and trends in the overall crystallization kinetics. For example, the sample labeled ABL 2 has a growth rate about 1 order of magnitude lower than that of the perfectly alternating sample, while the overall crystallization kinetics is only slightly lower. These trends have also been discussed in Section 5.4.

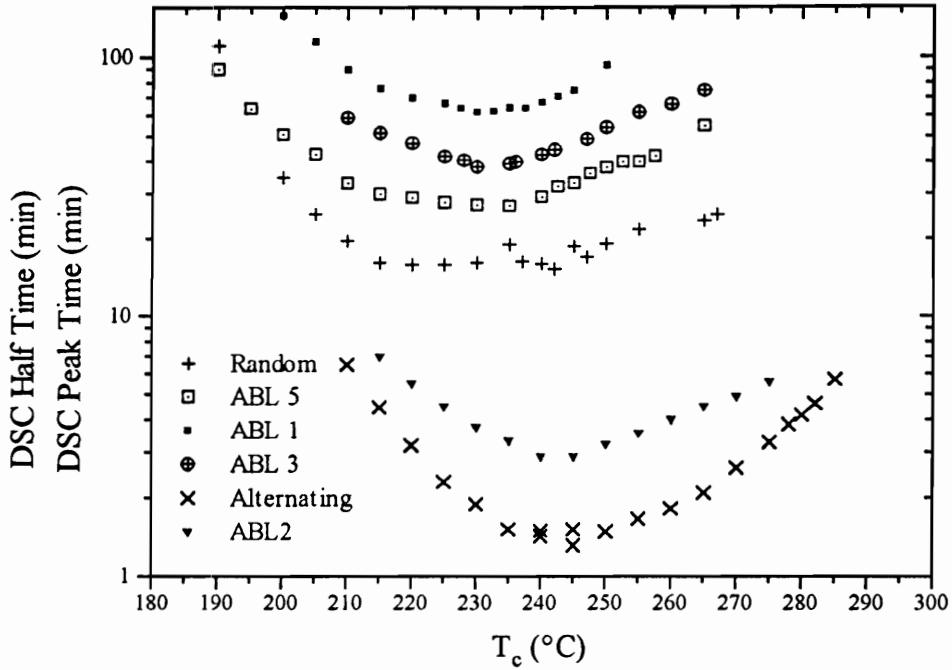


Figure 4.2: Crystallization kinetics as manifest in the DSC half time (ABL 1, ABL 3, ABL 5, and Random) and DSC peak time (perfectly alternating and ABL 2) vs crystallization temperature.

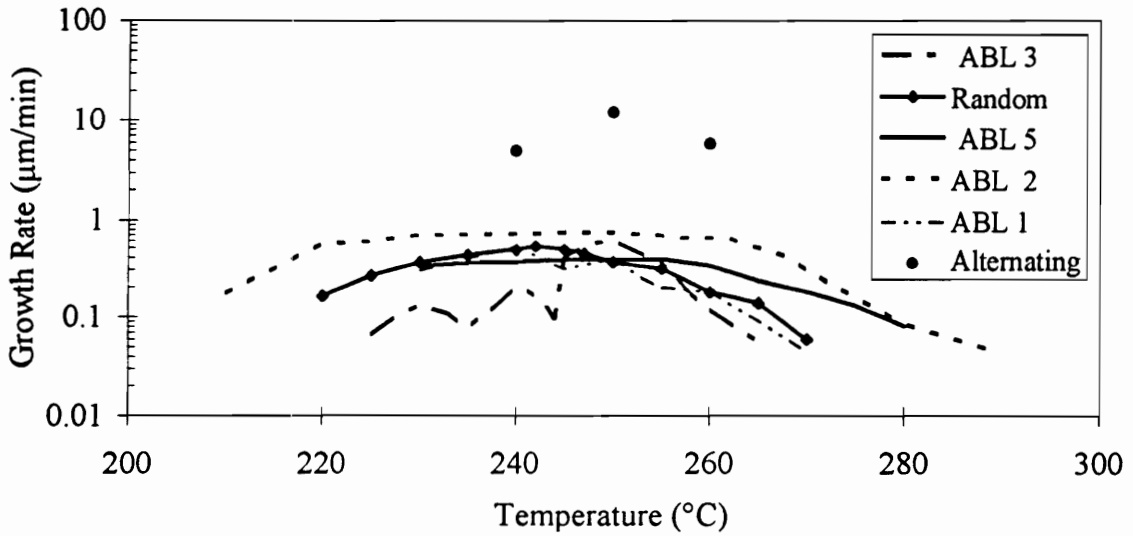


Figure 4.3: Spherulitic growth rate vs crystallization temperature for the different synthesized PEKK 50/50 samples, and also a perfectly alternating sample.

Figure 4.4 depicts the raw SAXS data (plot A) and also the Lorentz corrected SAXS data (plot B) for PEKK 50/50 ABL 3 crystallized at different temperatures. These plots are typical of all the PEKK 50/50 samples. For ABL 1, the lamellar thickness was estimated as  $L_b/35$  Å, where  $L_b$  is the long spacing estimated by applying Bragg's law on the maxima in the Lorentz corrected plot. Raw SAXS data can be Fourier inverted to obtain a correlation function. A typical correlation function is depicted in Figure 2.19. The correlation function can be analyzed using the method of Strobl and Schneider (see Section 2.5) to obtain the long spacing ( $L_c^M$ ) the lamellar thickness ( $l_1$ ) and the amorphous layer thickness ( $l_2$ ). Results of such calculations are depicted in plots A of Figures 4.5 through 9.

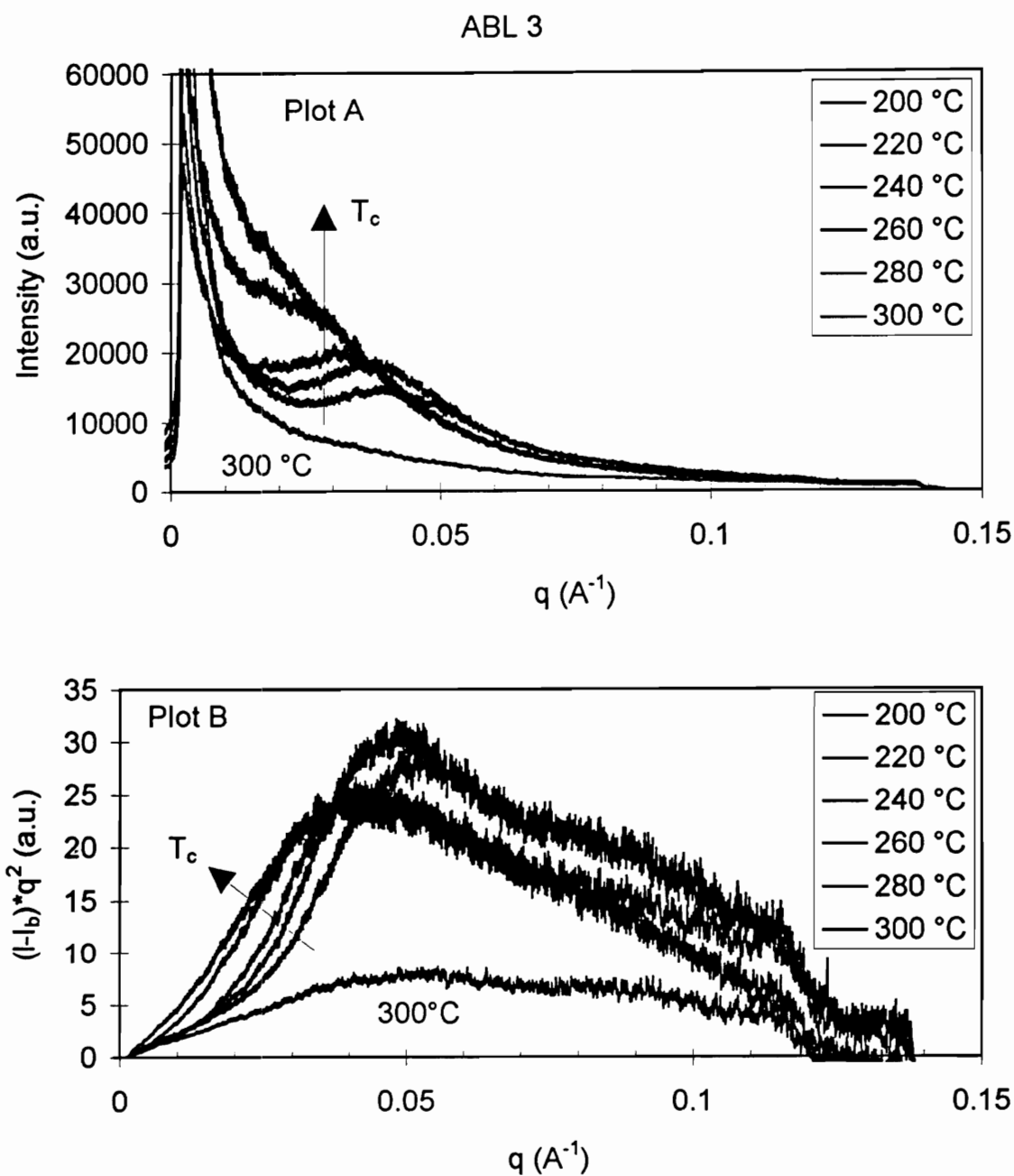


Figure 4.4: Example of raw SAXS data after parasitic correction (plot A) and after Lorentz correction (plot B). Sample: PEKK 50/50 ABL 2 crystallized at different temperatures (arrow indicates increasing crystallization temperature).

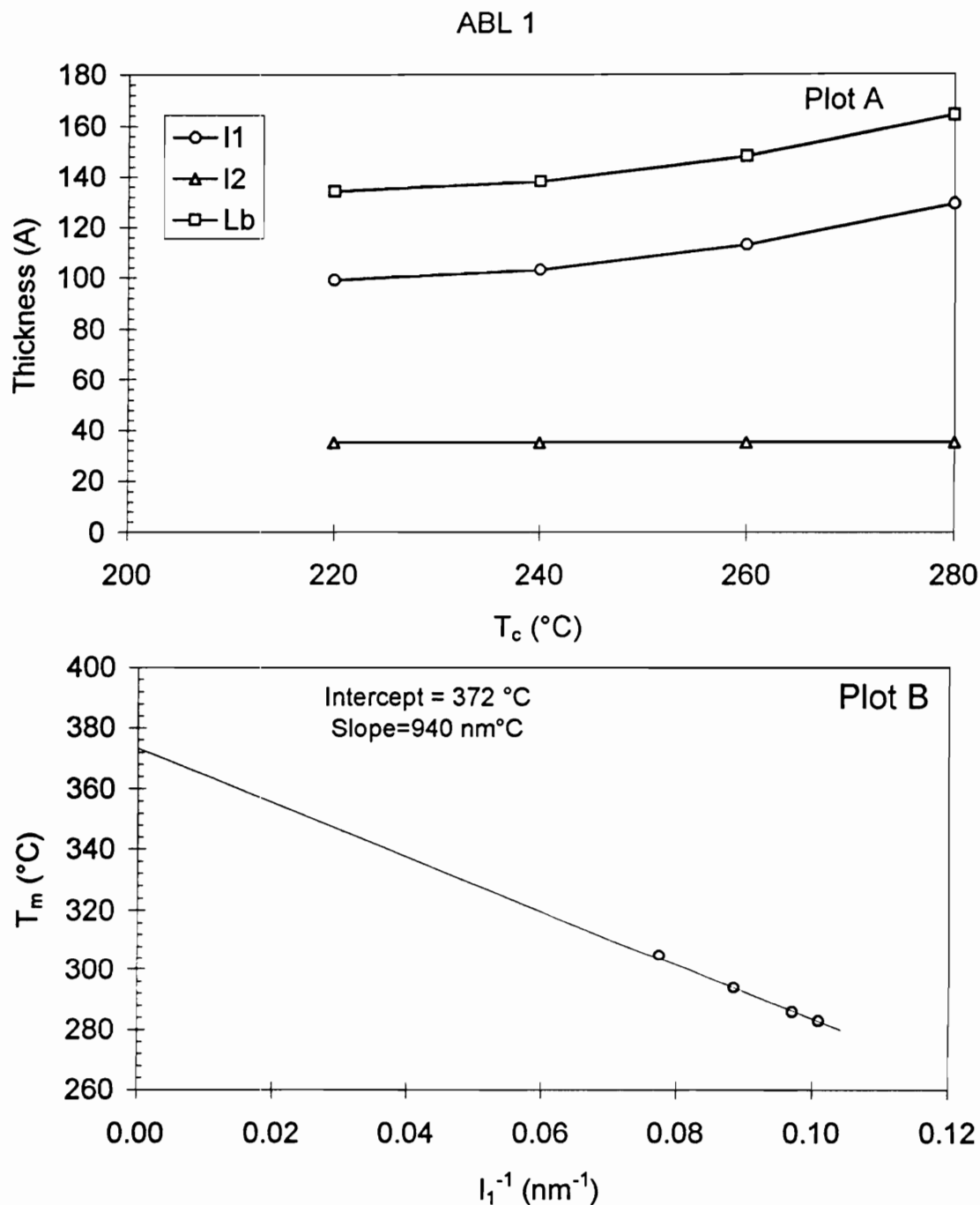


Figure 4.5: Plots summarizing the lamellar variables (plot A) and the Gibbs-Thomson-Tammann plot (plot B) for PEKK 50/50 ABL 1.  $l_b$ ,  $l_1$  and  $l_2$  in plot A refer to the long spacing, lamellar thickness and amorphous layer thickness.  $l_b$  is determined from the maxima in the Lorentz corrected desmeared plot and  $l_1$  is assumed to be 35 Å.



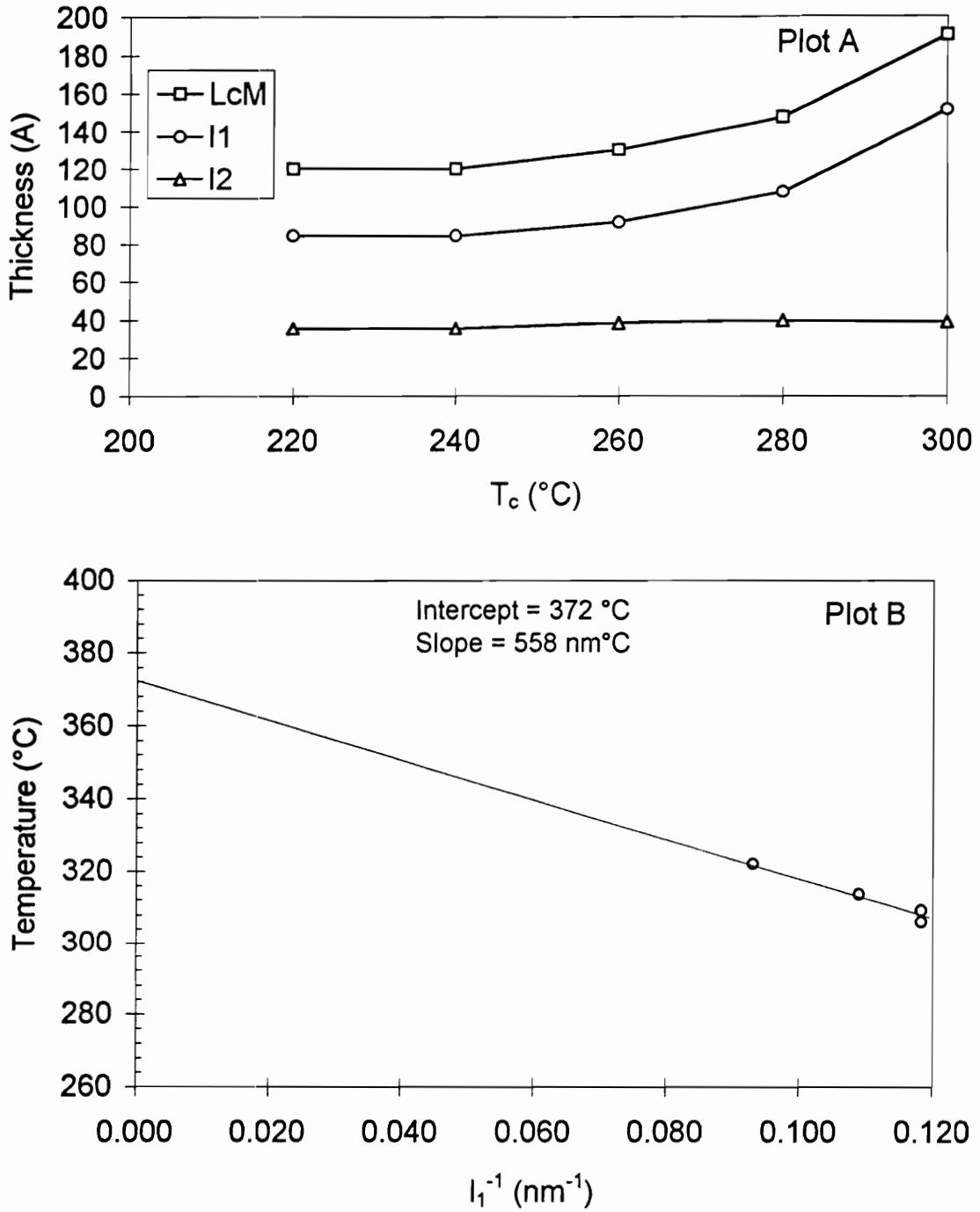


Figure 4.6: Plots summarizing the lamellar variables (plot A) and the Gibbs-Thomson-Tammann plot (plot B) for PEKK 50/50 ABL 2.  $L_c^M$ ,  $l_1$  and  $l_2$  in plot A refer to the long spacing, lamellar thickness and amorphous layer thickness determined from a correlation function analysis.

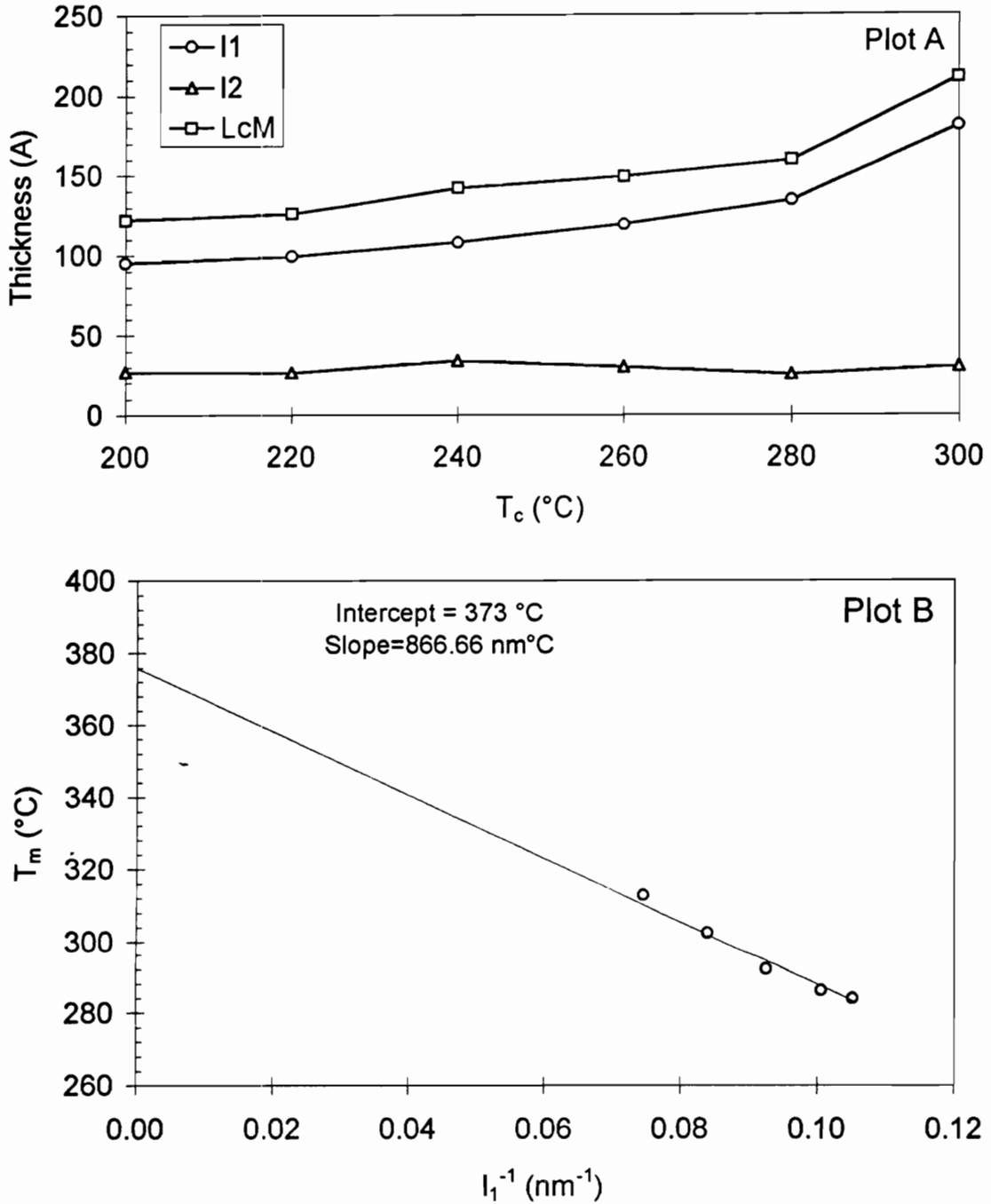


Figure 4.7: Plots summarizing the lamellar variables (plot A) and the Gibbs-Thomson-Tammann plot (plot B) for PEKK 50/50 ABL 3.  $L_c^M$ ,  $l_1$  and  $l_2$  in plot A refer to the long spacing, lamellar thickness and amorphous layer thickness determined from a correlation function analysis.

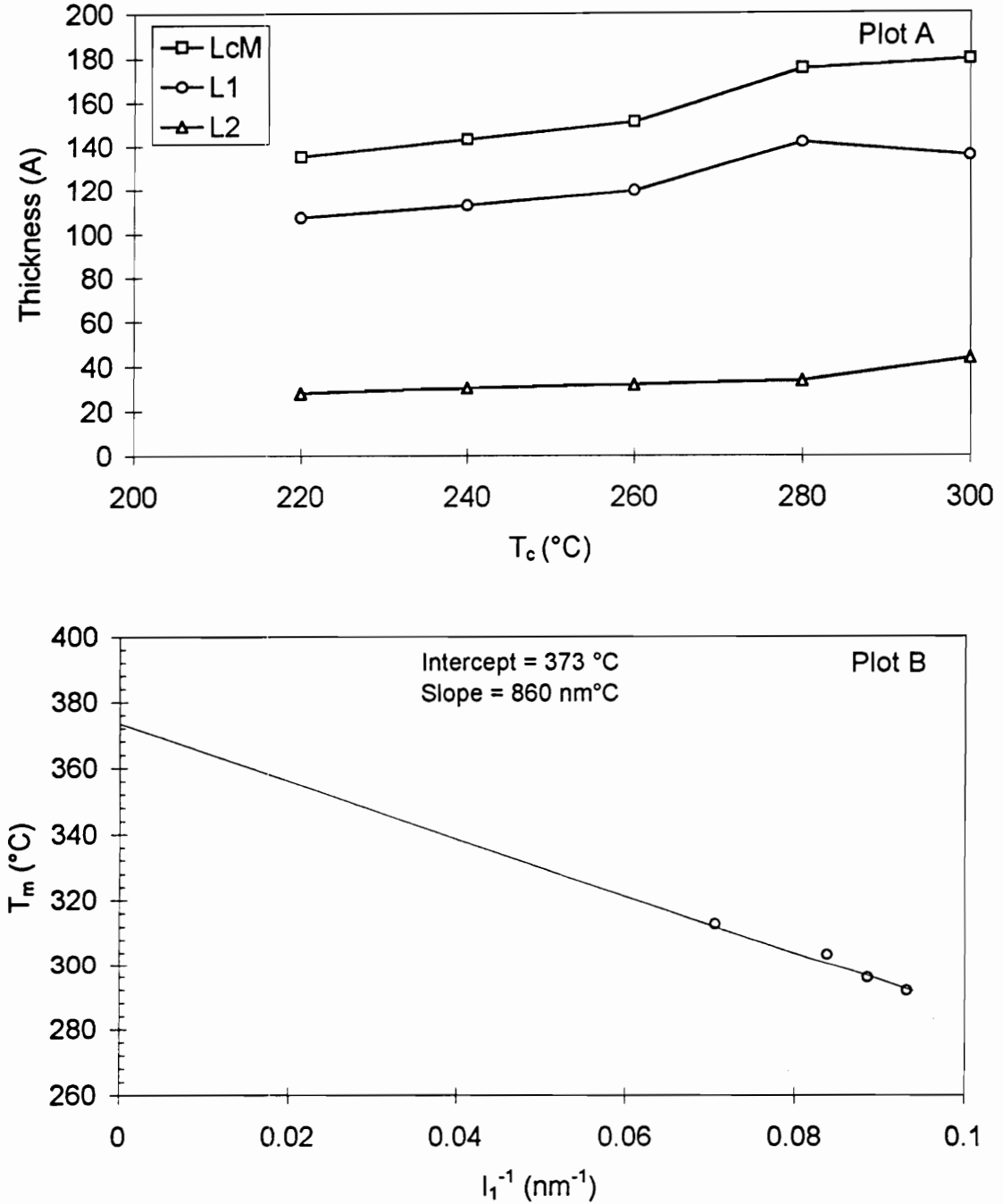


Figure 4.8: Plots summarizing the lamellar variables (plot A) and the Gibbs-Thomson-Tammann plot (plot B) for PEKK 50/50 ABL 5.  $L_c^M$ ,  $l_1$  and  $l_2$  in plot A refer to the long spacing, lamellar thickness and amorphous layer thickness determined from a correlation function analysis. The data point for  $T_c = 300^\circ\text{C}$  has been omitted in plot B.

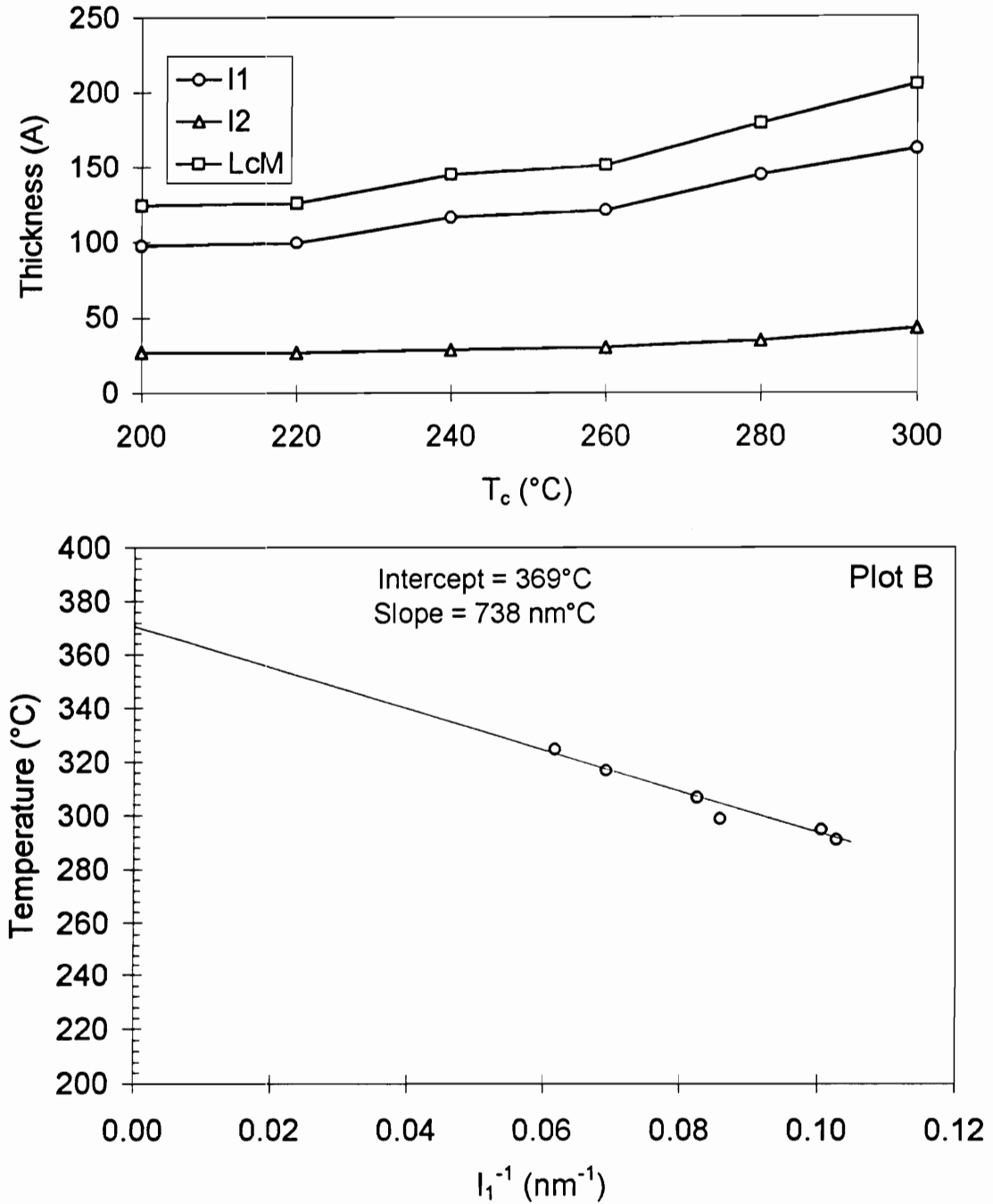
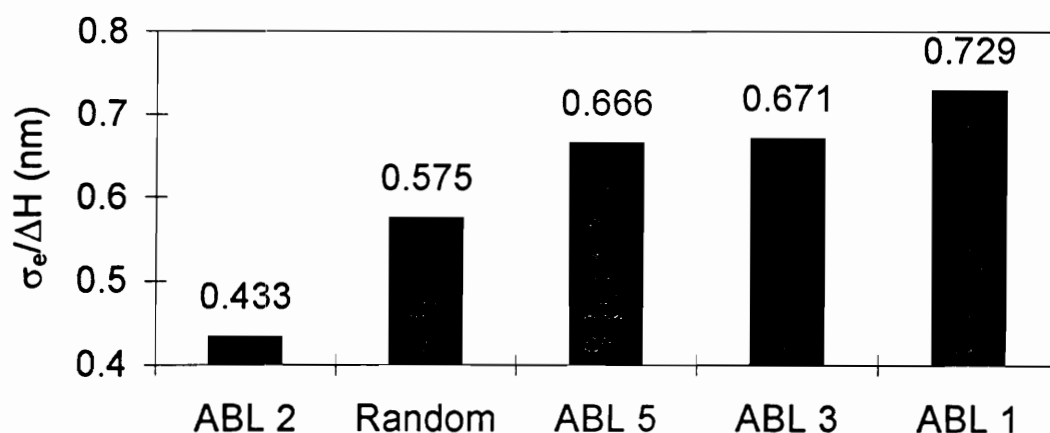


Figure 4.9: Plots summarizing the lamellar variables (plot A) and the Gibbs-Thomson-Tammann plot (plot B) for PEKK 50/50 Random.  $L_c^M$ ,  $l_1$  and  $l_2$  in plot A refer to the long spacing, lamellar thickness and amorphous layer thickness determined from a correlation function analysis.

Plot B in Figures 4.5 through 4.9 summarizes the Gibbs-Thomson-Tammann type extrapolations (see Equation 2.7 in Section 2.6) for the different PEKK 50/50 samples. As already described in Section 2.6, plots of  $T_m$  vs  $1/l_1$ , when extrapolated to the  $T_m$  axis, gives an estimate for the equilibrium melting temperature ( $T_m^{GTT}$ ). Such extrapolations have also been depicted in the 4 plots. From the slope of the extrapolated lines, the ratio of the end surface free energy ( $\sigma_e$ ) to the heat of fusion ( $\Delta H$ ) can be estimated. Figure 4.10 depicts this ratio ( $\sigma_e/\Delta H_f^\circ$ ) for the different PEKK 50/50 samples. Figure 4.11 depicts a  $T_m$  vs  $T_c$  type plot and the Hoffman-Weeks type extrapolation for the different PEKK 50/50 samples. As already described in Section 2.6, the Hoffman-Weeks approach involves extrapolating the high endotherm to the  $T_m=T_c$  line (also depicted in the 5 plots) and gives another estimate for the equilibrium melting temperature ( $T_m^{HW}$ ).

The equilibrium melting temperature determined from both techniques are depicted in Figure 4.12. Note that the Hoffman-Weeks type analysis cannot be rigorously applied to a semi-crystalline copolymer because of changes in crystalline phase composition (and therefore heat of fusion & unit cell parameters) with crystallization temperature. It will be demonstrated in a later section that the uncertainty that results from such considerations is about 13°C. This uncertainty has also been depicted in Figure 4.12. Within this uncertainty, the different non-alternating PEKK 50/50 samples have about the same  $T_m^{HW}$ , and they all have a substantially higher  $T_m^{HW}$  than the perfectly alternating PEKK 50/50 sample. Further, as depicted in Figure 4.12, the estimate for the equilibrium melting temperature from the Gibbs-Thomson-Tammann approach ( $T_m^{GTT}$ ) is higher than the estimate from the Hoffman Weeks approach ( $T_m^{HW}$ ). This discrepancy is due to the underestimation of  $T_m^{HW}$  as discussed in Section 2.6. Also note that the estimated  $T_m^{GTT}$  is nearly constant (~369-375°C) for the different PEKK 50/50 samples studied. These and other factors which affect the equilibrium melting temperature are discussed in more detail in Section 5.3

A WAXS pattern typical of a melt crystallized non-alternating PEKK 50/50 sample has already been depicted in Figure 2.10 in Section 2.2. The WAXS patterns have been fitted with Gaussian peaks (as described in Section 2.2). The area of the fitted peaks corresponding to some crystallographic plane can be divided with the total area of the WAXS pattern to estimate a crystallinity index. The estimated crystallinity index for the different PEKK 50/50 samples is depicted in Figure 4.13. Also, as already discussed, the ratio of the area of the peak at  $18^\circ$  (110 crystallographic plane) and the area of the peak at  $20^\circ$  (111 crystallographic plane  $\sim 18^\circ/20^\circ$  Intensity Ratio) can be used to calculate the composition of the crystalline phase. This ratio has been depicted as a function of crystallization temperature in Figures 4.14 for the different PEKK 50/50 samples. The same ratio for a crystalline phase with 50% and 100% T have also been depicted. Note that for all non-alternating PEKK 50/50 samples, the crystalline phase has about 65% T when crystallized at  $200^\circ\text{C}$  and about 95% T when crystallized at  $300^\circ\text{C}$ . Figure 4.15 depicts the heat of fusion of the two endotherms as a function of crystallization temperature for the different non-alternating PEKK 50/50 samples. **Test samples were held at the crystallization temperatures for durations of several times the half time. Therefore, crystallization time is not a factor and the estimated heat of fusions are reflective of complete crystallization. Based on the observed heat of fusion and crystallinity values, the estimated thermodynamic heat of fusion is about 7 kcal/g. Based on this estimate, and the observed values for heat of fusion vs. crystallization temperature (see Figure 4.15), it can be concluded that the crystallinity decreases as the crystallization temperature increases. These factors are discussed in Sections 5.1 and 5.2.**



**Figure 4.10:** The ratio between the end surface free energy and the heat of fusion for the different PEKK 50/50 samples.

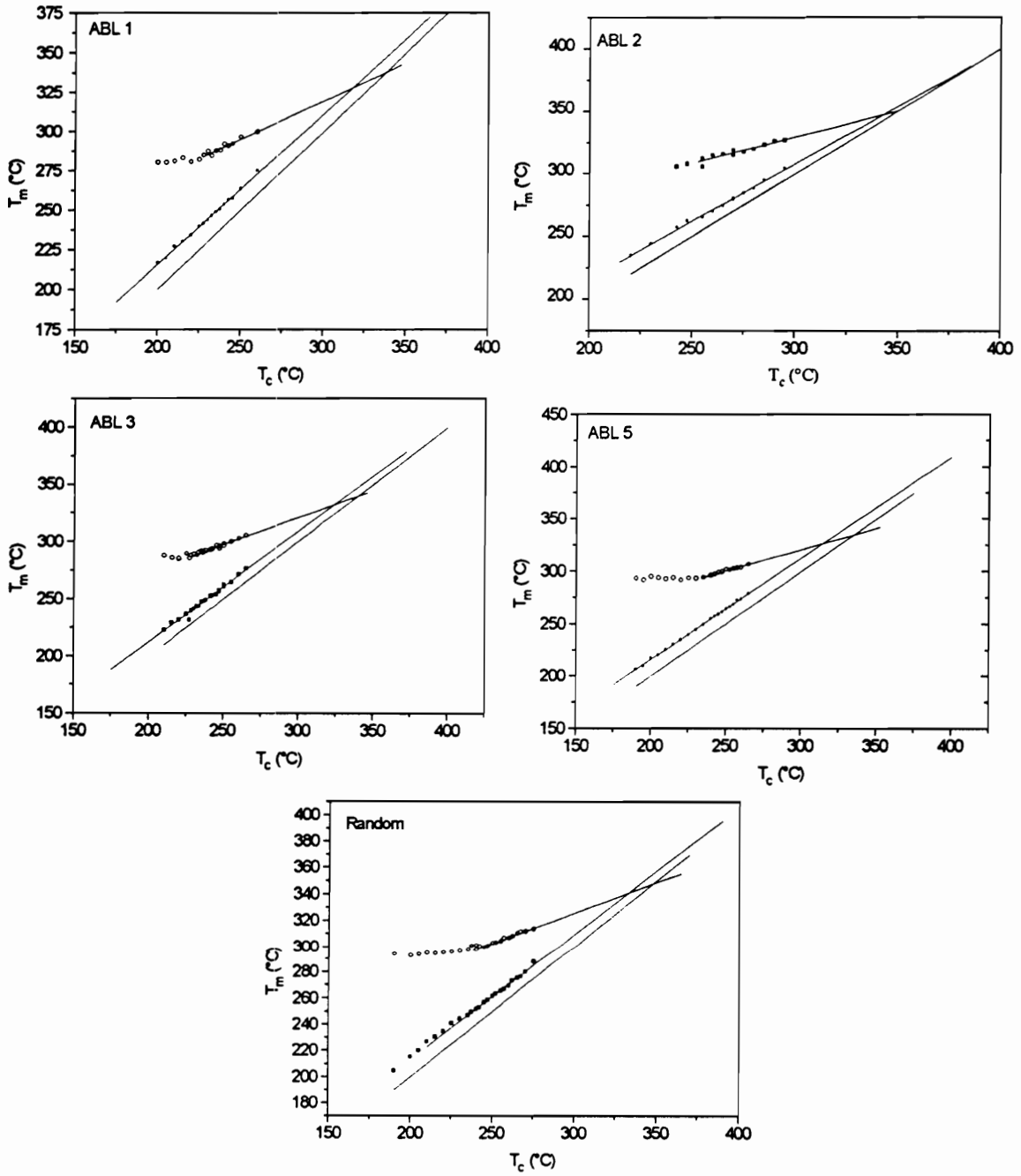


Figure 4.11: The Hoffman-Weeks type extrapolation for the 5 different synthesized PEKK 50/50 samples.



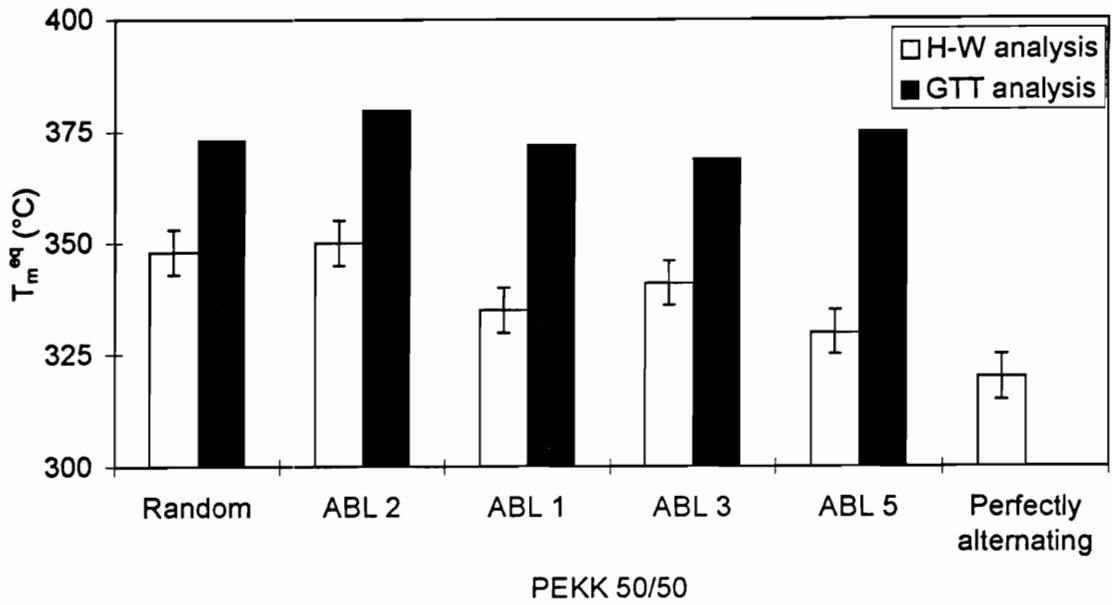


Figure 4.12: The equilibrium melting temperature estimated by the Hoffman-Weeks and the Gibbs-Thomson-Tammann analysis for the different PEKK 50/50 samples.

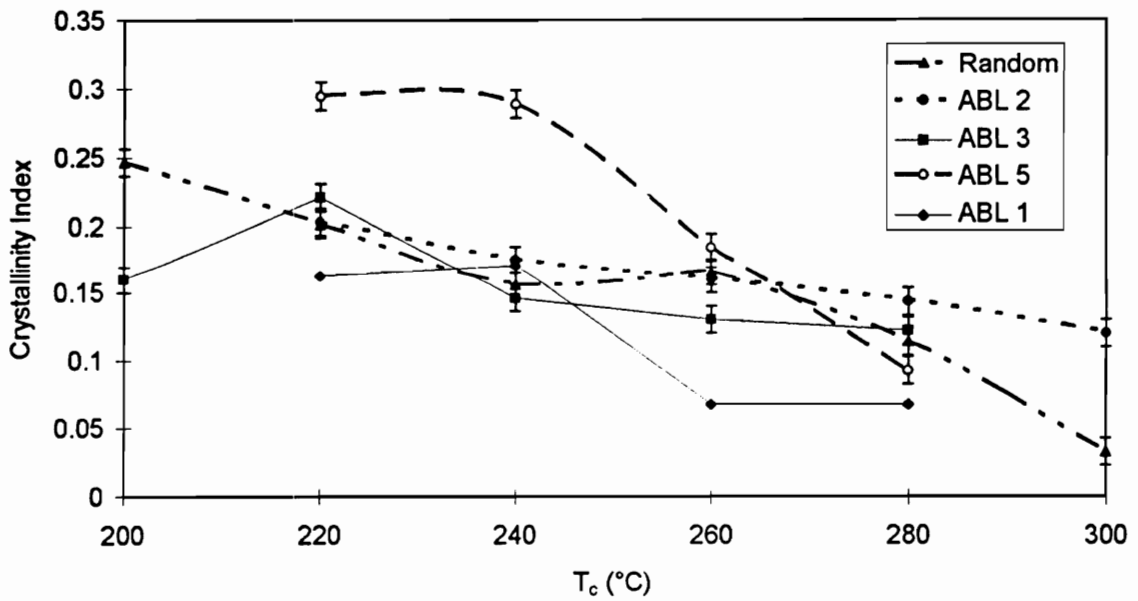


Figure 4.13: The estimated crystallinity index vs crystallization temperature for the different PEKK 50/50 samples.

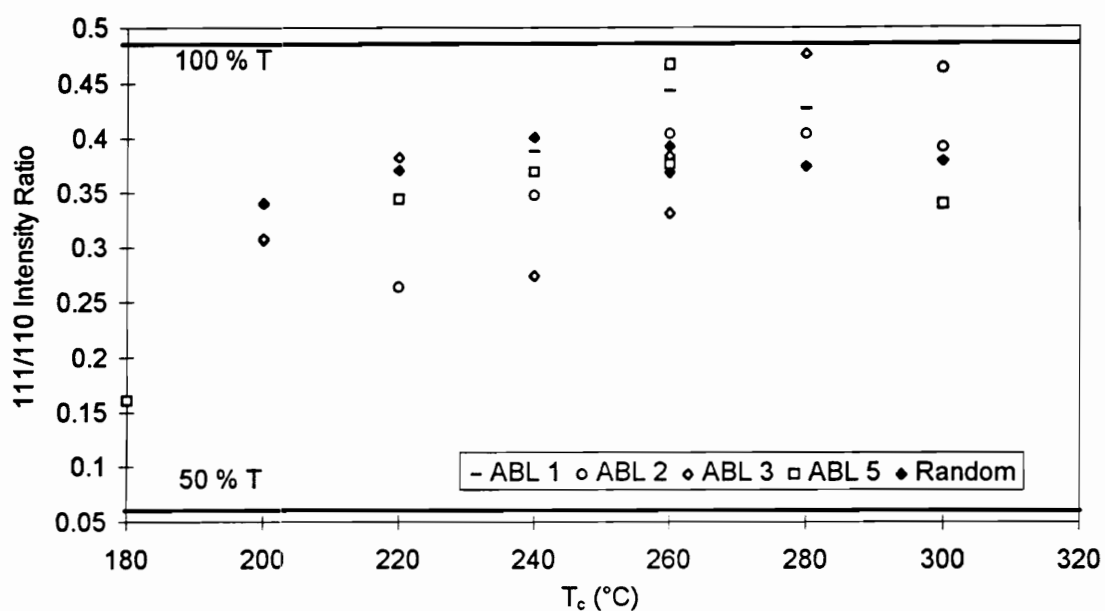


Figure 4.14: The estimated crystalline phase composition vs crystallization temperature for the different PEKK 50/50 samples.

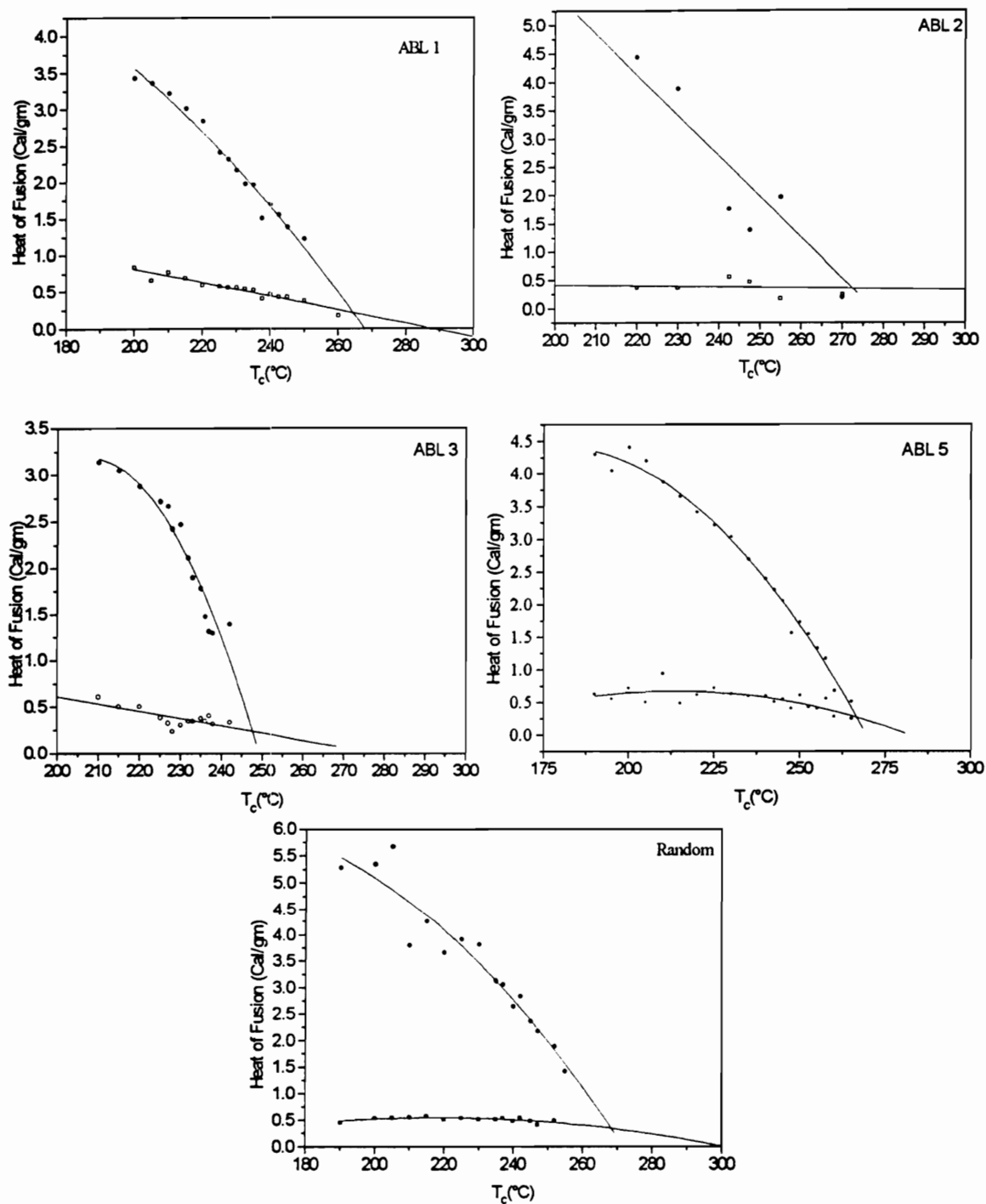


Figure 4.15: The heat of fusion vs crystallization temperature for the different PEKK 50/50 samples. The two traces for each sample are for the low and high endotherm.

## CHAPTER 5

### DISCUSSION

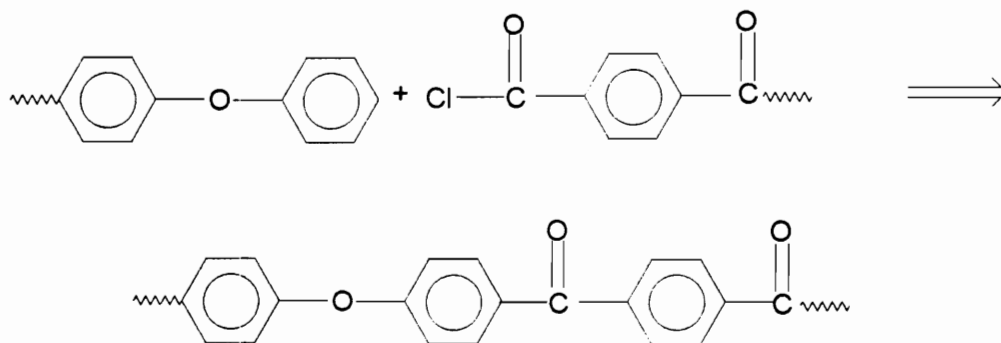
Work done in this study focuses on two issues. The first issue is the effect on the crystallization and melting behavior when the perfectly alternating PEKK 50/50 structure is replaced by non alternating structures. This issue has largely been addressed in the previous section. The second issue deals with the HOW's and WHY's of WHAT happens, and is addressed in this Section. First, a discussion on the defects (branching etc.) expected in the linear chain structure has been provided (Section 5.1). Next, the tendency of the non-alternating samples to exclude the DI monads from the crystalline phase is examined in Section 5.2. This is followed by Section 5.3, which is a discussion on the elevation of melting temperature brought about by the exclusion of such defects. Lastly, the factors affecting crystallization kinetics are summarized in Section 5.4.

Before an analysis of the crystallization mechanism, it might be useful to summarize the experimental observations. In order to study the effect of changing chain architectures on the crystallization behavior of copolymers, a series of non-alternating PEEK 50/50 copolymers were synthesized. The crystallization and melting behavior of these copolymers is compared to that of the perfectly alternating copolymer studied by

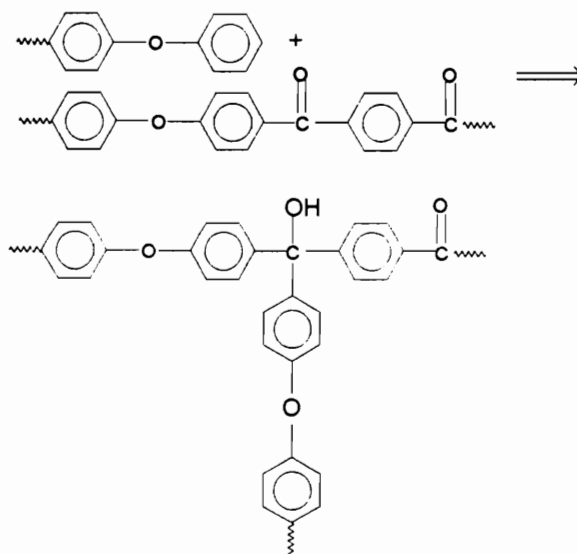
Gardner et al. When the structure is changed from alternating to non-alternating, 3 major effects are observed. First, the crystallization kinetics slows down substantially. Second, the  $T_m^{eq}$  is raised substantially. This increase in  $T_m^{eq}$  does not manifest in faster crystallization kinetics. Finally, the crystalline phase has a substantially lower percentage of defects as opposed to the overall melt.

## 5.1 Linear Chain Defects

During the prepolymerization step, excess amounts of DPE are reacted with either ICl (for ABL 1,3&5) or TCl (for ABL 2) or both (for the Random structure). The desired reaction during this step is of the general type.



However, there are other possible reactions made possible by the fact that the catalyst ( $\text{AlCl}_3$ ) is still attached to the ketone linkages and by the presence of excess amounts of DPE. These side reactions are summarized below:



As suggested by the above scheme, these side reactions will result in a branched type of chain structure. Since these branch points have to be excluded from the crystalline

phase, their presence will affect the crystallization behavior (discussed in more detail in Section 5.4). The triphenyl hydroxyl groups normally result in peaks at a shift of about 6.0 ppm. The NMR scan in Figure 3.3 depicts distinct peaks in this region which are compatible with the above hypothesis. Table 3.1 summarizes the areas of these peaks in comparison with the area of an assigned peak for the different PEKK 50/50 samples.

Note that the samples labeled ABL 5 and ABL 2 do not demonstrate any trace of such branching, while the sample labeled Random demonstrates intermediate amounts (less than ABL 1 and ABL 3). The structure labeled Random was prepared using a prepolymerization step with 4 parts DPE, 1 part TCl and 1 part ICl. In general, it appears that using a high DPE:ICl ratio in the prepolymerization step increases the amount of branching in the final polymer.

It should be pointed out that the difference in crystallization behavior exhibited by ABL 5 and ABL 2 suggests that blockiness is an important factor which affects the crystallization behavior. These trends have been discussed in more detail in Section 5.4.

To summarize, in order to obtain the desired chain structures (with varying Average Block Lengths), the amount of excess DPE in the prepolymerization step has to be controlled. However, this excess DPE results in the formation of branch points in the linear chain molecule. Since these branch points have to be excluded from the crystalline phase, their presence will affect the crystallization kinetics as discussed in Section 5.4.

## 5.2 Defect Exclusion

It has been experimentally demonstrated (see Figure 4.14) that the DI monads (which can be treated as defects) are preferentially excluded from the crystalline phase. Also, the tendency for defect exclusion increases with crystallization temperature. Various factors can be responsible for this behavior. These include thermodynamic factors (such as the enthalpy and entropy associated with defect inclusion), kinetic factors (time available for defect exclusion i.e. crystallization time vs the time scale for motion at the crystallization temperature) and lamellar thickness factors (thicker lamellae will tend to include more defects).

The preferential exclusion of defects can be thermodynamically modeled by the Helfand-Lauritzen Equilibrium theory (H-L theory). Details of the HL theory has been summarized in Section 2.4 and will not be discussed here. Briefly, the HL theory can be used to relate the composition of a crystalline phase with the thermodynamic factors associated with defect exclusion (see Equation 2.1)

From Figure 4.14 it can be seen that for  $T_c=260^\circ\text{C}$ , the crystalline phase composition is about 80% T and 20% I. Further, from the enthalpy of fusion measured from DSC and the crystallinity index measured by WAXD, it is determined that the heat of fusion is about 7kcal/mole. Using these values and Equation 2.1 it can be determined that  $\epsilon=0.7$  kcal/mole. In other words, the energy associated with defect inclusion is about 10% of the heat of fusion of the 100% T PEKK structure. Note that these values are consistent with the melting results obtained by Gardner et al. (see Figure 2.8). They have observed a 12% increase (in Kelvin scale) in the Hoffman-Weeks melting temperature as the overall composition changes from 50%T to 100%T. Using the relation

$$T_m^{eq} = \frac{\Delta H_f^\circ}{\Delta S_f^\circ}$$



and assuming that the entropy change is about constant, a 10% increase in heat of fusion would increase the melting temperature by 10%. This consistency between the expected melting temperature rise and the observed melting temperature rise supports the calculated values for defect inclusion energy.

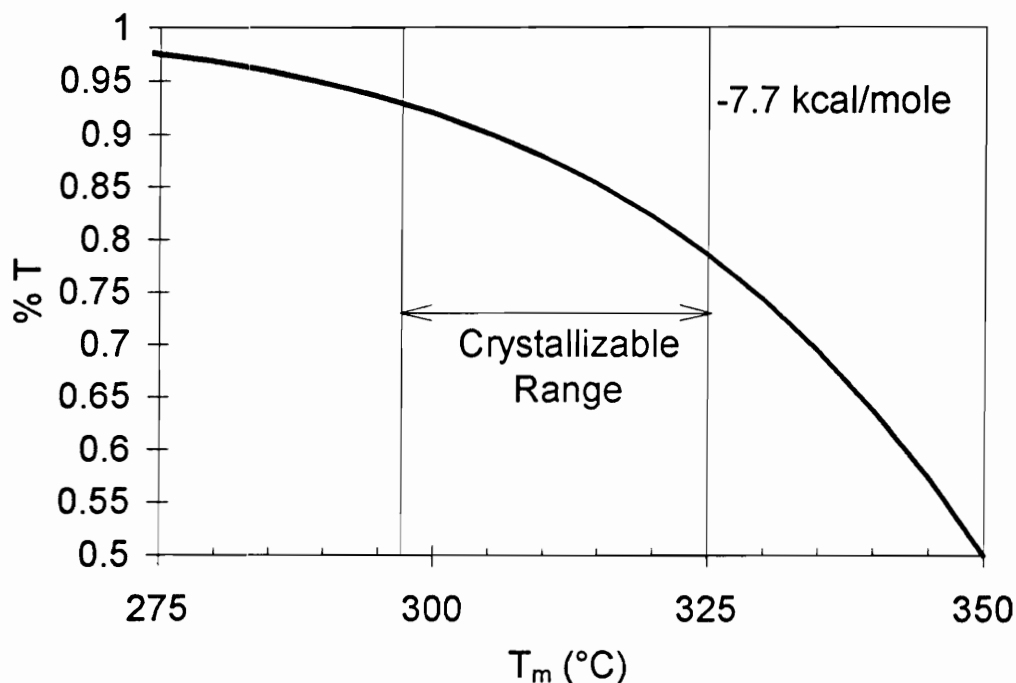


Figure 5.1: Defect exclusion vs melting temperature calculated using the Helfand-Lauritzen equilibrium theory. The values used were (see Equation 2.1 and 2.2)  $\epsilon$  : 0.7 kcal/mole;  $\Delta H_f$  : 7.7 kcal/mole; and  $T_m^{eq}$  : 350 °C.

Figure 5.1 depicts the composition of the crystalline phase as expected from the Helfand-Lauritzen theory and the values discussed above. The trends depicted in this plot can be compared to the experimentally observed trends in the crystalline phase composition as portrayed in Figure 4.14. Note that while the values predicted by the Helfand-Lauritzen theory lie in the same range as the experimental observations, the trends are in the opposite direction. Therefore it can be concluded that while thermodynamic factors play an important role in the exclusion of defects from the crystalline phase, there are other important factors which need to be considered.

Lamellar thickness can also be a factor. For all the copolymers in this study, lamellar thickness ranges from 80 to 140 Å. The length of a chemical repeat unit is about 15 Å. Therefore, a lamellae will consist of 6 to 10 repeat units (depending on the crystallization temperature). Further the average block length of all samples in this study ranges from 1 to 5 and the crystalline phase can contain upto 90% T unit. Therefore, crystallizing lamellae need segments with an average defect free segment length greater than the average block length. Since the exact distribution of the block lengths around the average block length is not known, the effect of lamellar thickness cannot be quantified. However, increasing lamellar thickness will make defect exclusion less favorable. Note that the experimentally observed trends are contrary to this expectation. Also, in the range 180-240°C, the lamellar thickness is about constant, whereas the composition of the crystalline phase changes drastically in this range. Therefore, it can be concluded that lamellar thickness has a minor effect on the exclusion of defects from the crystalline phase.

The only remaining factor in the exclusion of defects is related to the kinetics of crystallization and the time scale for molecular motion. These factors are summarized in Figure 5.2. Note that increasing crystallization temperature decreases the time scale for molecular motion. On the other hand, the crystallization time first decreases and then increases. Also, it has been shown that a crystallizing lamellae grows by the addition of a stem. For the unique case of the partially excluding copolymer being discussed, the stem needs to have a lower percentage of I units than the overall melt. Therefore, the chain adjacent to the growing lamellae needs to move lateral to the growing lamellae such that the stem has a high enough percentage of T units. Therefore, as the crystallization temperature is increased, and as the time scale for molecular motion decreases, the ease of defect exclusion should increase. However, superimposed on that is the effect of the time available for crystallization. As the crystallization temperature is increased, the half time decreases initially (upto about 220°C), then remains about constant (till about 240°C) and then increases as the thermodynamic driving force decreases. As the crystallization time increases, the chain has more time for the lateral motions necessary for defect exclusion.

Therefore increasing crystallization time will also ease defect exclusion. The amount of defect exclusion will be determined by the rate at which the chain can move compared to the crystallization time.

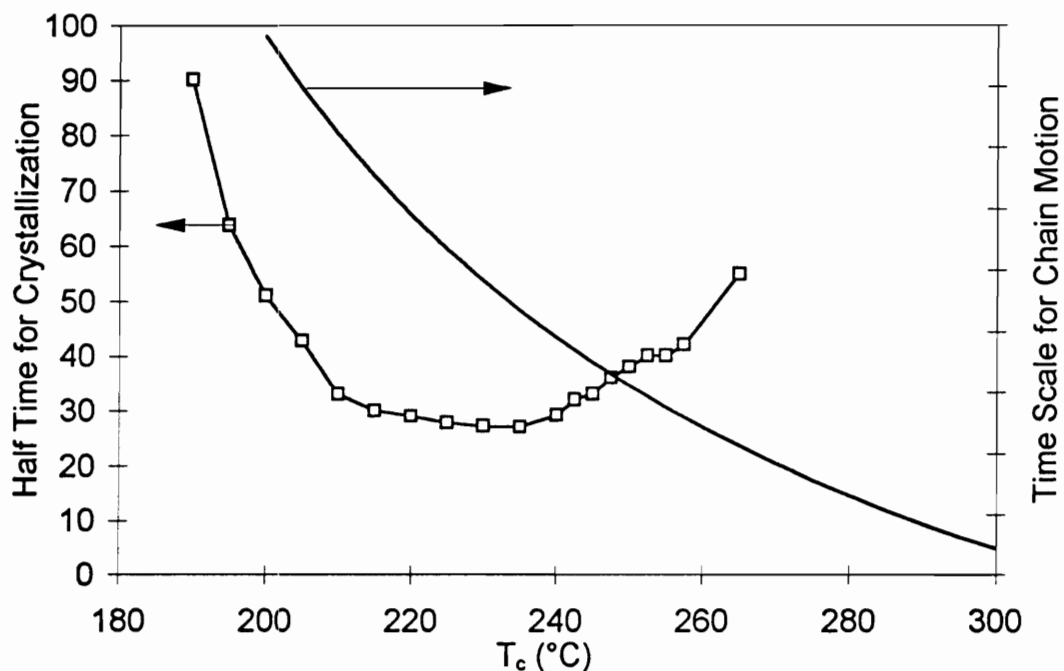


Figure 5.2: Summary of crystallization kinetics and time scale for molecular motion vs crystallization temperature. These factors affect the kinetics of defect exclusion as discussed in the text.

Note that crystallization kinetics is determined by two factors (1) the thermodynamic driving force and (2) the time scale for molecular motion. At temperatures close to  $T_g$ , the time scale for molecular motion is the dominant factor because it increases exponentially as the temperature is decreased. At temperatures close to the equilibrium melting temperature, the thermodynamic driving force (which is inversely proportional to the undercooling) becomes dominant.

Based on the above arguments, the following predictions can be made: (1) if the melt were to crystallize at  $T_g$ , the crystalline phase would have the same composition as the overall melt. This is because the chain adjacent to a growing lamellar tip would not

move in the manner necessary for defect exclusion. Obviously, the melt will never crystallize at the  $T_g$ , but at temperatures close to  $T_g$ , the crystalline phase composition should be close to the overall melt. Note that the experimentally observed data trends (see Figure 4.14) are consistent with this argument. (2) As the crystallization temperature is increased above  $T_g$ , the time scale for molecular motion decreases exponentially. This increases the ease of defect exclusion. In this range, the composition of the crystalline phase increases sharply to about 80% T at about 220°C. (3) Above 220°C, the time scale for motion decreases at a slower rate. Note that the two effects act opposite to each other at temperature below 220°C.

To summarize, the amount of defect exclusion is determined by 3 factors. These are the thermodynamic factors associated with defect inclusion, the factor brought about by changing lamellar thickness (thicker lamellae will obviously tend to include more defects) and kinetic factors like the time scale for chain motion compared to the growth rate of the spherulite. While the thermodynamic factors can be used to explain the amount of defect exclusion, the trends as a function of crystallization temperature are opposite to experimental observations. The effect of changing lamellar thickness cannot be quantified, however, the experimental trends are opposite to that expected from lamellar thickness considerations. Only the kinetic factors can be used to explain the trends in the crystalline phase composition.

### 5.3 Elevation of $T_m^{Eq}$

The equilibrium melting temperature has been estimated from a Hoffman-Weeks analysis ( $T_m^{HW}$ ) as well as the Gibbs-Thomson-Tammann analysis ( $T_m^{GTT}$ ). The Hoffman-Weeks approach has been used to compare the equilibrium melting temperature of the different PEKK 50/50 copolymers with the value reported by Gardner et al. for the perfectly alternating PEKK 50/50 structure. The Gibbs-Thomson-Tammann analysis has been used to estimate the absolute values for the equilibrium melting temperature for the different non-alternating PEKK 50/50 samples. This is because of the errors inherent in the Hoffman-Weeks technique as already discussed in Section 2.5

Note that the Hoffman-Weeks analysis, which is suspect even for homopolymers, cannot be rigorously applied to copolymers for the following reason. As the crystallization temperature changes, the unit cell parameters, the crystalline phase composition and the heat of fusion etc. change. Therefore, lamellae crystallized at different temperatures will have different 'quasi-equilibrium' melting temperatures associated with them. The Hoffman-Weeks approach assumes one equilibrium melting temperature, and therefore cannot be applied to a copolymer. However, it has been shown that for PEKK, the unit cell structure does not change. Further, as the crystallization temperature increases from 220 to 280°C, the composition of the crystalline phase increases from about 70% T to about 80% T. Also, it has been determined that as the overall T/I ratio increases from 50/50 to 100/0, the equilibrium melting temperature increases by about 65°C. Therefore, it can be deduced that a 10% fluctuation (in absolute terms) of the crystalline phase composition will cause an uncertainty of about 13°C in the Hoffman-Weeks analysis. This uncertainty has been incorporated in the Hoffman-Weeks plots depicted in Figure 4.4.

Note that within this error in the Hoffman-Weeks analysis, all the non-alternating samples have about the same equilibrium melting temperature. Further, the equilibrium

melting temperature of all the non-alternating samples are substantially higher than that of the perfectly alternating sample.

The Gibbs Thomson Tammann analysis has also been used to determine the equilibrium melting temperature. As suggested by Equation 2.5, a plot of  $T_m$  vs  $1/l_{av}$  should result in a straight line with slope  $2T_m^{GTT}\sigma_e/\Delta H$  and an intercept on the  $T_m$  axis of  $T_m^{GTT}$ . Figure 4.12 also summarizes the results of the Gibbs-Thomson-Tammann analysis for the equilibrium melting temperature ( $T_m^{GTT}$ ) for the different non-alternating samples (data for the alternating sample is not available). Note that all the non-alternating samples have the same melting temperature (369-373°C) within experimental errors. Further, the underestimation of the experimental equilibrium temperature from the Hoffman-Weeks method ( $T_m^{HW}$ ) when compared to the Gibbs-Thomson-Tammann method ( $T_m^{GTT}$ ) is in the range of 20-45°C, which is in good agreement with the theoretical underestimation depicted in Figures 2.20 & 2.21.

It was stated earlier that the melting temperature elevation is consistent with the observed exclusion of the defects from the crystalline phase. Equations relating the melting temperature of a copolymer to the overall composition, the composition in the crystalline phase, the heat of fusion of the homopolymer and the defect exclusion energy have been developed by Sanchez and Eby<sup>39,40</sup>. Their relation is summarized in 2.3. The values obtained for the heat of fusion (7.7 kcal/mole), the defect exclusion energy (0.7 kcal/mole) and the reported value for the equilibrium melting temperature of PEKK 100/0 (about 405°C)<sup>2</sup> can now be used in Equation 2.3. With a simple calculation, it can be easily demonstrated that the predicted melting temperature for a PEKK 50/50 copolymer with a crystalline phase of PEKK 70/30 is about 375°C. This value is in excellent agreement with the Gibbs-Thomson-Tammann estimate for equilibrium melting temperature for the different non-alternating PEKK 50/50 copolymers. However, the melting temperature for a PEKK 50/50 copolymer with a crystalline phase of the same

composition as estimated from Equation 2.3 is about 370°C. This estimate is substantially higher than the reported value of about 325°C.

The good agreement between the estimated melting temperature and the estimate using Equation 2.3 *for the non-alternating samples* supports the basic thermodynamic approach. However, the discrepancy for the *perfectly alternating sample* is obvious and suggests that equilibrium thermodynamics of Helfand and Lauritzen<sup>38</sup> does not fully describe perfect inclusion. While no definite proof can be provided at this stage, some hypothetical arguments can be proposed to account for this discrepancy. In the perfect exclusion model proposed by Flory<sup>36</sup>, the underlying philosophy is that changes are caused by the requirement of preferential ordering of the copolymer chains. In other words, the effect is entropic rather than enthalpic. In the Helfand-Lauritzen Equilibrium theory<sup>38</sup>, and in the Sanchez-Eby extensions<sup>39-40</sup>, the underlying philosophy is enthalpic rather than entropic. The enthalpic approach assumes that entropic changes can be ignored, and it is possible that this assumption breaks down for cases of perfect inclusion. Another possible reason for the discrepancy is that kinetic factors become dominant for cases of perfect inclusion and the thermodynamic trends in melting temperature are lost.

Note that the estimated melting temperatures for the non-alternating samples can also be explained by the entropic approach (the final equations for melting temperature have a similar form<sup>36-39,64</sup>). It is possible to distinguish between the entropic and the enthalpic approaches if accurate estimates for heat of fusion and crystallinities are available<sup>39</sup>. However, given the errors inherent in any estimate of crystallinity, no such attempts were made in this study.

## 5.4 Crystallization kinetics

The crystallization kinetics are substantially affected by changes in chain architecture. These changes have been depicted in Figures 4.2 and 4.3. The two plots depict the growth rates and crystallization half times vs crystallization temperature for the different PEKK 50/50 samples. Note that the non-alternating samples crystallize at substantially slower rates than the perfectly alternating PEKK 50/50 sample studied by Gardner et al. This decrease in the kinetics of crystallization is contrary to what would have been expected from the observed increase in equilibrium melting temperatures. In this section, the HOW's and WHY's of the crystallization kinetics has been discussed.

The two common parameters that determine crystallization kinetics are glass transition and melting temperatures. At any given crystallization temperature, the first factor affects the mobility of the individual polymer chains and the second factor affects the driving force for crystallization. As already pointed out, the glass transition temperature remains about constant even as the block length is changed. Further, the equilibrium melting temperature determined by the Gibbs-Thomson-Tammann analysis ( $T_m^{GTT}$ ) remains about constant as the average block length is varied. Further, the experimental data suggests that the slowdown in crystallization kinetics is accompanied by an increase in equilibrium melting temperatures. This observation is contrary to theoretical expectations. Clearly, the drastic change in crystallization kinetics must be affected by factors which are not commonly associated with crystallization kinetics.

These factors can include entropy ( $\Delta S_f$ ) and enthalpy of fusion ( $\Delta H_f$ ), lateral surface free energy ( $\sigma$ ) and end surface free energy ( $\sigma_e$ ). An increase in  $\Delta H_f$  would increase the thermodynamic driving force for crystallization, thereby speeding the process. This is contrary to experimental trends. Therefore, it can be concluded that changes in  $\Delta H_f$  is not a major factor in affecting the crystallization kinetics. Also, it can be safely assumed that changes in  $\sigma$  are small and will not affect the crystallization kinetics.



Further, as demonstrated earlier, changes in  $\Delta H_f$  are small. Hence it can be assumed that changes in  $\Delta S_f$  are also small. In any case, most of the entropy change (about 75% for polyethylene<sup>36</sup>) is brought about by changes in the configuration. Therefore  $\Delta S_f$  and  $\sigma$  have been ignored in this study.

The only remaining factor that might explain trends in the crystallization behavior is  $\sigma_e$ . An examination of the slopes in the Gibbs Thomson Tammann plots suggests that  $\sigma_e$  follows the same trend as the crystallization kinetics. Plot A in Figure 5.3 summarizes  $\sigma_e$  for the different PEKK 50/50 samples. The Figure also includes a plot depicting the half time or the peak time (Plot B) for the different PEKK 50/50 samples. As Figure 5.3 depicts, the end surface free energy correlates well with the crystallization kinetics. Note that there is considerable uncertainty in estimating the lamellar thickness through the SAXS correlation function approach (see Section 2.5). Therefore the above correlation might be within the errors associated with the techniques. However, given that trends in crystallization kinetics cannot be explained by any other factor, it is likely that the observed correlation between  $\sigma_e$  and the crystallization kinetics is real. Also note that there is an approximate correlation between the branch ratio as estimated from <sup>1</sup>H NMR analysis and the estimated end surface free. A higher branch ratio seems to result in a higher end surface free energy.

Lastly, note that blockiness also affects crystallization kinetics. This is illustrated by the samples labeled ABL 2 and ABL 5, and the perfectly alternating sample studied by Gardner et al.<sup>2</sup> (all 3 do not demonstrate any trace of branching). The crystallization kinetics in these samples follows the trend ALTERNATING > ABL 2 > ABL 5. Therefore, it can be concluded that increasing block lengths results in slower crystallization kinetics. Changes in the  $\sigma_e$  have to be related to changes in the architecture of the linear chain. The ultimate origin of these changes probably lie in a mechanism related to secondary nucleation. However, at this stage no definite conclusions can be made about the exact mechanism.

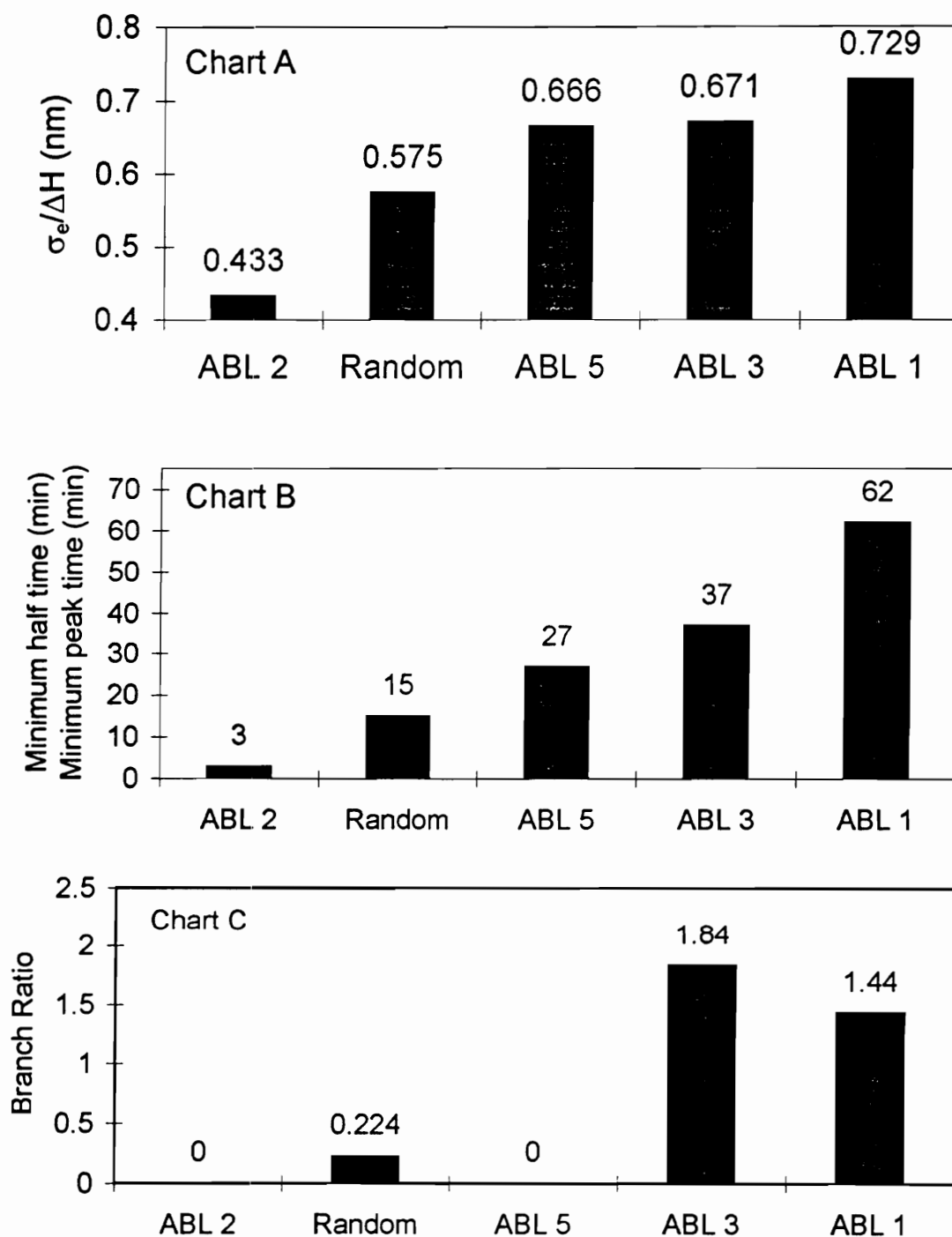


Figure 5.3: Summary of the end surface free energy as determined by the GTT analysis (Chart A); the crystallization kinetics as determined by DSC studies (Chart B) and the branching ratio estimated from  $^1\text{H}$  NMR (Chart C).

## CHAPTER 6

### CONCLUSION

The crystallization and melting behavior of a partially excluding copolymer (PEKK 50/50) has been studied. A series of copolymers with the same overall composition (PEKK 50/50), but with varying chain architectures within that composition has been synthesized. The chain architecture was manipulated by varying the diphenyl ether to isophthaloyl chloride ratio (DPE:ICl ratio) in the prepolymerization step so as to obtain average block lengths (ABL) of 1,3&5. Because of the unique synthesis route, the 3 samples have different amounts of branching which follow the trend  $ABL\ 3 > ABL\ 1 > ABL\ 5$ . The sample labeled ABL 3 demonstrated the highest amount of branching while the sample labeled ABL 5 did not demonstrate any trace of branching. An additional copolymer was prepared by using a DPE:TCl ratio of 3:2 in the prepolymerization step (ABL 2). This copolymer also did not demonstrate any trace of branching. Another copolymer was prepared by using both ICl and TCl along with DPE in the prepolymerization step. This copolymer demonstrates intermediate amounts of branching and is expected to result in a random type of chain structure. In general, it appears that

increasing the DPE:ICI ratio in the prepolymerization step increases the amount of branching in the final copolymer.

The crystallization and melting behavior of these copolymers was studied and compared with the reported behavior of a perfectly alternating PEKK 50/50 copolymer. The following interesting features were observed:

1. The crystallization kinetics is slowed for all non-alternating copolymers. This slowdown in crystallization kinetics is attributed to changes in the blockiness of the copolymer *and* to the presence of branches in the linear chain structure. It appears that the presence of branches is aggravated by use of a high DPE:ICI ratio in the prepolymerization step. The presence of these branch points increases the end surface free energy, thereby decreasing the spherulitic growth rates by about 1-2 orders of magnitude.

2. The crystalline phase substantially excludes the DI monads in all non-alternating PEKK 50/50 samples. The exclusion of such monads is more prominent at higher crystallization temperatures. The driving force for the exclusion of such DI monads is the change in the  $\Delta H$  term associated with the inclusion of such monads in the crystalline phase. The tendency for defect exclusion increases with increasing crystallization temperatures because the time scale for molecular motion decreases at a faster rate than the time available for crystallization. From an analysis of the composition of the crystalline phase when crystallized at 260°C, it was estimated that the enthalpy change for crystallization decreases by about 10% when a DT monad is replaced by a DI monad. This value compares well with the reported increase in equilibrium melting temperatures (of about 12%) when the overall composition is varied from PEKK 50/50 to PEKK 100/0.

3. Because of the exclusion of such DI monads from the crystalline phase, the equilibrium melting temperature of all the non-alternating copolymers is substantially higher than that of the perfectly alternating copolymer. The equilibrium melting

temperature lies in the range of 335-360°C (as estimated by Hoffman-Weeks analysis) and 369-375°C (as estimated by Gibbs-Thomson-Tammann analysis) for all non-alternating samples. This compares with the values of 320°C and 375°C obtained by Gardner et al. (Hoffman Weeks analysis) for perfectly alternating PEKK 50/50 and PEKK 80/20 respectively. Note that in the range of temperatures used for the Gibbs-Thomson-Tammann analysis, the crystalline phase has a composition of about PEKK 80/20, which is compatible with the values obtained by Gardner et al.<sup>2</sup>.

4. This increase in equilibrium melting temperature will tend to increase both the nucleation and the growth rates of the non-alternating samples. However, the growth rates are slowed down by the presence of branch points in the linear chain structure. Therefore, the overall effect on the crystallization kinetics can be summed up by two factors. First, the nucleation rate (which was not measured!) should increase because of the increase in the equilibrium melting temperature. Secondly, the growth rate which decreases because the presence of branch points. The overall effect on the crystallization rate is dominated by the presence of branches. Therefore, the crystallization rate decreases with increasing amounts of branching in the linear chain.

The objective of this dissertation is a better understanding of the crystallization and melting behavior of copolymers. Towards this end, a series of copolymers with the same overall composition, but with varying chain architectures were synthesized. While the value of the final results are diluted somewhat by the presence of branch points in the linear chain structure, some definite conclusions have been made. These have been listed below:

1. Data presented in this paper supports the simplistic Flory<sup>36</sup> model for the crystallization behavior of copolymers consisting of crystallizable and non-crystallization comonomers. Following his arguments, at temperatures slightly below the equilibrium melting temperature, the requirement of large lamellae for crystallization and the ensuing

requirement of very long blocks free of non-crystallizing monads would drastically reduce the degree of crystallinity. As the crystallization temperature is reduced, this requirement of large lamellae, and the ensuing requirement of long blocks free of non-crystallizable monad is relaxed. Therefore, the degree of crystallinity should rise as the crystallization temperature is decreased. Indeed, the estimated crystallinity does rise as the crystallization temperature is decreased.

2. The Helfand-Lauritzen<sup>38</sup> equilibrium theory is useful in describing several aspects of the crystallization and melting behavior. However, the equilibrium theory starts deviating from reality and kinetic factors become important when the trends are examined in detail. It is always useful to understand the extent of validity of the equilibrium theory. The equilibrium theory can predict the average exclusion of the defects from the crystalline phase. It can relate the crystalline phase composition to the melting temperature. However, it cannot model the trends in the crystalline phase composition vs crystallization temperature plot. Also, it cannot model the limiting case of perfect inclusion.

3. Kinetic factors play an important role in determining trends in the crystalline phase composition vs crystallization temperature. The experimental trend of increasing exclusion with increasing crystallization temperature can only be explained when kinetic factors (such as the time scale for chain motion vs the crystallization time) are taken into account. Also, In the limiting case of perfect inclusion, the entropy effects probably become important, which probably accounts for the breakdown of equilibrium thermodynamics based on enthalpic affects.

4. The architecture of the linear chain affects the kinetics of crystallization. This can be definitely concluded by comparing the ALTERNATING sample with ABL 2 and ABL 5. These samples have drastically different crystallization behavior, although they do not demonstrate any traces of branching. In general, larger blocks in the linear

chain results in slower crystallization kinetics. This slowdown in crystallization kinetics is probably related to a secondary nucleation mechanism. However, at the current level of understanding, no definite conclusions can be made about the exact fundamental origin of the slowdown.

5. Branching in the linear chain also affects the crystallization kinetics. Samples with more branches tend to crystallize slower than samples with less branching. Further, both branching and linear chain architecture affect the crystallization kinetics via the end surface free energy. Increased amounts of branching and increased lengths of the blocks in the linear chains translate into a higher end surface free energy, which then translates into slower crystallization kinetics.

## CHAPTER 7

### FUTURE WORK

The objective of this dissertation is a better understanding of the factors which affect copolymer crystallization and melting. The quality of that “understanding” is a function of the quality of the samples used, the kind of tests performed on those samples and the quality of the data analysis procedures employed. Improvements can be made in each of these departments. With that in mind, some thoughts on possible avenues for future research have been listed in this chapter. First, the factors which might affect the quality of the synthesized samples are discussed. That is followed by a discussion on the kind of tests and the data analysis procedure that should be employed.

Since branching in the linear chain structure follows the same trend as chain architecture, it is hard to separate the effect of one from the other. However, there are a few conceivable approaches around this problem. All of them involve novel synthesis routes. Some of these approaches were tried out during the course of this study and were determined to be unfeasible. All of these are listed below, along with any relevant comments.



1. The first approach involves synthesis of PEKK 50/50 from a derivative of the 2 step route used by Gardner et al<sup>2</sup>. Gardner et al. chain extended DTD with ICl (which therefore results in a perfectly alternating structure). Similar routes have been described by Gay et al<sup>11</sup>. In order to synthesize non-alternating structures, various amounts of DID and DTD can be chain extended with appropriate amounts of ICl and TCl. While the resulting PEKK 50/50 structure should be non-alternating, there would be no a-priori way of predicting the average block length (which is why the direct method was chosen for this study). However, this synthesis route would result in less defects in the linear chain structure.

2. Another approach would be synthesis of PEKK 50/50 using two different subsets of the direct method. The first would involve DPE and TCl in the prepolymerization step. The second would involve DPE and ICl. Since the DPE + TCl route is expected to result in a smaller amount of chain defects, it is conceivable that the effects of blockiness could be separated from that of branching. Unfortunately, attempts to proceed along these lines were unfruitful because of premature precipitation of long blocks of DT units during the prepolymerization step. Further, it is possible that branching will alter the average block length of the copolymer. Therefore, no definite conclusions would be extracted from that study.

3. The last approach involves synthesis of blocks of DT and DI of predetermined length. These blocks could then be purified, isolated and reacted together so as to result in PEKK 50/50 with known, monodisperse block lengths. These copolymers would also have the added advantage of being virtually defect free. And while this approach is the hardest in terms of the synthesis route, it would result in very powerful information on copolymer crystallization.

Once the desired copolymers are synthesized, they can be studied using similar thermal and scattering techniques. In addition, the glassy-liquid transition can be

characterized using techniques such as dynamic mechanical analysis (DMA); dielectric thermal analysis (DETA) etc. However, each of those techniques need improvements so as to enable stronger conclusions. These have been listed below:

1. Crystallinities were estimated from WAXD data using a simple peakfitting procedure outlined in Section 2. While this procedure suffices in giving an estimate for the crystallinity (or a crystallinity index), it does not correct for incoherent scattering, thermal motion and other lattice defects. In future analysis of WAXD data, the method outlined by Ruland<sup>63</sup> should be employed. Ruland's method gives an estimate for absolute crystallinity and also a parameter  $k$  related to thermal motion and lattice defects. It is likely that  $k$  will be affected by the presence of -DI- monads within the crystalline phase. Therefore, employing Ruland's method on WAXD data would give more accurate and precise estimates for crystallinity, and potentially, the amount of defects within the crystalline phase. Ruland's method requires more information (such as WAXD data collected over larger scattering angles) and is difficult to implement. However, the benefits should potentially outweigh the effort. For example, accurate estimates of crystallinities would enable a distinction between the entropic and enthalpic approaches<sup>39</sup>.

2. The Gibbs-Thomson-Tammann analysis for melting temperature and end surface free energy relies on the accuracy of the estimated lamellar thickness. This in turn relies on the SAXS data analysis procedure. While the analysis procedure employed in this dissertation is pretty rigorous for the available data, better estimates can be obtained by collecting SAXS data to higher angles (e.g.  $2\Theta$  of  $5^\circ$ ). Further, if samples covering a larger range of lamellar thickness is available, then the accuracy of the extrapolation will increase. Therefore future studies should concentrate on the synthesis of two types of samples. (1) Samples which demonstrate crystallization kinetics fast enough to enable crystallization at relatively high temperatures, but slow enough to enable quenching to room temperature without additional crystallization on the cool down cycle. (2) Samples which demonstrate fast crystallization kinetics, and which can therefore be crystallized

from the melt at high temperatures in relatively short periods of time. These samples could be crystallized from the melt in a hot stage and SAXS data collected at high temperatures.

3. The thermal analysis technique used (DSC) can also be improved upon. For example, the melt crystallized samples were heated directly from the crystallization temperature to the melting. While this ensures that no crystallization takes place on a cool down cycle, it also results in some uncertainty in the estimation of the heat of fusion for the two endotherms (see Figure 4.1c). Future studies could employ a small cooling ramp (e.g. about  $10^{\circ}\text{C}$ ) before the heating ramp or heating at slower rates (e.g.  $2^{\circ}\text{C}/\text{min}$ ) so as to enable better baseline estimations.

4. No attempts were made to estimate the heat of fusion using standardized heat capacities values. It is likely that the errors that result in the estimates for melting temperature and heat of fusion is small, however care should be taken in future DSC studies so as to get accurate heat capacity estimates.

5. The half time for crystallization is difficult to estimate for slow crystallizing samples. The problem has been illustrated in Figure 4.1b. For slow crystallizing systems, the crystallization exotherm is broad and not well defined. The estimated half time for crystallization then becomes a function of the baseline. Care was taken in this dissertation to report the average half time from multiple estimates on multiple samples (usually about 5 estimates on 1 sample, and 2 samples per data point). However, it is advisable that the estimated crystallization kinetics be confirmed with other techniques. These could include real time light intensity measurements under cross polarized light using a hot stage.

With more available data, it is possible that the theory for copolymer crystallization and melting could be further developed. In homopolymers, equilibrium theories are used to predict the minimum lamellar thickness for a given crystallization temperature. Kinetic factors are then incorporated to model the crystallization kinetics and the actual lamellar

thickness<sup>61</sup>. Melting is then modeled as an equilibrium manifestation of the actual lamellar thickness (an example of which is depicted in Section 2.6). The theory for copolymers could potentially be developed in a similar manner. Equilibrium theories could be used to predict an average crystalline phase composition independent of the crystallization temperature and also the minimum lamellar thickness. Kinetic factors could then be incorporated to predict the actual lamellar thickness, the crystallization kinetics and the crystalline phase composition. Melting would then be an equilibrium manifestation of the actual lamellar thickness and the crystalline phase composition.

## BIBLIOGRAPHY

1. Herold, F. and Schneller, A. Advanced Materials, 1992, **4**,3, 143
- 2a. Gardner, K. H., Hsiao, B. S., Matheson, R. R. and Wood, B. A. Polymer, 1992,
- 2b. Gardner, K. H., and Hsiao, B. S. Personal Communications.
3. Radhakrishnan, S. and Nadkarni, V. M. Journal of Polymer Materials, 1985, **2**, 93.
4. Dawson, P. C. and Blundell, D. J. Polymer, 1980, **21**, 577
5. Hay, J. N., and Kemmish, D. J. Polymer Comm., 1989, **30**, 77
6. Matheson, R.R., Chia, Y. T., Avakian, P. and Gardner, K. H. Polymer Prep, 1988, **27**, 468.
7. Chang, I. Y SAMPE Quarterly, 1988, **19**, 29
8. Avakian, P., Gardner, K. H., and Matheson, R.R Journal of Polymer Science: Polymer Letters, 1990, **28**, 243.
9. Sauer, B. B., Avakian, P., Starkweather, H. and Hsiao, B. S. Macromolecules, 1990, **28**, 5119
10. Hsiao, B. S., Chang, I. Y. and Sauer, B. B. Polymer, 1991, **32(15)**, 2799
11. Gay, F. P. and Brunette, C U. S. Patent # 4,816,556 1989
12. Bassett, D. C.; Olley, R. H.; Raheil, I. A. M. Polymer, 1988, **29**, 1745
13. Lee, Y.; Porter, R. S. Macromolecules 1987, **20**, 1336
14. Cheng, S. Z. D.; Cao, M. Y.; Wunderlich, B. Macromolecules 1986, **19**, 1868
15. Hsiao, B. S., Gardner, K. C., Wu, D. Q., and Chu, B. Polymer 1993,
16. Hsiao, B. S., Gardner, K. C., Wu, D. Q., and Chu, B. Polymer 1993,

17. Velikov, V., Vivirito, J., and Marand, H. submitted to Macromolecules.
18. Verma, R. K., Kander, R. G., Velikov, V., Chu, B., Hsiao, B. S., and Marand, H. Macromolecules In Press.
19. Bonner, W. H. US Patent # 3065205(1962).
20. Goodman, I., McIntyre, J. E. and Russell, W. British Patent Application # 971227.
21. Iwakura, Y., Uno, K. and Takiguchi, T. J. Polym. Sci. 1968,**6**,3345.
22. Marks, B. M. US Patent Application # 1387303 1969.
23. Dahl, K. US Patent # 3,953,400, 1976
24. Nieme, K., Toda, F., Uno, K and Iwakura, K. Polymer Letters Edition 1977,**15**,283.
25. Colquhoun, H. M. and Lewis, D. F. Polymer 1988, **29**, 1902.
26. Ueda, M. and Oda, M. Polymer Journal 1989, **21**, 9, 673.
27. Clendinning, R. A., Farnham, A. G., Hall, W. F., Johnson, R. N. and Merriam, C. N. J. Polym. Sci. 1967, **5**, 2375.
28. Attwood, T. E., Dawson, P.C., Freeman, J. L., Hoy, L. R. J., Rose, J. B. and Staniland, P. A. Polymer 1981, **22**, 1096
29. Mohanty, D. K., Lowery, R. C., Lyle, G. D. and McGrath, J. E. 32<sup>nd</sup> SAMPE Symposium 1987, **32**, 4081
30. Lyon, K. R., Mohanty, D. K., Lyle, G. D., Glass, T., Marand, H., Prasad, A. and McGrath, J. E. SAMPE Symposium
31. Sakaguchi, Y., Tokai, M., and Kato, Y. Polymer 1993, **34**, 7 1512
32. Clendinning, R. A., Kelsey, D. R., Botkin, J. H., Winslow, P. A., Youssefi, M. Cotter, R. J., Matzner, M., and Kwiatkowski, G. T. Macromolecules 1993, **26**, 2361

33. Harris, J. E., Winslow, P. A., Botkin, J. H., Maresca, L. M., Clendinning, R. A., Cotter, R. J., Matzner, M., and Kwiatkowski, G. T. Macromolecules 1993, **26**, 2366
34. K. L. Faron Personal Communications
35. Memory, J. D., and Wilson, N. K. "*NMR of Aromatic Compounds*" John Wiley & Sons 1982.
36. Flory, P. J. Transactions of the Faraday Society 1955, 848
37. Wunderlich, B. Macromolecular Physics 1976, **2**, 259
38. Helfand, E., and Lauritzen, J. I. Jr. Macromolecules 1973, **6**, 4, 631
39. Sanchez, I. C., and Eby, R. K. Macromolecules 1975, **8**, 5, 638
40. Sanchez, I. C., and Eby, R. K. Journal of Research of the National Bureau of Standards A 1973, **77**, 353
41. Lauritzen, J. I. Jr., DiMarzio, E. A., and Passaglia, E. Journal of Chemical Physics 1966, **45**, 4444
42. Nojima, S., Ono, M., and Ashida, T. Polymer Journal 1992, **24**, 11, 1271
43. Ito, J-I, Mitani, K., and Mizutani, Y Journal of Applied Polymer Science 1992, **46**, 1221
44. Ito, J-I, Mitani, K., and Mizutani, Y Journal of Applied Polymer Science 1992, **46**, 1235
45. Alamo, R. G., Chan, E. K. M., Mandelkern, L. and Voigt-Martin, I. G. Macromolecules 1992, **25**, 24, 6381
46. Sanchez, I. C., and Eby, R. K. Journal of Research of the National Bureau of Standards- A. Physics and Chemistry 1973, **77A**, 3, 353
47. Allegra, G., Marchessault, R. H., and Bloembergen, S. Journal of Polymer Science, Part B, Polymer Physics 1992, **30**, 809

48. Allegra, G. Polymer Preprints 1988, **29**, 615
49. Strobl and Schneider Journal of Polymer Science Part B, Polymer Physics, 1981,
50. Koberstein J. T. Stein R. S. J. Polym. Sc., Polym. Phys. Ed 1983, **21**, 2181
51. Ruland, W. Colloid Polym. Sci 1977, **255(5)**, 417
52. Biswas, A. Personal Communications.
53. Lovinger, A. J.; Hudson., S. D.; Davis, D. D. Macromolecules 1992, **25**, 1752
54. Sauer B. B., and Hsiao, B. S. In Press.
55. Line broadening analysis performed on the 111 peak (assuming infinite dimensions along a & b axes) for alternating PEKK 50/50 crystallized at 260°C without instrumental correction results in a "lower limit" for lamellar thickness of 80 Å, which was consistent with the higher value of  $X_{CL}$  obtained from SAXS.
56. Vonk, G. G. J. Appl. Cryst. 1973, **6**, 81
57. Wunderlich, B. "*Thermal Analysis*" Academic Press, 1990
58. Hoffman, J. D., and Weeks, J. J., Journal of Research of the National Bureau of Standards 1962, **66A**, 13
59. Hoffman, J. D., Davis, G. T., Lauritzen, J. I. Jr. In Treatise on Solid State Chemistry Hannay, N. B., Ed. Plenum Press: New York, 1976, Volume 3 Chapter 7.
60. Hoffman, J. D., and Miller, R. L. In Press.
61. Hoffman, J. D., and Lauritzen, J. I. Jr. Journal of Research of the National Bureau of Standards 1961, **65A**, 297
62. Glatter, O. Journal of Applied Crystallography 1974, **7**, 147
63. Ruland W., Acta Crystallography. 1961, **14**, 1180.
64. Equation 6 in Reference 39.



## VITA

Ravi Kant Verma was born on October 24, 1968 of Krishna and Verma in Ranchi, Bihar (India). He graduated from St. Xavier's College in Ranchi in 1986 and in the same fall joined the Indian Institute of Technology at Kharagpur, graduating with a degree in Metallurgical Engineering in 1990. The same fall, he joined the Materials Science and Engineering Department at Virginia Polytechnic Institute and State University. He obtained an M. S. degree under the guidance of Dr. Ronald George Kander in May 1992, and started pursuing a PhD.